Cardiac analysis of endothelin-1 transgenic and endothelial nitric oxide synthase knock-out mice

Dissertation zur Erlangung des akademischen Grades des
Doktors der Naturwissenschaften (Dr. rer. nat.)

eingereicht im Fachbereich Biologie, Chemie, Pharmazie
der Freien Universität Berlin

vorgelegt von

Nicolas Vignon-Zellweger

aus Suresnes, Frankreich

2009

Hiermit bestätige ich, dass ich die vorliegende Arbeit selbständig angefertigt habe. Ich versichere, dass ich ausschließlich die angegebenen Quellen und Hilfen in Anspruch genommen habe.

Hereby I declare that I have written this thesis by myself, marked the sources of any quotations or content obtained otherwise and mentioned any personal help by name.

This work was carried out from January 2006 to December 2009 under the supervision of Prof. Dr. Franz Theuring at the Center for Cardiovascular Research, Institute for Pharmacology, Charité University of Berlin.

1st reviewer: Prof. Dr. Franz Theuring
2nd reviewer: Prof. Dr. Burkhardt Wittig

Day of the oral examination: February 26th, 2010

"Si l'intelligence n'a dans la hiérarchie des vertus
que la seconde place, il n'y a qu'elle capable de
proclamer que l'instinct doit occuper la première."

Marcel Proust
Contre Sainte-Beuve

"Wir versuchen genau zu sein, einseitig aber nicht. Dies ist
eine Herausforderung, die uns jedoch nicht aufhalten soll.
Das Wissen, soweit es reichen kann, ist Genauigkeit.
Die Fantasie jedoch bleibt dabei unverzichtbar."

Paul Klee
Über die moderne Kunst

Acknowledgement

I am sincerely grateful to my supervisor Prof. Dr. Theuring for having received me in his group and for his daily support these four last years. His intellectual guidance and direction has accompanied me through the learning of the profession of researcher. Together with Prof. Dr. Hocher, to whom I'd like to address my sincere gratitude, Prof. Dr. Theuring has been all along a source of inspiration.

I deeply thank Prof. Dr. B. Wittig for reviewing this manuscript.

I thank my colleagues from AG Theuring, K. Schwab, M. Gluth, N. Gül and A. Fischer for their support and help. Thank you to J. Rahnenführer and P. Seider for their engagement during their diploma within our group. This work would have not been possible without the technical advices of C. Tanneberger, B. Seelhorst, M. Magbagbeolu and A. Thoma as well as many members of the CCR. Thank you all for your help making my work easier and more efficient day after day.

I express my gratitude to the people of the Proteome Factory AG: Dr. Christian Scheler, and particularly B. Neumann and Dr. K. Lehmann for their inexhaustible expertise on mass spectrometry and two dimensional electrophoresis, respectively.

The member of Prof. Hocher's lab, particularly K. Relle and Ph. Kalk, thank you for your fruitful collaboration in the project.

This work was supported by grants from the Deutsche Forschungsgemeinschaft to Prof. Theuring (DFG Th 466/7-1) and by the European Commission via the Marie Curie Host Fellowship for Early Stage Training CARDIOVASC (MEST-CT-2005-020268). I thank Prof. P. Ruiz and Dr. D. Michel for their organization skills contributing to the success of the CARDIOVASC program.

My family and friends, and of course my dear Susi, for your encouragement, understanding and support, thank you!

Abbrevations

Note: the abbreviations for the protein names are in the table 8.

18S	18S ribosomal RNA	DNase	Deoxyribonuclease
1D	One dimensional	dNTP	Deoxyribonucleotide
2D	Two dimensional	dpi	Dots per inch
2DE	Two dimensional electrophoresis	DTT	Dithiothreitol
aa	Amino acid	ECE	Endothelin converting enzyme
Ab	Antibody	ECM	Extracellular matrix
ADF	Actin-depolymerizing factor	EDTA	Ethylenediaminetetraacetic acid
ADP	Adenosine phosphate	eNOS	Endothelial nitric oxide synthase
ANP	Atrial natriuretic peptide	eNOS-/-	eNOS knock out
APS	Ammonium persulfate	ESI	Electrospray Ionisation
ATP	Adenosine triphosphate	ESI/MS	Electrospray ionisation/tandem mass spectrometry
BCIP	5-Bromo-4-chloro-3-indolyl phosphate	ET	Endothelin
BH4	Tetrahydrobiopterin	ET+/+	Endothelin-1 transgenic
BLAST	Basic local alignment and search tool	ET-1	Endothelin-1
BNP	Brain natriuretic peptide	ETA	Endothelin receptor A
bp	Base pair	ETB	Endothelin receptor B
BSA	Bovine serum albumin	ETR	Endothelin receptor
C57BL/6	C57 black 6	FAD	Flavin adenine dinucleotide
cDNA	Complementary DNA	h	Hour
cGMP	Cyclic guanosine monophosphate	H_2O_2	Hydrogen peroxide
CoA	Coenzyme A	HE	Hematoxylin Eosin
Col	Collagen	hET-1	Human endothelin-1
Ct	Threshold cycle	hPPET1	Human preproendothelin-1
Da	Dalton	HPRT	Hypoxanthine guanine phosphoribosyl transferase
DAB	3,3` -Diaminobenzidine	IEF	Isoelectric focusing
ddH_2O	Double-distilled water	Ig	Immunoglobulin
DIG	Digoxigenine	iNOS	Inducible nitric oxide synthase
DMSO	Dimethyl sulfoxide	iNOS-/-	iNOS knock out
DNA	Deoxyribonucleic acid	IP3	Inositol triphosphate

Abbrevations (continued)			
IPTG	Isopropyl β-D-1-thiogalactopyranoside	PCR	Polymerase chain reaction
jpeg	Joint Photographic Experts Group	PDE	Phosphodiesterase
kDa	Kilo dalton	PDH	Pyruvate dehydrogenase complex
LB	Lysogeny broth	PFA	Paraformaldhyde
LC	Liquid Chromatography	pI	Isolectric point
L-NAME	N-Nitro-L-Arginine Methyl Ester	PLC	Phospholipase C
L-NMMA	N-Methylarginine	PPET1	Preproendothelin-1
L-NNA	N-omega-nitro-L-arginine	PVDF	Polyvinylidene difluoride
LVEDP	Left ventricular end diastolic blood pressure	PVP	Polyvinylpyrrolidone
M	Mole per liter	qRT-PCR	Quantitative real time PCR
MALDI	Matrix-assisted laser desorption/ionization	RBG	Red blue green
mET-1	Murine endothelin-1	RNA	Ribonucleic acid
min	Minute	RNAse	Ribonuclease
MMP	Matrix metalloproteinase	ROS	Reactive oxygen species
mPPET1	Murine preproendothelin-1	rpm	Revolutions per minute
mRNA	Messenger RNA	RT	Room temperature
MS	(tandem) Mass spectrometry	SDS	Sodium dodecyl sulfate
MW	Molecular weight	SEM	Standard error of the mean
NaCl	Sodium chloride	sGC	Soluble guanylate cyclase
NAD	Nicotinamide adenine dinucleotide	SSC	Sodium saline concentration
NADPH	Nicotinamide adenine dinucleotide phosphate	TBS	Tris buffered saline
NBT	Nitro blue tetrazolium	TCA	Tricarboxylic acid
NCBI	National centre for Biotechnology information	TE	Tris EDTA
NMRI	Naval Medical Research Institute	TEMED	Tetramethylethylenediamine
nNOS	Neuronal nitric oxide synthase	tiff	Tagged Image File Format
NO	Nitric oxide	TNFα	Tumor necrosis factor alpha
NTE	NaCl EDTA Tris-HCl	tRNA	Transfer RNA
O_2^-	Superoxide	U	Unit
$ONOO^-$	Peroxynitrite	V	Volt
PAGE	PolyAcrylamide Gel Electrophoresis	vs.	Versus
PAH	Pulmonary arterial hypertension	WB	Western blot
PBS	Phosphate buffered saline	WT	Wild type

Table of content

1 Introduction 4
1.1 The discovery of two vasoactive substances 4
1.2 Physiology of endothelin-1 4
1.2.1 Generation of endothelin 4
1.2.2 Endothelin-1 action 5
1.2.2.1 Vessels 5
1.2.2.2 Heart 7
1.2.2.3 Kidney 7
1.2.2.4 Lung 7
1.2.2.5 Nervous system 7
1.3 Nitric oxide 8
1.4 Mouse models 8
1.4.1 ET-1 transgenic mice 8
1.4.2 eNOS-/- mice 10
1.4.3 Combination of ET+/+ mice with iNOS-/- and eNOS-/- mice 11
1.4.3.1 ET+/+iNOS-/- mice 11
1.4.3.2 ET+/+eNOS-/- mice 12
1.5 The NO / ET interplay in cardiovascular disease 12
1.6 Clinical applications 14
1.7 Proteomics 15
1.8 Aim of the study 17
2 Material and methods 19
2.1 Mice 19
2.2 Chemicals 20
2.3 Equipment 21
2.4 Software 22
2.5 Quantitative Real Time PCR 23
2.5.1 RNA extraction 23
2.5.2 qRT-PCR 23
2.5.3 Computations 24
2.6 Immunohistochemistry 25
2.7 In situ Hybridization 27
2.7.1 ETAR and ETBR cloning 27

2.7.2 RNA probes production 28
2.7.3 Staining protocol 28
2.7.4 Relative quantification 30
2.8 Histology 31
2.8.1 Staining 31
2.8.2 Measurements 32
2.9 Proteomics 33
2.9.1 Protein preparation 33
2.9.2 2DE: IEF and SDS-PAGE 34
2.9.3 Silver staining 35
2.9.4 MS compatible silver staining 35
2.9.5 Computer Analysis 35
2.9.6 Nano Liquid Chromatography-Electrospray Ionization / tandem Mass Spectrometry (ESI/MS) and protein identification 36
2.9.7 Protein classification 37
2.10 1D Western Blotting 37
2.11 Statistics 38
3 Results 39
3.1 Quantitative RT-PCR 40
3.1.1 Cardiac tissue 40
3.1.2 Aortic tissue 41
3.2 In situ hybridization 42
3.3 Western Blot of ETAR, ETBR, eNOS and iNOS 43
3.3.1 Cardiac tissue 43
3.3.2 Aortic tissue 45
3.4 Histology 46
3.4.1 Cardiac interstitial and perivascular ECM deposition 46
3.4.2 Cardiomyocyte diameter 48
3.4.3 Cardiac arteriole morphology 49
3.5 Immunohistochemistry 51
3.6 Proteomics 52
3.6.1 2DE: characteristics and reproducibility 53
3.6.2 Number of differentially expressed spots 53
3.6.3 Spot identification 54
3.6.4 Protein classification 57

3.6.5 Observed post-translational modifications 60
3.6.6 Validation 62
3.6.6.1 Oxidative stress 63
3.6.6.1.1 Peroxiredoxin-6 (PRDX6) 63
3.6.6.1.2 Peroxiredoxin-1 (PRDX1) 65
3.6.6.1.3 Superoxide dismutase [Cu-Zn] (SODC) 67
3.6.6.1.4 Glutathione S transferase Mu 2 (GSTM2) 68
3.6.6.2 Contractile machinery 68
3.6.6.2.1 Myosin regulatory light chain 2, ventricular/cardiac muscle isoform (MLRV) 68
3.6.6.3 Metabolic proteins 69
3.6.6.3.1 3-methylcrotonyl-CoA carboxylase alpha subunit (MCCA) 69
4 Discussion 71
4.1 Expression of ET components 72
4.2 Histology 74
4.2.1 Interstitium 74
4.2.1.1 Matrix protein expression 74
4.2.1.2 Metalloprotease expression 74
4.2.2 Perivascular area 75
4.2.3 Cardiomyocyte diameter 76
4.2.4 Cardiac arteriole morphology 76
4.3 Proteomics 77
4.3.1 Oxidative stress 78
4.3.2 Contractile machinery 81
4.3.3 Hypertrophy 84
4.3.4 Metabolism 85
4.3.4.1 Fatty acid metabolism 86
4.3.4.2 Glucose metabolism 88
4.3.4.3 TCA cycle and oxidative phosphorylation 91
4.3.4.4 Other metabolisms 93
4.4 Conclusions 94
5 Summary 95
6 Zusammenfassung 97
7 References 99

1 Introduction

1.1 The discovery of two vasoactive substances

Endothelin-1 (ET-1) has been discovered in the late 1980s. Yanagisawa and colleagues extracted from porcine aortic tissue a small peptide responsible for a strong and long lasting elevation of blood pressure after intravenous administration in rats.[1] The effect of ET-1 was observed to be even stronger than angiotensin II or vasopressin in elevating blood pressure. Almost simultaneously, a strong endothelium derived vasodilator was identified as nitric oxide (NO). These two discoveries demonstrated the importance of the endothelium in the control of blood pressure. Very rapidly, these two new vasoactive compounds have been found to belong to a complex and delicate regulatory system inside the vessel wall and in many organs, where subtle alterations might have prominent influences in the induction of pathologies. Twenty years after, the knowledge about NO and ET-1 exploded and led to the development of powerful treatments for cardiovascular diseases targeting both of these systems. Still, the underlying cellular and molecular mechanisms of this interplay and the clinical relevance of it are only partially understood.

1.2 Physiology of endothelin-1

1.2.1 Generation of endothelin

Endothelins compose a family of three peptides, ET-1, ET-2 and ET-3 derived from three distinct genes. The expression of ET-2 and ET-3 differ from ET-1 relatively to the tissue type.[2, 3] ET-1 is the predominant isoform *in vivo*. The human and mouse Edn1 genes code for a biologically inactive 212 and 202 amino acids (aa) preproendothelin-1 (PPET1), respectively. PPET1 is cleaved into the 38 aa big endothelin-1 (big ET-1) by specific furin-like proteases.[4] The active 21aa peptide ET-1 is produced from big ET-1 through the proteolytic action of the endothelin converting enzyme (ECE).[5] Human and mouse ET-1 amino acid sequences are identical. Other proteases, the chymases, can cleave big ET-1 into a 31aa active peptide ($ET\text{-}1_{1\text{-}31}$).[6] Big ET-1 has been shown to bind to the endothelin receptors also, but with a much lower affinity.[7] However, because of its longer half-life in serum, big ET-1 is sometimes preferred as pathological marker.[8, 9] Big ET-1 has no biological function apart from the protection from proteolysis

cleavage during transport in blood of endothelin. ET-1, for its part, exhibits a low plasma concentration[10] and acts as a para- and autocrine hormone. ET-1 is expressed in epithelial cells of the vasculature. In the kidney, ET-1 is expressed in the collecting duct, the thick ascending limb and endothelial cells.[11] In the heart, mammalian (but not human) cardiomyocytes,[12] endothelial and endocardial cells secrete ET-1.[13] ET-1 is also produced by neurons.[14] In the lung, ET-1 is expressed by endothelial cells of the pulmonary vasculature as well as in the different cell types of the airways (pulmonary neuroendocrine cells, endothelial cells, alveolar epithelial cells, and alveolar macrophages).[15-17] Macrophages produce ET-1 in many organs as well.[17] Transforming growth factor-beta, tumor necrosis factor-alpha, interleukins, insulin, norepinephrine, angiotensin II, and thrombin stimulate ET-1 transcription.[18-20] Atrial and brain natriuretic peptides, NO, prostacyclin, and prostaglandin inhibit ET-1 transcription.[21-23]

1.2.2 Endothelin-1 action

Shortly after the discovery of ET-1, two types of seven transmembrane G protein-coupled receptors were cloned called endothelin receptor A (ETAR)[24] and B (ETBR).[25] No specific agonist for ETAR and only two ETBR agonists, sarafotoxin 6c and IRL1620, are actually available.[26] However, the study of each receptor's role has been facilitated with the development of selective antagonists for both ETAR (e.g. BQ-123)[27] and ETBR (e.g. BQ-788)[28] and dual antagonists, like bosentan.[29] ET-1 has a similar affinity for both receptors.[24, 25] The intracellular pathways installed after ET-1 induced ETAR and ETBR activation involve Gq, Gs and Gi small G-proteins leading to stimulation of phospholipase C. The consecutive production of inositol triphosphate (IP3) and diacylglycerol increases the concentration of intracellular Ca^{2+}. Calcium is recruited from the reticulum by activation of the IP3 receptor and external calcium influx is increased by opening of the Ca^{2+} channels on the cellular membrane.[30]

1.2.2.1 Vessels

Historically, ET-1 is considered as a hormone controlling vascular tone. ETAR is expressed on vascular smooth muscle cells and ETBR on both endothelial and vascular smooth muscle cells (figure 1). 80% of ET-1 produced by endothelial cells diffuses through the basal side in the vascular wall and binds to both ETAR and ETBR on smooth muscle cells, which leads to a

vasoconstriction of the vessels.[31] Selective blockade of ETAR leads to a vasodilation mediated by enhanced production of NO.[32] In contrast, ET-1 which diffuses in the plasma activates ETBR on endothelial cells, which promotes endothelial Nitric Oxide Synthase (eNOS) derived NO release through a tyrosine kinase-dependent and a calcium/calmodulin-dependent pathway.[33] NO, in turn, reduces the concentration of intracellular Ca^{2+} with concomitant vasodilation[34] (figure 1). Moreover, ETBR plays a key role in the clearance of circulating ET-1.[35, 36] Beside its major role on vascular tone, ET-1 has mitogenic effects on vascular smooth muscle cells[37] and fibroblasts[38] and induces cytokine production through the ETAR receptor on macrophages.[39]

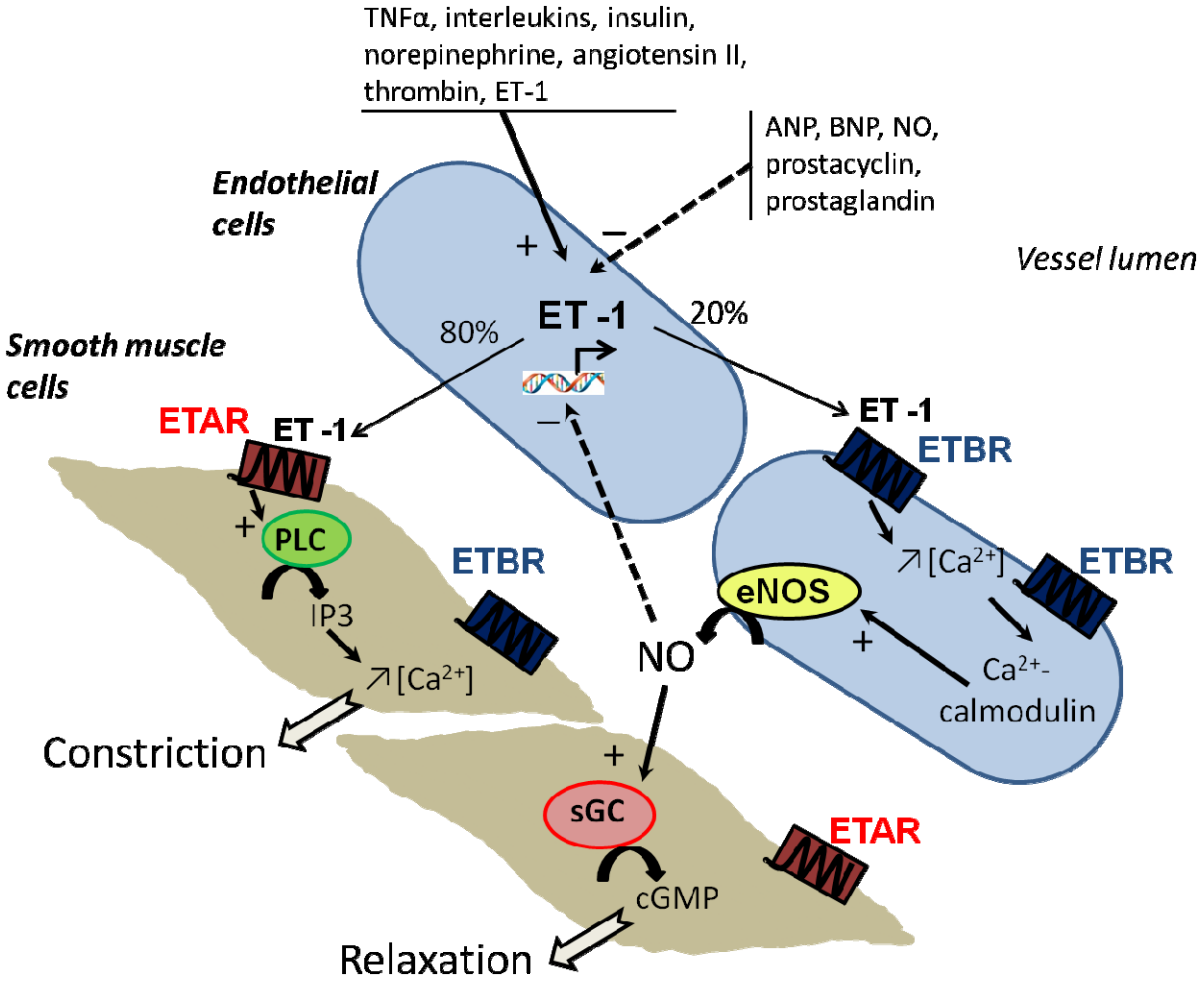

Figure 1: Basic scheme on ET-1 expression, regulation and actions inside the vessel wall. ET-1: endothelin-1, NO: nitric oxide, ETAR: endothelin receptor A, ETBR: endothelin receptor B, eNOS: endothelial nitric oxide synthase, PLC: phospholipase C, sGC: soluble guanylyl cyclase, IP3: inositoltriphosphate, cGMP: cyclic guanoside monophosphate, TNFα: tumor necrosis factor alpha, ANP: atrial natriuretic peptide, BNP: brain natriuretic peptide.

1.2.2.2 Heart

Both ETAR and ETBR are expressed throughout the cardiac muscle, including the coronary vasculature. The ratio between both depends on the cell types.[13] ETAR is the most represented type in the myocardium: its activation has constrictive and inotropic effects.[40] An ETAR antagonist treatment increases left ventricular pressure, when an ETBR antagonist has the opposite effects.[41] ET-1 promotes myocytes hypertrophy, these effects can be antagonized by NO.[42] On the other hand, ET-1 actions in the heart include cell survival mechanisms.[43]

1.2.2.3 Kidney

In the kidney, both ETAR and ETBR receptors are present. ET-1 induced ETAR activation provokes mesanglial cells contraction[44] and proliferation.[45] ETAR and ETBR are expressed on podocytes and may play a role in glomerular filtration.[46, 47] In the collecting duct, ETBR is the predominant receptor type. ETBR activation has diuretic[48] and natriuretic[49] effects, by enhancing NO release. This is true in the medullary thick ascending limb,[50] endothelial and interstitial cells.[11] ET receptors (ETR) are typically present on renal vessels and control renal blood flow.[51] Finally, ET-1 plays a role in the inflammatory response in the kidney as well.[52]

1.2.2.4 Lung

Endothelin receptors are present on airway smooth muscle cells. Ratio between ETAR and ETBR is species as well as region specific.[53-55] Nevertheless, ET-1 induced ETBR and ETAR activations contract airway smooth muscle cells[56] and has mitogenic effects on these cells[57] and on epithelial cells.[58] ET-1 modifies airway mucus secretion.[59] Finally, ET-1 can induce pulmonary inflammation and fibrosis.[60]

1.2.2.5 Nervous system

ET-1 and its receptors are expressed in many cell types of the central and peripheral nervous systems. The role of ET-1 as neurotransmitter has been reviewed by Dashwood and Loesch.[61] Briefly, ETR activation is thought to be implicated in the central control of blood pressure, cardiac and pulmonary functions in rodents and humans.[62, 63] Moreover, intracerebral injection of ET-1 modifies behavior in rats.[64] Finally, ET-1 mediates nociception at the central level[65] and in the periphery through ETBR in rodents.[66]

1.3 Nitric oxide

NO has been identified in 1987 as an endothelium-derived factor responsible for relaxation of vessels.[67] It's a gaseous vasoactive substance, whose production is catalyzed from L-arginine by three types of NOS. The endothelial and neuronal NOS (eNOS and nNOS) are constitutively expressed and their activation is calcium dependent. The inducible NOS (iNOS) expression is stimulated by cytokines in case of inflammation and is calcium independent. eNOS is the most important isoform in the vasculature. NO diffuses through the cell and binds the soluble guanylyl cyclase (sGC) on its iron heme. The sGC is thereby activated and produces the second messenger cGMP[68] (figure 1). Under physiological conditions, NO is constantly produced and contributes to vascular smooth muscle cells tone.[69] The amount of vascular NO depends on shear stress forces[70] and is therefore higher in arteries and veins with smaller rather than larger diameters in mammalians.[71] NO is responsible for plethoric effects in the cardiovascular system. In the vasculature, NO is protective by inhibiting leukocyte[72] and platelet adhesion,[73] relaxes vascular smooth muscle cells[67] and also inhibits vascular smooth muscle cells proliferation and mitogenesis.[74] In the heart, eNOS and iNOS derived NO is produced in endothelial cells and cardiomyocytes and controls contractile functions, in physiological and pathological situation, respectively.[67] NO reduces renal vascular resistance and increases glomerular filtration rate in many species including rodents and humans.[75] All these positive cardiovascular effects are to be seen in balance with the pathological consequences of oxidative stress provoked by an excessive production of NO. In fact, the reactive oxygen species superoxide (O_2^-) inactivates NO by forming the highly reactive peroxynitrite (ONOO−). NO derived oxidative stress plays indeed a role in several cardiovascular diseases, such as cirrhosis induced nephropathy,[76] artherosclerosis,[77] and hypertension.[78] In case of eNOS co-factors deficiency, tetrahydrobiopterin (BH4) and L-arginine, the so-called uncoupled eNOS produces superoxide rather than NO.[79]

1.4 Mouse models

1.4.1 ET-1 transgenic mice

The transgenic approach consists in inserting one or more copies of a gene of interest into the genome of an animal. It permits the study of the product of one gene in a whole living animal.

Even though the permanent overexpression of a gene results in some compensatory mechanisms, it remains a powerful technique. The role of ET-1 *in vivo* has been better understood with the generation of ET-1 transgenic (ET+/+) mouse lines by microinjection of linear human ET-1 genomic DNA fragments into one-cell embryos. Surprisingly, these mice remain normotensive.[80] They develop however age-related renal cysts, interstitial fibrosis, and glomerulosclerosis, leading to a progressive decrease in glomerular filtration rate and subsequent lethality.[80, 81] Elevation in laminin expression is in both interstitium and glomeruli mainly responsible for fibrosis.[82] The mechanisms underlying this pathological phenotype is probably an imbalance between cell proliferation and apoptosis.[83] In the lung, the chronic overexpression of ET-1 leads to an increase of interstitial matrix expression and a CD4 positive cells characterized inflammation.[60] This does not lead to pulmonary hypertension either. The endothelin receptor expression is similar in transgenic and wild type (WT) mice;[60] the reorganization of the receptors expression can therefore not explain the lack of hypertension. In the heart of ET+/+ mice, overexpression of ET-1 promotes interstitial fibrosis in aged mice, mainly characterized by an elevation in the expression of collagen type III and laminin.[82]

A second independent mouse line overexpressing ET-1 has been generated characterized also by renal interstitial fibrosis, renal cysts, glomerulosclerosis and narrowing of arterioles.[84] Because of this renal phenotype, these mice develop a salt sensitive hypertension. Furthermore their creatinine clearance is reduced and proteinurea is enhanced but, most importantly, no high blood pressure is detected in these mice compared to WT.[84]

A recently generated mouse model, in which human ET-1 is specifically overexpressed in the endothelium, develops endothelial dysfunction associated with oxidative stress[85] and a chronic vascular inflammation, again in the absence of hypertension.[86]

The contractile response to ET-1 of aortic rings in ET+/+ mice is reduced compared to WT and the elevation of maximum contraction to ET-1 after preincubation with the NOS inhibitor N-Nitro-L-Arginine Methyl Ester (L-NAME) is more pronounced in ET+/+ mice than in WT[87] indicating that NO bioavailability is elevated in ET+/+ mice. Consistently, urinary nitrite and nitrate excretion, a marker of NO production, in ET+/+ mice is higher than in WT. Furthermore, the elevation of blood pressure after an L-NAME treatment is greater in ET+/+ mice than in WT.[87, 88] Moreover, iNOS is overexpressed in the vasculature of ET+/+ compared to WT[88] and an

L-NAME induced pulmonary fibrosis and inflammation occurs in ET+/+ but not in WT mice.[89] Taken together, these results strongly suggest that NO synthesis is increased in ET+/+ mice, thereby demonstrating its role as natural functional antagonist of ET-1.

1.4.2 eNOS-/- mice

Knock-out technology consists in inactivating a gene through the insertion of a cassette in the open reading frame. It results in the absence of the expression of the functional protein and provides therefore insights into the functions of this protein in a living animal. L-Arginine analogs are used as NOS inhibitors (L-NAME, L-NNA, L-NMMA). They are powerful tools to reduce NO production, but are not specific for the different NOS isoforms. Knock-out technology is thus particularly important for the *in vivo* study of NOS functions. Four independent eNOS knock-out (eNOS-/-) lines have been generated and published.[90-93] Even though the different eNOS-/- mice differ according to some parameters because of their different genetic background, they all develop high blood pressure. Despite the compensatory effects observed, particularly regarding the expression of the other NOS isoforms[94] and prostaglandins,[90] these models have enabled the study of the functional role of eNOS. eNOS plays an important role in cardiac function and structure since eNOS deficient mice display enhanced cardiac contractility and show age-related cardiac hypertrophy.[95] The age-related cardiac hypertrophy and early lethality affect more dramatically male than female eNOS-/- mice.[95] The protective role of eNOS was demonstrated in eNOS-/- mice generated by Huang *et al.*, which develop an increased infarct size compared to WT.[96] The strain generated by Shesely *et al.* exhibit however a reduced infract size[96] describing the importance of the genetic background on development of pathologies. eNOS derived NO plays a role in the acetylcholine response in heart[90] and aorta[92] and β-adrenergic response in heart.[97] Hypertension in eNOS-/- mice can be in part explained by a higher renin production.[93] ET-1 plasma level is not altered in these mice, but ET-1 induced elevation of blood pressure is more pronounced than in WT mice.[98] ET-1 tissue level is elevated in mesenteric arteries and ETBR expression is reduced in cardiac tissue of eNOS-/- mice.[99] Studies prove eNOS implication in the regulation of renal function through an L-arginine induced inhibition of NaCl absorption.[100] Interestingly, generation of eNOS-/- mice confirmed the role of NO in modulating energy metabolism, oxygen

consumption, cardiac glucose and fatty acid metabolism, here again with some differences between the strains.[101-104] Finally, eNOS is required for normal cardiovascular development: eNOS-/- mice are characterized by defected aortic valve[105] and septum[106] as well as impaired coronary vasculature at birth.[107]

1.4.3 Combination of ET+/+ mice with iNOS-/- and eNOS-/- mice

Counter regulatory interactions between the NO and ET systems are well established.[80, 108] NO release is stimulated by ET-1 via the activation of the endothelial ETBR-eNOS pathway and in turn, endothelium derived NO inhibits the production of ET-1 via a cyclic GMP-dependent pathway (figure 1).[88, 109, 110] The lack of hypertension observed in ET+/+ mice is therefore assumed to be the result of an increased generation of NO, thus counterbalancing the activated ET system.[87, 88]

1.4.3.1 ET+/+iNOS-/- mice

To further investigate in more details this hypothesis and disrupt the probable compensatory effect of NO in ET+/+ mice, and because vascular iNOS expression was shown to be elevated in ET+/+ mice,[88] ET+/+ mice have been crossbred with iNOS-/- mice. Compared to ET+/+ animals, the ET+/+iNOS-/- mice show a significant lower endothelium-dependent relaxation. Therefore, in ET+/+ mice, additional knock-out of iNOS results in an impairment of vasodilative capability. However, this leads only to a slight elevation of blood pressure in the ET+/+iNOS-/- compared to ET+/+. ET+/+iNOS-/- mice are nevertheless not hypertensive compared to WT mice.[111] Moreover, in aged animals (12 months old), both ET+/+ and iNOS-/- mice develop cardiac perivascular fibrosis and left ventricular diastolic dysfunctions, characterized by an elevated end diastolic pressure and stiffness constant. In spite of that, in the ET+/+iNOS-/- mice, combination of both genetic manipulations restores these parameters to WT level.[89] Thus this study describes the age-related development of cardiac dysfunctions in ET+/+ mice and the ambivalent role of iNOS, since genetic inactivation of iNOS alone causes reduction of cardiac functions but improves them on an ET+/+ background.

1.4.3.2 ET+/+eNOS-/- mice

iNOS expression is mostly induced in case of inflammation though.[112] In addition, the endothelial form of NOS (eNOS) is the most abundant form of NOS in vessels[113] and accordingly NO is mostly produced by this isoform. On account of this, the ET+/+eNOS-/- mice have been generated. This model, like the eNOS-/- mice, shows an elevation of blood pressure in comparison to WT and ET+/+ mice.[114] The endothelium-independent aortic relaxation to sodium nitroprusside is not affected in this model, suggesting intact relaxation properties of the smooth muscle cells. Endothelium-dependent relaxation to acetylcholine is blunted by the lack of eNOS, supporting eNOS as the predominant source of endothelial NO, but is enhanced in ET+/+ mice, confirming an enhanced bioavailability of NO in ET+/+ mice.[87]

Finally contraction to ET-1 is similar in ET+/+ and ET+/+eNOS-/- but reduced compared to WT, when lack of eNOS alone does not affect it. Quaschning *et al.*[114] made the assumption that this reduction of exogenous ET-1 induced contraction in both ET+/+ and ET+/eNOS-/- animals is due to a saturation of receptor occupation. Both ETAR and ETBR are however overexpressed in aorta of crossbred animals but this does not correlate necessarily with receptor responses. The use of the selective ETAR and ETBR antagonists, BQ-123 and BQ-788 respectively, shows that aortic contraction in this model is ETAR dependent, and ETBR does not play a contractile role.[114]

In conclusion, the results from these two mouse models indicate that a transgenic overexpression of ET-1 is not able to provoke hypertension. It is rather an imbalance between ET-1 and eNOS produced NO actions which is responsible for the development of hypertension. Nevertheless, the exact role of both vasoactive substances in this delicate interplay remains to be fully investigated.

1.5 The NO / ET interplay in cardiovascular disease

Extrapolation from animal models to the human situation can sometimes be dubious. However, with regard to the interplay between the endothelin and NO systems, a rich literature demonstrates the joint roles of both vascular substances in development of many cardiovascular diseases in both humans and animal models.

The development of bosentan, a dual ETR antagonist, and its commercialization for pulmonary arterial hypertension (PAH) is the strongest evidence of the importance of studying the role of endothelin in biomedical research. Interestingly, NO production in the pulmonary airways is reduced in PAH patients and bosentan treatment restores NO production to a normal level;[115] reduced NO production is therefore thought to be one of the causes of PAH. The other way around, ET-1 gradients between central venous and pulmonary arterial plasma levels are reduced in PAH patients receiving an inhalation of nitric oxide.[116] Rabelink and Bakris reviewed how an imbalance between endothelium-derived reactive nitrogen species and reactive oxygen species as well as an increased expression of ET-1 may contribute to a loss of renal function in diabetes.[117] In diabetic nephropathy, renal iNOS expression is activated, total renal NO is however reduced; both of these parameters can be restored by a dual ETR antagonist treatment.[118] Papalambros *et al.* showed positive correlation between ET-1 and iNOS production in an arterial anastomotic rat model.[119] Changes in the sensitive balance between NO generation and ET-1 production have also been described in a variety of other cardiovascular diseases: in coronary artery disease patients, NO/ET-1 ratio is impaired; pharmacological reduction of oxidative stress in these patients can restore the physiological ratio and this is accompanied by improved systolic functions.[120] In congestive heart failure, ET-1 is overexpressed and blunts NO derived endothelial relaxation by increasing the level of asymmetric dimethylarginine, a natural NOS inhibitor.[121] In preeclamptic women, hypertension goes along with elevated endothelin and reduced NO plasma levels.[122] In patient with essential hypertension, vasoconstrictive effects of ET-1 are increased, because of an impaired NO bioavailability.[123] Obese patients with metabolic syndrome suffer from endothelium dysfunction characterized by reduced NO and increased ET-1 vascular activity; this imbalance can be readjusted by the unique treatment with the growth hormone grehlin.[124]

The importance of ET-1 and NO in numerous cardiovascular diseases has become evident. More than the absolute ET-1 and NO plasma levels, the ratio between both seems to be a good prognostic indicator for cardiovascular disease.[125] However, the underlying molecular mechanisms controlling the balance between NO and ET-1 are not clear yet. It is difficult to settle if the elevated ET-1 and reduced NO levels observed in many pathological situations are two independent events or, in contrary, if these two events are closely related to one another.

Moreover, the question whether these mechanisms are a consequence or a cause of cardiovascular failure remains open. However, the fact that by pharmacologically targeting one system the other is affected, strongly indicates a close regulatory relationship between the NO and ET systems.

1.6 Clinical applications

The knowledge on the ET-1 and NO systems in pathophysiology led to the development of powerful therapies. Inhaled NO has been approved for persistent pulmonary hypertension of neonates. By limiting the breakdown of NO induced cGMP, phosphodiesterase (PDE) inhibitors potentiate the NO pathway. Sildenafil, a PDE inhibitor, is in clinical praxis for treatment of PAH. To date, three ETR antagonists have been approved for marketing, all of them for the treatment of PAH (bosentan from Actelion since 2001, sitaxentan from Pfizer since 2006 and ambrisentan from GlaxoSmithKline since 2007).

Riociguat, a stimulator of sGC, the cellular NO target, is under investigations for treatment of PAH.[126] Several clinical studies currently explore the potential clinical advantages of L-arginine supplementation on preeclampsia and essential hypertension.

At the same time, results from clinical trials using a dual ETR antagonist in preventing other cardiovascular diseases such as acute heart failure are controversy.[127] Several clinical studies are ongoing to clarify the potential of ETR antagonists for other indications. Macicentan, a new dual ETR antagonist, is under investigations for symptomatic PAH in the phase III study SERAPHIN. The clinical benefits of ambrisentan, bosentan and macicentan on idiopathic pulmonary fibrosis will be revealed by the ARTEMIS-PH, BUILD-3 and MUSIC studies, respectively. Macitentan can also reduce end organ damage in diabetic rats.[128] Avosentan, another dual ETR antagonist, reduces proteinurea in diabetic patients, as shown in the phase III trial ASCEND.[129] Zibotentan, an ETAR blocker, is currently being evaluated in a phase III trial program (ENTHUSE) for prostate cancer.

Compared to the tremendous work achieved at the preclinical level since the discovery of ET-1 and NO, more than twenty years ago, the actual clinical applications may look modest. If more basic research and clinical studies are needed, the ET and NO systems remain, nevertheless, promising therapeutic targets for the treatment of cardiovascular disease.

1.7 Proteomics

Together with appropriate animal models, research on ET-1 and NO thus needs an open-minded approach. Proteomics, the study of the proteome, represents a hypothesis free technique, which is able to dissect molecular mechanisms without particular expectations.

The proteome is defined as the complete complement of proteins in a given system (cell culture, organ, or organism). Virtually every protein is post-translationally modified, according to time, localization and stress, physiological and pathological situations. These modifications are extremely diverse and can be methylation, phosphorylation, and glycosylation to name a few. The term protein species represents the products of one single gene including the protein in all its different post-translational states.

The idea of protein separation in two dimensions goes back to the 1950's.[130] Two decisive inventions made it look as we know it today. The first is PolyAcrylamide Gel Electrophoresis (PAGE), which consists in separation of proteins according to their molecular weight through a polyacrylamide gel,[131] improved by Laemmli in 1970 by the use of the detergent sodium dodecyl sulfate (SDS).[132] The second is isoelectric focusing (IEF) which separates proteins according to their isoelectric point.[133] Combination of both was used by several groups to separate proteins in the seventies and particularly by Klose *et al.*[134] and at the same time but independently by O'Farell *et al.*.[135] Further development occurred during the following two decades till the work of Klose *et al.*,[136] who reached both high resolution and reproducibility and on which the technique employed here is based. From the discovery of two dimensional electrophoresis (2DE), we needed to wait almost twenty years for the development of mass spectrometry techniques able to sequence peptides: Matrix-assisted laser desorption/ionization (MALDI)[137] and electrospray ionization (ESI),[138] the two most common mass spectrometric techniques used today for the analysis of biomolecules. After trypsin digestion of proteins excised from the polyacrylamide gels, the resulting peptides can be sequenced by mass spectrometry (figure 2). Using MALDI, the peptide preparation is crystallized into a matrix, while ESI uses an electrospray to disperse the peptide solution into the mass spectrometer. To identify with the minimal doubt the proteins corresponding to the sequenced peptides, the need for reliable protein databases was fulfilled with the creation of, among others, the Swissprot database (figure 2). Thereby, the

rapid development of the World Wide Web was a crucial step making these databases easily accessible.

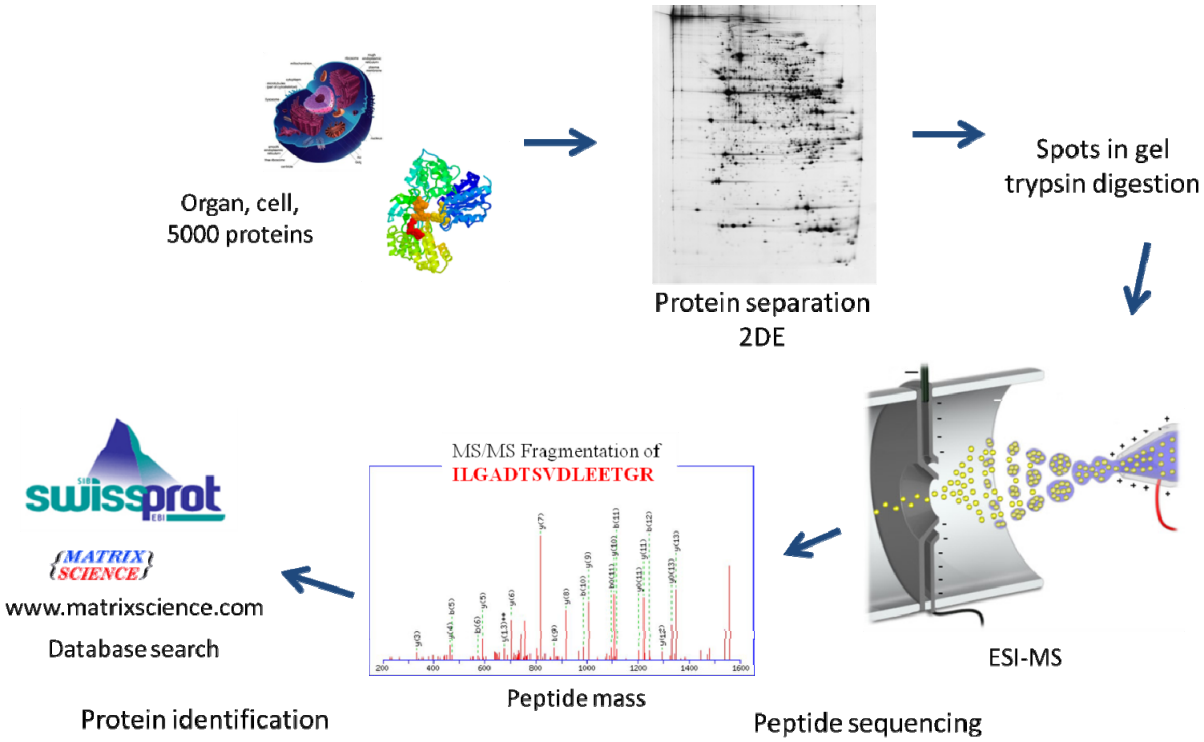

Figure 2: Proteomics study workflow. Proteins are extracted from a given system and separated on two dimensional electrophoresis (2DE). After gel analysis, spots of interest are excised from the gel and the proteins are digested. The peptide solution is applied to the electron spray ionization/tandem mass spectrometer (ESI/MS) for sequencing. Peptide sequence is matched to a database for identification of the protein.

While a part of the scientific community was concentrated on the study of the genome, also called genomics, the combination of IEF/PAGE based 2DE and MALDI or ESI/MS opened the era of Proteomics. The study of the protein has an immense advantage on genomics, because proteins are the biological active molecules in the cells. Moreover, 2DE/MS can distinguish between the different post-translational forms of the proteins, which are, in most of the cases, essential for their biological activities, localization and functions. In addition, the non linear correlation between gene expression and protein abundance has been proven as consequences of mRNA stability and denaturation,[139] alternate splicing, and protein processing[140] and denaturation.[141] This might make proteomics much more biologically relevant than genomics.

Proteins work as complex and sensitive networks within and between the cells. Therefore the genetic manipulation of one single gene (overexpression or inactivation) brings about a change in a wide proportion of the proteome. Proteomics is therefore a method of choice to study the consequences of a genetic manipulation in a hypothesis free approach.

1.8 Aim of the study

In spite of the acknowledged role of ET-1 as a strong vasoconstrictor, ET-1 overexpressing mice remain normotensive. Evidences showed that the NO system, the natural functional ET-1 antagonist, was activated in ET-1 mice. This led to the hypothesis that NO participated in the maintaining of normal blood pressure in ET+/+ mice. Prof. Hocher and Prof. Theuring decided therefore to crossbreed ET+/+ mice with eNOS-/- mice. This should have disrupted the presumed compensatory effects from the NO system in ET+/+ mice. Thus, this approach was thought to mimic the imbalance between NO and ET-1 actions observed in many cardiovascular diseases and therefore provide an important *in vivo* model to study the pathophysiological consequences of a disrupted ET-1/NO ratio. K. Relle showed that, at the age of nine months, both eNOS-/- and ET+/+eNOS-/- mice develop elevated blood pressure compared to WT and ET+/+ mice. However, heart catheterization experiment performed in cooperation with Bayer Schering Pharma, revealed that eNOS-/- mice, but not ET+/+eNOS-/-, developed diastolic dysfunctions, characterized by elevated end diastolic pressure and time of left ventricular relaxation. The crossbred animals may have established mechanisms to compensate lack of eNOS. Transgenic overexpression of ET-1 seems therefore to be beneficial for cardiac functions on an eNOS-/- background.

The aim of this study was to characterize and analyze the morphological and molecular changes taking place in the groups resulting from the crossbreeding, i.e. WT, ET+/+, eNOS-/-and ET+/+eNOS-/- mice, in order to understand the molecular and cellular mechanisms leading to the functional differences between the groups.

The first goal was to determine the expression pattern of components of the ET system in cardiac tissue at the mRNA level, by employing *in situ* hybridization and quantitative Real Time-PCR (qRT-PCR), as well as at the protein level by using Western Blot (WB). Secondly, cardiac myocyte and arteriole morphology as well as the expression level of cardiac extracellular matrix

(ECM) proteins have been analyzed using standard histological methods and immunohistochemistry.

The ultimate goal of this study was to define, in a hypothesis free approach, the changes in the cardiac proteome pattern between the different genotypes. To do so, the state-of-the-art 2DE coupled to ESI/MS technique was applied. Alterations of cardiac functions have been observed in eNOS-/- mice, but not ET+/+eNOS-/-, at the age of nine months. Because the hypothesis was that this was the cause of compensations happening over time due to the transgenic overexpression of ET-1 and in order to elucidate the early events, young animals (three months old) were analyzed. In this way, this study aimed at revealing which proteins are driving the pathological processes, depicting the causes and not the consequences.

2 Material and methods

2.1 Mice

Human ET-1 transgenic mice were generated by microinjection of linear human ET-1 genomic DNA fragments into one-cell embryos obtained from hormone-primed NMRI females mated the night before injection with NMRI males.[80] After microinjection, viable eggs were transferred to the oviducts of pseudopregnant NMRI mice. After birth, genotype was confirmed by PCR of genomic DNA using standard techniques. eNOS-/- mice were a gift from Prof. David Rodman and originally generated by homologous recombination by Huang et al. Inactivation of the eNOS gene was achieved through the replacement of the exons of the eNOS gene coding for the NADPH ribose and adenine binding sites by a neomycine cassette in C57BL/6 mice.[92] Female eNOS-/- mice and male homozygous ET-1 transgenic mice were used for breeding.[114] The four genotypes (ET+/+, eNOS-/-, ET+/+eNOS-/- mice and their wild-type (WT) littermates) were further bred to produce inbred strains of mice with mixed genetic background NMRI/ C57/BL6. Mice were kept under controlled environmental conditions with respect to temperature (20°C), humidity (64%), and a 12h night-day light cycle. Mice were fed on a standard breeding rodent diet and received water *ad libitum*. Study groups were composed as follows: WT, ET transgenic mice (ET+/+), eNOS knock-out mice (eNOS-/-), and crossbred mice (ET+/+eNOS-/-) (male and female). Two subsets of each group were killed by cervical dislocation at the age of three and nine months; hearts and aortas were harvested for further studies.

2.2 Chemicals

product	Cat #	supplier
3,3` -Diamino benzidine	SK-4100	Vector
Acetanhydrid	CP28	Carl-Roth
Acetic acid	3738	Carl-Roth
Aceton	8002	J.T. Baker
Acrylamid	10674	Serva
Agarose low melt	6351	Carl-Roth
Ampholyte 2-4	42902	Serva
Ampholyte pH 2-11	42900	Serva
Ampholyte pH 3.5-10	A5274	Sigma-Aldrich
Ampholyte pH 4-7	42948	Serva
Ampholyte pH 5-8	42949	Serva
Ampholyte pH 6-9	42913	Serva
APS	A3678	Sigma-Aldrich
BCIP	B6274	Sigma-Aldrich
Benzamidin	12072	fluka
Bisacrylamid	29195	serva
Blocking reagent	1096-176	Boehringer
BSA	8076	Carl-Roth
Coumaric acid	C9008	Sigma-Aldrich
Cybergreen	4312704	Applied Biosystems
Denhardts	750018	Invitrogen
DMSO	D8418	Sigma-Aldrich
DTT	6908	Carl-Roth
EDTA	8043	Carl-Roth
Ethanol	8006	J.T. Baker
Ethidium bromide	7870	Carl-Roth
Ethylendiamine	80094 72500	Merck
Ficoll	F2637	Sigma-Aldrich
Formaldehyde	7398	Carl-Roth

Product	Cat #	supplier
Low melt agarose	6351	Carl-Roth
Luminol	9253	Fluka
Maleinacid	3538	Carl-Roth
Methanol	10600 92500	Merck
$MgCl_2$	1005482	Quigen
Milk powder	T145	Carl-Roth
Na_2HPO_4 x $2H_2O$	4984	Carl-Roth
Na-citrat x $2H_2O$	3580	Carl-Roth
NaCl	9265	Carl-Roth
NBT	4421	Carl-Roth
Normal serum	S-1000	Vector
Page Ruler	SM0671	Fermentas
Paraffin Typ 6	8336	Richard-Allan-Scienfitic
Paraffin Typ 9	8337	Richard-Allan-Scienfitic
Paraformaldehyde	335	Carl-Roth
p-Coumarinacid	28200	Fluka
Phosphoric acid	6366	Carl-Roth
Picric acid solution	80456	Fluka
Picro-Fuchsine, van Gieson	2E-50	Waldeck GmbH
Piperazin diacrylamid	D1538	Sigma-Aldrich
Proteinase K	AM2542	Invitrogen
PVP	4606	Carl-Roth
RNAse A	R6513	Sigma-Aldrich
rRNAsin	N2511	Promega
SDS,	2326	Carl-Roth
Sephadex G100	G10050	Sigma-Aldrich
Silver nitrate	7908	Carl-Roth
Sodium acetate 3xH2O	6779	Carl-Roth
Sodium hydrogen carbonate	6885	Carl-Roth

Product	Cat #	Supplier
Formamid	A2156	Applichem
Glutaraldehyde	3778	Carl-Roth
Glycerin	3783	Carl-Roth
Glycine	3908	Carl-Roth
Hematoxylin solution	X906	Carl-Roth
Heringssperma	S-3126	Sigma-Aldrich
Hydrogen peroxide	T1377	Merck
IPTG	2316	Carl-Roth
Isopropanol	8067	J.T. Baker
KCl	HN27	Carl-Roth
KH_2PO_4	1 .12034	Merck
LB Agar	3002-222	MP Biomedicals
LB medium	3002-022	MP Biomedicals
Leupeptine	9783	Sigma-Aldrich
LiCl	L-9650	Sigma-Aldrich

Product	Cat #	Supplier
Sodium thiosulfate 5xH2O	P034	Carl-Roth
TEMED	2367	Carl-Roth
Thimerosal	6389	Carl-Roth
Thiourea	9531	Carl-Roth
Tissue Tek OCT	E62550-01	Science Services
Triethanolamine	4804	Sigma-Aldrich
Tris	4855	Carl-Roth
Tris-HCl	9090	Carl-Roth
Trizol	15596-026	Invitrogen
tRNA	10109 517001	Roche
Tween-20	9127	Carl-Roth
Urea	3841	Carl-Roth
Urea (for IEF)	161-0731	Biorad
Xgal	B9146	Sigma-Aldrich
Xylol	8080	J.T. Baker

2.3 Equipment

Equipment	Model	Supplier
Balance	LP605	Sartorius
Balance	AE240	Mettler
Centrifuge	Mikro22R	Hettich
Cryostat	Jung Frigocut 2800E	Leica
Cuvette spectrophotometer	DU 530	Beckmann
Developper	Curix 60	Agfa
Digital camera	PL-A662	Pixelink
Electrophoresis chamber	V10-WDCD	Wilten instrumenten
Electrophoresis chamber	Desaphor VA 300	Desaga
Electrospray	PicoTip emitter	New Objective
Incubator	UV5	Biometra
Incubator	Unitron	Infors AG

Equipment	Model	Supplier
Magnetic stirrer with heating	RCT basic	Ika Labortechnik
Mass spectrometer	Esquire 3000 plus ion trap MS	Bruker
Microplate spectrophotometer	BenchmarkPlus	BioRad
microscope	DMLB2	Leica
Microtome	RM2025	Leica
Mixer	Vortex-Genie2	Scientific industries
Mixer	KS-15	Edmund Bühler
Mixer	RM5 CE 348	Karl Hecht
Nano liquid chromatography system	Agilent 1100	Agilent
Paraffin Embedding Center	Microm EC-350	Thermo Scienfitic
pH meter	pHM92	Radiometer Copenhagen
Power supply	EV233	Consort
Power supply	Power Pac 200	BioRad
Real time thermocycler	Mx3000P	Stratagene
Scanner	FB2080	Umax
Scanner	Canonscan 5000F	Canon
Thermocycler	T3 thermocycler	Biometra
Thermomixer	5436	Eppendorf
Tissue processor	Shandon Citadel 1000	Thermo Scientific
Water bad	Typ 16800	Medax

2.4 Software

Software	Developer
ImageJ 1.37V	National Institutes of Health
AlphaEaseFC 3.1.2	Alpha Innotech Corporation
Microplate Manager 5.2	BioRad
SPSS 17.0	SPSS Inc.
Photoshop CS3	Adobe
Excel 2007	Microsoft
Word 2007	Microsoft
Reference Manager 11	Thomson ResearchSoft.
Ingenuity Pathways Analysis	Ingenuity
Prism 5	GraphPad Software Ltd.
Primer3	Whitehead Institute, Howard Hughes Medical Institute
CanoScan Toolbox 4.1.	Canon

2.5 Quantitative Real Time PCR

2.5.1 RNA extraction

Total RNA was extracted from snap-frozen aortic and cardiac tissue using Trizol reagent (Invitrogen 15596-026, Carlsbad, CA). Tissue was pulverized under liquid nitrogen. Powder was incubated with 1mL Trizol and vortexed 10min at RT. 200µL chloroform were added and the probes were mixed 15s. After a 3min long incubation at RT, the probes were centrifuged at 4°C, 12000rpm 15min. The water phase was taken in a new tube and the RNA was precipitated by adding of 500µL isopropanol for 10min at RT. The probes were centrifuged again at 12000rpm, 4°C for 10min The supernatant was discarded and the pellet was washed in 75% Ethanol, 25% ddH_2O and centrifuged finally at 7500rpm, 4°C for 5min The pellets were air dried and resuspended in ddH_2O. DNase treatment was performed using the Nucleospin RNA II extraction kit from Mecherey & Nagel (cat. no. 740955). The RNA concentration was determined by absorbance at 260nm.

2.5.2 qRT-PCR

mRNA was reverse-transcribed to cDNA using the Superscript III reverse transcriptase (18080-044 Invitrogen) according to the manufacturer's protocol (500ng RNA were mixed with random poly-A primers).

The primers specific for mouse and human ET-1, and binding to both mouse and human ET-1 as well as the primers for hypoxanthine guanine phosphoribosyl transferase (HPRT) and 18S ribosomal RNA (18S) were designed with the online available computer program Primer3,[142] using as template the sequence from the Ensembl Database[143] (human ET-1 Ensembl Transcript ID ENST00000075232; murine ET-1 Ensembl Transcript ID ENSMUST00000021796; murine HPRT Ensembl Transcript ID ENSMUST00000026723, murine 18S Ensembl Transcript ID ENSMUST00000122786). The specificity of the primers was verified by sequence analysis using the BLAST program from NCBI.[144] The other primers used were derived from the literature (Table 1). A total of 5µL of cDNA 10µg/ml (50ng) was used as template for the amplification. A total of 0.5µL of each specific primer (5pmol), 6.5µL of water, and 12.5µL of SYBR Green PCR Master Mix (4309155; Applied Biosystems, Foster City, CA) were added. All spots were

performed in triplicate. The PCR was performed on an Mx3000P thermal cycler (Stratagene, La Jolla, CA). Reaction conditions were 95°C for 10min followed by 40 cycles of the amplification steps (95°C for 15s, 60°C for 30s, and 72°C for 45s). The relative gene expression (sQ) of ETAR, ETBR, murine ET-1, endothelin-converting enzyme (ECE), eNOS, and iNOS were obtained for each genotype in comparison to WT. The gene expression of the human ET in the crossbred mice was compared with its expression in human ET-1 transgenic animals.

Gene	Primer Sequence 5' to 3'	Amplicon Length (bp)	Spanned Intron	Reference
ETAR	+GCTGGTTCCCTCTTCACTTAAGC	129	6	[145]
	-TCATGGTTGCCAGGTTAATGC			
ETBR	+TGTGCTCTAAGTATTGACAGATATCGAG	240	2,3	[145]
	-GGCTGTCTTGTAAAACTGCATGA			
mET-1	+GGAAACTACGAAGGTTGGAGGC	235	4	
	-CTGTAGAAGCCACACAGATGGTCT			
hET-1	+AAGTTCAGAGGAACACCTAAGACAAAC	170	4,5	
	-GAGGCTATGGCTTCAGACAGG			
ET-1	+CAAGGAGCTCCAGAAACAGC	168	1,2	
	-GATGTCCAGGTGGCAGAAGTA			
iNOS	+CAGCTGGGCTGTACAAACCTT	95	17,18	[146]
	-CATTGGAAGTGAAGCGTTTCG			
eNOS	+CCTTCCGCTACCAGCCAGA	105	10,11,12	[147]
	-CAGAGATCTTCACTGCATTGGCTA			
ECE	+ATGACGCCGCCCATGGTGAAC	128		[148]
	-TGGTTGGGCTAAGACATAAC			
HPRT	+CAGGCCAGACTTTGTTGGAT	147	7,8,9	
	-TTGCGCTCATCTTAGGCTTT			
18S	+GTAACCCGTTGAACCCCATT	151		
	-CCATCCAATCGGTAGTAGCG			

Table 1: List of primer used for qRT-PCR.

2.5.3 Computations

For the study of aorta, the relative quantity (Q) was normalized to the expression of HPRT using the following formula:

$$nQ = \{2^{[\text{minCt(gene of interest)} - \text{Ct(gene of interest)}]}\}/\{2^{[\text{minCt(HPRT)} - \text{Ct(HPRT)}]}\}$$

The normalized quantity (nQ) was then normalized to the expression in WT mice using the formula:

$$sQ = nQ_{test}/mQ_{WT}$$

where $Ct_{(gene\ of\ interest)}$ and $Ct_{(HPRT)}$ represent the threshold cycle for the gene of interest and for HPRT, respectively; $minCt_{(gene\ of\ interest)}$ and $minCt_{(HPRT)}$ are the lower Ct values for the gene of interest and HPRT, respectively; nQ_{test} is the normalized quantity in a given genotype, and mQ_{WT} is the mean of the nQ in WT mice.

For the cardiac tissue, the relative intensity (Q) of mET-1, hET-1 and ET-1, normalized to the expression of 18S RNA, were obtained using the delta Ct (ΔCt) method:

$$Q = 2^{[\Delta Ct\ (gene\ of\ interest) - average\ \Delta Ct\ (gene\ of\ interest\ in\ WT)]}$$

$$\Delta Ct_{(gene\ of\ interest)} = Ct_{(gene\ of\ interest)} - Ct_{(18S)}$$

where $Ct_{(gene\ of\ interest)}$ and $Ct_{(18S)}$ represent the threshold cycle for the gene of interest and for 18S RNA, respectively.
The relative intensity of hET-1 in crossbred animals was compared to its intensity in the ET+/+ group.

2.6 Immunohistochemistry

For immunohistochemical staining, 6µm thick frozen sections of hearts from nine months old animals were used. The sections were cut at -25°C on a cryostat (Jung Frigocut 2800E, Leica), placed on glass slides (Super Frost Plus, 03-0060, R.Langenbrinck) and stored at -80°C. The sections were then treated as shown in the following table:

step	solution	incubation time	temperature	composition
1	acetone	7min	RT	acetone
2	PBS	5min	RT	137mM NaCl, 2.7mM KCl, 8.1mM Na_2HPO_4 x $2H_2O$, 1.5mM KH_2PO_4, pH 7,4
3	normal serum/peroxide	3min	RT	normal serum (Vector S-1000) 1drop in 3mL PBS/ 0,3% H_2O_2
4	PBS	5min	RT	
5	Avidin-Blocking solution	45min	RT	Avidin/Biotin– Blocking Kit (Vector SP-2001) 1drop in 5ml normal serum
6	Primary antibody	1h	RT	primary antibody diluted in biotin blocking solution (Avidin/Biotin– Blocking Kit, SP-2001, Vector)
7	PBS	5min	RT	
8	PBS	5min	RT	
9	PBS	5min	RT	
10	Secondary antibody	30min	RT	ABC Kit elite Vectastain Rabbit Ig (PK6101, Vector)
11	PBS	5min	RT	
12	PBS	5min	RT	
13	PBS	5min	RT	
14	avidin biotin ABC	30min	RT	Avidin/biotin mix (1 drop avidin, 1drop biotin in 5mL PBS/Tween 1%) (ABC Kit elite Vectastain Rabbit Ig, PK6101, Vector), 30min on ice before use
15	PBS	5min	RT	
16	PBS	5min	RT	
17	PBS	5min	RT	
18	DAB	1min	RT	3,3` -Diaminobenzidine (DAB-Substrat-Kit, SK-4100, Vector)
19	stop solution	5min	RT	water

Table 2: Protocol for immunohistochemistry.

For detection of matrix proteins, rabbit anti-MMP2 (Chemicon AB19167), anti-MMP9 (Chemicon AB19016), anti-Col I (Chemicon AB765P) and anti-Col III (Calbiochem 234189) primary antibodies were diluted 1/200 in an avidin/biotin normal serum blocking solution. Binding of the antibodies were revealed using the ABC Kit elite Vectastain Rabbit Ig (Vector PK6101). The same procedure omitting primary antibody was used as negative control. Slices were photographed with a digital camera plugged to the microscope with 200x magnificence. The relative intensity of the signal was measured on 8bit pictures using the threshold function of the software ImageJ

as percentage of tissue area. The images from the negative controls were analyzed the same way. The signal measured on the negative controls was considered as background and therefore subtracted.

2.7 In situ Hybridization

2.7.1 ETAR and ETBR cloning

For the production of RNA probes needed for *in situ* hybridization, a part of the ETAR and ETBR genes have been cloned in an expression vector. Primers for the cloning of ETAR and ETBR were designed using Primer3 using as template the sequences from the Ensembl Database[143] (ETAR: Ensembl Transcript ENSMUST00000034029, ETBR: Ensembl Transcript ENSMUST00000022718). The forward and reverse primers were flanked with the restriction sites of Bsu15I and BcuI, respectively, and the GAT sequence as spacer (table 3).

Gene	Primer Sequence 5' to 3'	Amplicon Length (bp)
ETAR	+gatatcgatCAACCATTACGCCACAGATG	1224
	-gatactagtCAGTGCTATCTCGCCCAAGT	
ETBR	+gatatcgatATGACGCCACCCACTAAGAC	1218
	-gatactagtAGTGAGATTCGGCGAGTGTT	

Table 3. Primers used for the cloning of ETAR and ETBR

Amplification by PCR of the correspondent sequence was performed using as template cDNA from mouse. The PCR was performed with 0.02 U/µL Phusion DNA Polymerase (F-530, Finnzymes) in Phusion HF Puffer added of 200µM of each dNTP, 3% (v/v) DMSO and 0.5µM of each primer, using the following protocol: initial denaturation at 98°C, 30s; 30 cycles: denaturation at 98°C, 20s; annealing at 63°C, 30s; elongation at 72°C, 30s, final elongation at 72°C, 10min. The DNA fragment was separated on a 1% low melt agarose/0.1% ethidium bromide gel and the size of the amplicon was checked. The band was excised from the gel and the DNA was extracted using the gel extraction kit QIAquick (28704, Qiagen). The DNA fragments as well as the pBluescript KS (-) expression vector (#21220, Stratagene) were cut using 20u Bsu15I (ER0141, fermentas) and 20u BcuI (ER1251, fermentas) for 2h at 37°C followed by heat inactivation at 65°C for 20min. 100ng of the fragments were ligated in the presence of

pBluescript vector using 2u of T4 ligase (EL0015, fermentas) in appropriate buffer overnight at 16°C. The correct insertion of the fragment was verified by separation of the plasmid obtained after digestion with EcoRV (ER0301, fermentas) on agarose gel.

Chemically competent Oneshot Top10 *E. coli* cells (C4040, Invitrogen) were transformed as recommended by the provider with 2µL vector solution, incubated 30min on ice, 30 sec. at 42°C and put again on ice. The cells were then supplemented with 250µL LB medium and incubated 1h at 37°C on a shaker and finally plated on LB Agar/Xgal 20µg.mL^{-1}/IPTG 0.1mM. Positive colonies were picked, cultivated overnight in 5mL LB medium. The plasmid was extracted and an aliquot of the culture was stored at -80°C in glycerol.

2.7.2 RNA probes production

Plasmid extraction was done using a plasmid extraction kit (NucleoSpin Plasmid 740588, Macherey-Nagel). The plasmid was linearized with 0,5 u.µL^{-1} of either BcuI or Bsu15I restriction enzyme in corresponding buffer for 2h at 37°C, for T3 or T7 RNA polymerase, respectively. DNA was then precipitated and washed with SureClean (BIO-37047, Bioline) and resuspended in water. The labeled RNA probe was produced using a DIG labeling kit (11 175 033 910, Roche). 1µg DNA was incubated with 1x DIG labeling dNTP mix, 10mM DTT, 20u.µL^{-1} RNAse inhibitor (rRNAsin, Promega) and 1u.µL^{-1} T3 or T7 RNA Polymerase in appropriated buffer for 2h at 37°C. DNA was then digested with 1µL DNAse I (18047-019, Invitrogen) 15min at 37°C. RNA was washed with EtOH70%/LiCl 0.1M and incubated 30min at -80°C. The probe was resuspended in water and its concentration was measured by spectrophotometry.

2.7.3 Staining protocol

The *in situ* hybridization was performed on 7µm thin heart paraffin slices. The different steps are listed in the following table. Steps 1 to 27 were done by incubating the glass slide in a cuvette. The following steps were performed by pipetting 600µL on the slice. The RNA probes were denaturated 5min at 85°C before diluting at 0,5 - 1,5 µg.ml^{-1} in hybridization buffer. The steps 29 and 33-38 were done in a chamber humidified with 2x SSC solution. Negative controls were run in every experiment by omitting the RNA probe. At the end, the slices were mounted with Hydromount (HS-106, National diagnostics).

	step	solution	incubation time	temperature	composition
Day 1	1	xylol	10min	RT	xylol 100%
	2	xylol	10min	RT	
	3	xylol	10min	RT	
	4	EtOH 95%	1min	RT	EtOH 95%
	5	EtOH 90%	1min	RT	EtOH 90%
	6	EtOH 80%	1min	RT	EtOH 80%
	7	EtOH 70%	1min	RT	EtOH 70%
	8	EtOH 50%	1min	RT	EtOH 50%
	9	EtOH 30%	1min	RT	EtOH 30%
	10	PBS	5min	RT	137 mM NaCl, 2.7 mM KCl, 8.1 mM Na_2HPO_4 x $2H_2O$, 1.5 mM KH_2PO_4, pH 7,4
	11	PBS	5min	RT	
	12	PBS 4% PFA	30min	RT	PBS 4% Paraformaldhyde
	13	PBS	5min	RT	
	14	PBS	5min	RT	
	15	Proteinase K	10min	RT	20 mM Tris-HCl, 1 mM EDTA, 10 µg/ml Proteinase K (Sigma), pH 7,2
	16	PBS	5min	RT	
	17	PBS 4% PFA	30min	RT	
	18	PBS	5min	RT	
	19	PBS	5min	RT	
	20	2x SSC	2min	RT	0.3 M NaCl, 30mM Na-citrat x $2H_2O$, pH 7,0
	21	2x SSC	2min	RT	
	22	Tris-Glycin	30min	RT	10 mM Tris Base, 100 mM Glycin, pH 7,0
	23	PBS	5min	RT	
	24	PBS	5min	RT	
	25	Acetylation buffer	10min	RT	1,2% (w/v) Triethanolamin, 0,25% (v/v) Acetanhydrid
	26	PBS	5min	RT	
	27	PBS	5min	RT	
	28	Hybridisation buffer	4h	RT	50% (v/v) Formamid, 5x SSC, 5x Denhardts (50x Denhardts: 1% (w/v) BSA, 1% (w/v) Ficoll, 1% (w/v) PVP), 200 µg/ml tRNA (*S.cerevisiae*, Sigma), 100 µg/ml Heringssperma (Sigma)
	29	Probe in hybridisation buffer	16h	70°C	

	step	solution	incubation time	temperature	composition
Day 2	30	5x SSC	20min	RT	0.75 M NaCl, 75mM Na-citrat x $2H_2O$, pH 7,0
	31	5x SSC	20min	RT	
	32	5x SSC	20min	RT	
	33	Formamide solution	40min	60°C	20% (v/v) Formamid, 0,5x SSC
	34	Formamide solution	1,5h	37°C	
	35	NTE-buffer	15min	37°C	0,5 M NaCl, 0,5 mM EDTA, 10 mM Tris-HCl pH 7,0
	36	RNAse A	30min	37°C	40 µg/ml RNAse A (Sigma) in NTE-buffer
	37	NTE-buffer	15min	37°C	
	38	Formamide solution	40min	60°C	
	39	2x SSC	15min	RT	
	40	2x SSC	15min	RT	
	41	buffer 1	5min	RT	0,1 M Maleinsäure, 0,15 M NaCl, pH 7,5
	42	buffer 1	5min	RT	
	43	Blocking solution	1h	RT	1% (w/v) Blocking reagent (Boehringer) und 1% (v/v) Tween20 in buffer 1
	44	DIG-AP	1h	RT	anti-DIG Ab 1/400 in blocking solution
	45	buffer 1	30min	RT	
	46	buffer 1	30min	RT	
	47	buffer 2	5min	RT	100 mM NaCl, 50 mM $MgCl_2$, 100 mM Tris-HCl pH 9,5, 0,1% (v/v) Tween20
	48	buffer 3	3h	RT	0,55 mM NBT, 0,4 mM BCIP in buffer 2
	49	TE-buffer	10min	RT	10 mM Tris, 1 mM EDTA, pH 8,0
	50	TE-buffer	10min	RT	
	51	PBS	30min	RT	
	52	water	5min	RT	

Table 4: Protocol for *in situ* hybridization.

2.7.4 Relative quantification

Slices were photographed under a light microscope (magnification x200) and saved as jpeg pictures at 150 dpi, RBG 24 bits. Consecutive pictures were taken to cover the whole left cardiac ventricle. Using ImageJ, the pictures were converted into 8 bit gray scale pictures. The signal was measured using the threshold function defined manually on a randomly chosen set of picture. Once the threshold segregating signal from background was chosen, all pictures were analyzed in the same way. A second threshold was used to measure the tissue area from each

picture. The final signal was defined as a signal percentage from tissue area. Negative control pictures were analyzed using the same thresholds.

2.8 Histology

2.8.1 Staining

Histological staining was performed on paraffin sections of hearts (3µm thin for Sirius red and Elastica-van Giesson staining and 1µm thin for Hematoxylin-Eosin staining). Sirius red stains collagens in red. Elastica- van Giesson staining is a combination of resorcin-fuchsin, which stains connective tissue in violet, picrofuchsin, which stains cytoplasm in yellow-red and hematoxylin, which stains cell nuclei in grey-blue. Eosin stains cytoplasm in blue-pink. Each staining was preceded by rehydration and followed by a dehydration of the slices. The different steps are listed in the following table.

step	solution	incubation time	temperature	composition
Rehydration				
1	xylol	5min	RT	
2	xylol	5min	RT	
3	EtOH 100%	2min	RT	EtOH 100%
4	EtOH 95%	2min	RT	EtOH 95%
5	EtOH 80%	2min	RT	EtOH 80%
6	EtOH 70%	2min	RT	EtOH 70%
7	water	30s		
Sirius Red staining				
8	Sirius Rot solution	1h	RT	Sirius Red 0,1% in saturated picrin acid solution
9	wash solution	30s	RT	0,01M HCl in Ethanol

Step	solution	incubation time	temperature	composition
Elastica van Gieson staining				
8	Resorcin-Fuchsin solution	10min	RT	
9		3min	RT	water
10	wash solution	30s	RT	0,01M HCl in ethanol
11		7min	RT	water
12	wash solution	30s	RT	0,01M HCl in ethanol
13		30s	RT	water
14	EtOH 70%	1min	RT	EtOH 70%
15	EtOH 80%	2min	RT	EtOH 80%
16	Hematoxylin solution	3min	RT	
17		3min	RT	water
18	wash solution	30s	RT	0,01M HCl in ethanol
19		7min	RT	water
20	van Gieson solution	30s	RT	
HE staining				
8	Hematoxylin solution	4min		
9		7min		water
10	wash solution	30s		0,01M HCl in ethanol
11		7min		water
12		30s		distilled water
13	eosin	4min		
14		30s		distilled water
Dehydration				
1	EtOH 70%	30s		EtOH 70%
2	EtOH 80%	30s		EtOH 80%
3	EtOH 95%	2min		EtOH 95%
4	EtOH 100%	2min		EtOH 100%
5	xylol	2min		xylol 100%

Table 5: Histology: Protocols for Sirius Red, Elastica van Gieson and HE staining of paraffin-embedded tissue slices.

2.8.2 Measurements

Interstitial fibrosis of the cardiac left ventricular wall and the septum was quantified using computer-aided histomorphometry as follows: After Sirius Red staining, about 30 randomly chosen pictures from every thin layer-section were taken under light microscope using a digital camera. The Sirius Red-positive area of every picture was then quantified using image

processing software ImageJ with a threshold derived from a subset of randomly chosen pictures. The Sirius Red-positive area was expressed as a percentage of total tissue area. Perivascular fibrosis of the left ventricular wall and the septum was quantified after Sirius Red staining using a relative quantitative scoring system: Two independent investigators, who were blinded to the study groups, graded the fibrosis around cardiac arteries using 5 different grades based on the relation between media diameter and the diameter of the surrounding collagen ring of the adventitia (Grade 1 = diameter collagen-ring-wall < 25% in comparison to diameter of media-wall; grade 2 = 25-50%; grade 3 = 50-75%; grade 4 = 75-100%; grade 5 = >100%). Perivascular fibrosis of the heart was then expressed as the mean value of the obtained grades.

For the assessment of Media-to-Lumen ratio, Elastica-van Giesson-stained sections of the left ventricular wall and the septum tissue sections were used. Virtually all visible small arteries were photographed under light microscope (magnification x400) using a digital camera. The area of the media and the lumen were then quantified using the freehand selection tool of the ImageJ software. Media-to-lumen ratio was calculated as quotient of media and lumen area.

For the measurement of cardiomyocyte diameter, HE-stained tissue sections were used. For each animal, thirty randomly chosen pictures of longitudinally cut myocytes with a visible and non-conspicuous cell-nucleus from the left ventricular wall and the septum were photographed under light microscope (magnification x600). The diameter was measured using the straight line selection tool of the ImageJ software.

2.9 Proteomics

2.9.1 Protein preparation

Protein preparation was done according to Aksu *et al.*,[149] with minor changes. Snap-frozen hearts were pulverized with mortar and pestle under liquid nitrogen. Six to nine individual hearts for each group were processed. The powder was dissolved in 600µL lysis buffer (Tris/HCl 25mM, KCl 50mM, EDTA 3mM, Benzamidin 2.9mM, Leupeptin, 2.1µM, Urea 7M, Thiourea 2M, Ampholyte 2-4 2%, DTT 70mM) for 100mg tissue. The samples were vortexed and incubated for 10min at room temperature and then centrifuged for 45min at 13000rpm, 20°C. The supernatants were collected, aliquoted and stored at -20°C. The protein concentration was

measured using the Bradford assay Roti-Nanoquant (Roth, K880.1) in triplicates in 96 well microtiter plates, using a standard curve of bovine serum albumin of known concentrations.

2.9.2 2DE: IEF and SDS-PAGE

The protocol used here was based on the work of Zimny-Arndt *et al.*.[150] The isoelectric gels consisted of a 20cm long separation gel (Acrylamide 3.5%, piperazin diacrylamide 0.3%, ampholyte pH 3.5-10 0.25%, ampholyte pH 2-11 0.25%, ampholyte pH 4-7 1.75%, ampholyte pH 5-8 0.5%, ampholyte pH 6-9 0.25%, urea 9M, glycerin 5%, TEMED 0.06%, APS 0.02%) and a 1cm long cap gel (idem with acrylamide 12%, piperazin diacrylamide 0.13%). The gels were loaded in 25cm long glass tubes with an inner diameter of 1mm. The polymerization lasted 3 days at 21°C. On the top of the gel, 3µL sephadex solution were given (Sephadex solution: 2g Sephadex G200 were incubated in 50mL water 5h at 90°C, supernatant was removed and Sephadex was incubated in 100mL Glycerin 25% 1h at RT, supernatant was removed and Sephadex was incubated in 100mL Glycerin 25% 1h at RT again, supernatant was finally again removed. 120µL aliquots were stored at -20°C; 108mg urea was freshly added to one aliquot, 10µL DDT 1.4M and 10µL ampholyte 2-11). Protein solution (100µg) was added and finally 5µL of sample protection solution were added (Urea 5M, glycerin 0.54M, ampholyte 2-4 5%). The upper part of the tube was filled with anode buffer. The isoelectric focusing was performed at 20°C under following conditions: 100V 1h, 200V 1h, 400V 16.5h, 600V 1h, 1000V 30min, 1500V 10min, 2000V 5min. Anode buffer was 3M urea, 5% phosphoric acid. Cathode buffer was 9M urea, 5% ethylendiamine, 5% glycerin. After focusing, geld were removed from the tube and equilibrated 10min in Tris 125mM, glycerin 4.3M, SDS 0,1M, DTT 65mM and finally stored at -20°C.

The second dimension gels contained acrylamide 2.25M, bisacrylamide 13.8mM, Tris 0.3M, TrisHCL 95mM, TEMED 2.75mM, SDS 3.7mM, APS 3.5mM. The SDS-PAGE gels were polymerized half an hour at RT, 1mL of SDS protection solution (Tris 1.15M, Tris/HCl 192mM, SDS 3,47mM) was added on top of the gel and they were further polymerized overnight at 8°C. The SDS protection solution was removed and the IEF gel was positioned on the SDS gel, bubble free. A low melt agarose solution (Agarose low melt 1%, Tris 0.1M, SDS 3,47mM, H3PO4 75mM) was dissolved at 70°C, cooled at 38°C and applied on the gels and polymerized 15min at RT. The electrophoresis buffer was Tris 25mM, Glycin 192mM, SDS 0.1%. Electrophoresis lasted 15min

at 65mA followed by 6h at 160mA in a chamber cooled at 15°C. The gels were then fixed overnight in ethanol 50%, acetic acid 20%.

For two dimensional western blots (2D-WB), small IEF gels were used (7.5cm) and 50µg of proteins were loaded. Compared to long gels, sephadex and protection solution were reduced to 2µL and the focusing conditions were reduced to 100V 75min, 200V 75min, 400V 75min, 600V 75min, 800V 15min, 1000V 5min. The second dimension electrophoresis lasted 15min at 60V followed by 3h at 110V. All other parameters were similar to the one used for the large gels. The gels were then treated as for 1D Western Blot (see below).

2.9.3 Silver staining

Gels were silver stained by incubation in the following solutions: incubation solution for 2h (ethanol 30%, glutaraldehyde 0.5%, sodium acetate 0.5M, sodium thiosulfate 8.6mM), water for 3 times 20min, silver solution for 30min (silver nitrate 5.9mM, formaldehyde 0.0001%), water for 2 times 10s, development solution for 10min (sodium carbonate 235mM, sodium thiosulfate 52µM, formaldehyde 0.0001%), stop solution 1 for 30min (EDTA 0.05M, thimerosal 0.25mM) and finally stop solution 2 (EDTA 0.05M).

2.9.4 MS compatible silver staining

Preparative gels were stained with the MS compatible silver staining method developed by Nebrich *et al.*.[151] Spots were excised from these gels for identification. Wash solution (20% Ethanol) for 20min, incubation solution (0,02% sodium thiosulphate) for 1min, water two times 1min, silver solution (0.1% silver nitrate) for 30min, water for 30s, development solution 1 (2,5% sodium carbonate) for 1min, development solution 2 (2,5% sodium carbonate / 0,02% formaldehyde / 0,025% thimerosal) for up to 20min and finally stop solution (EDTA 0.05M) for 20min The gels were then stored in water.

2.9.5 Computer Analysis

One gel for each heart (6-9 hearts per group) was scanned on an Umax scanner coupled to Photoshop 7.0 as 8 bit pictures at 150dpi and compressed as tiff file. Computer-assisted analysis of the gels was performed with the software Proteomweaver version 3.0.9.9 (Definiens, Munich, Germany). Spot detection, matching of protein spots, background subtraction and normalization

were performed by the software. The spots were first matched within the groups. Then matching was done between the groups: each genotype versus WT, males and females separately. Thus, each of the three genotypes (ET+/+, eNOS-/- and ET+/+eNOS-/-) was compared to WT (three comparisons for males and three comparisons for females). The matched spots were taken into account for analysis. Manual spot matching and spot design (drawing, growing or shrinking, splitting or merging) has been performed for every gel afterwards to correct for lack of accuracy of the software. Spots with a difference in average intensity with a factor of at least 1.6 (up or down versus wild type), new spots or vanished spots and shifted spots (compared to wild type) were taken into account. Spots had to be present in at least 80% of the gels to be analyzed. Finally, difference in the spot intensity had to be statistically significant as computed by the software using a Student's t-test (significance set for $p<0.05$).

2.9.6 Nano Liquid Chromatography-Electrospray Ionization / tandem Mass Spectrometry (ESI/MS) and protein identification

Protein identification using ESI/MS was performed by the Proteome Factory (Proteome Factory AG, Berlin, Germany). The MS system consisted of an Agilent 1100 nanoLC system (Agilent, Boeblingen, Germany), PicoTip emitter (New Objective, Woburn, USA) and an Esquire 3000 plus ion trap MS (Bruker, Bremen, Germany). Protein spots were in-gel digested by 200ng trypsin per spot in 50mM Ammoniumbicarbonate, 10% acetonitrile (Promega, Mannheim, Germany) overnight and applied to ESI/MS ion trap after acidification. After trapping and desalting the peptides on enrichment column (Zorbax SB C18, 0.3x5mm, Agilent) using 1% acetonitrile/0.5% formic acid solution for 5min peptides were separated on Zorbax 300 SB C18, 75 µm x 150mm column (Agilent) using an acetonitrile/0.1% formic acid gradient from 5% to 40% acetonitrile within 40min. MS spectra were automatically taken by Esquire 3000 plus according to manufacturer's instrument settings for ESI/MS analyses. Proteins were identified using MS/MS ion search of Mascot search engine (Matrix Science, London, England) and the Swiss-Prot protein database (Swiss Institute of Bioinformatics, Geneva, Switzerland)[152] limited to the mus musculus species. Variable modifications in search parameters were set to phosphorylation (serine/threonine), oxidation (methionine), propionamide (cysteine), carbamidomethyl

(cysteine), sulphinic and sulphonic acid (cysteine). Ion charge in search parameters for ions from ESI/MS data acquisition were set to "1+, 2+ or 3+" according to the instrument's and method's common charge state distribution. Peptide mass tolerance and fragment mass tolerance were set to 0.1% and 0.5Da, respectively. Proteins with the highest score were considered to be properly identified.

2.9.7 Protein classification

The biological function of every identified protein was defined according to the online available evolutionary relationships classification system Panther (http://www.pantherdb.org).[153] Panther is a public database generated by computational algorithms and classifies proteins according to their functions, using published scientific experimental evidence and evolutionary relationships. The biological function of a protein is defined as its function in the context of a larger network of proteins that interact to accomplish a process at the level of the cell or organism.

2.10 1D Western Blotting

The protein solution, as prepared for proteomics, (25µg) was heated 1min at 95°C in presence of loading buffer (K929.1, Roth) before loading on an SDS-PAGE gel 10% acrylamide. Stacker gel (5% (v/v) acrylamide / bisacrylamide, 12,5% (v/v) stacker buffer (1M Tris pH 6,8), 0,1% (w/v) SDS, 0,1% (w/v) APS, 0,1% (v/v) TEMED); Separation gel (10% (v/v) acrylamide / bisacrylamide, 25% (v/v) buffer (1,5M Tris pH 8,8), 0,1% (w/v) SDS, 0,1% (w/v) APS, 0,04% (v/v) TEMED); Electrophoretic separation was done under following conditions: 20min 40V, 90min at 90V and 90min at 110 V at 4°C. Molecular weight was visualized by loading on every gel a marker (Page Ruler SM0671, fermentas). Hydrophobic polyvinylidene difluoride (PVDF) (Amersham Hybond-P, RPN303F, GE Healthcare) membrane was activated 1min in methanol and incubated as well as the transfer paper and the gel in transfer buffer (methanol 20%, glycine 175mM, 32mM Tris). The proteins were transferred onto the PVDF membrane overnight at 4°C under 5 V tension using semidry transferring equipment (TransBlot SD, BioRad). The unspecific sites were blocked one hour with Tris buffered saline (TBS) (20mM Tris, 140mM NaCl, pH 7,6), Tween-20 0.1%, Milk 5%. The primary antibodies anti-ETAR (sc33536, Santacruz), ETBR (sc33538, Santacruz), PRDX6

(ab59543, Abcam), PRDX6SO_3 (ab28444, Abcam), PRDX1 (ab41906, Abcam), SODC (ab16831, Abcam), MYL2 (sc-34490, Santacruz), MCCA (sc-66988, Santacruz), and β-actin (sc1615, Santacruz), were diluted in TBS-Tween milk 4% and incubated overnight at 4°C. eNOS and iNOS antibodies were gift from Prof. J. Pfeilschifter. The horseradish peroxidase–coupled anti-rabbit (NA934V, Amersham Biosciences), anti-goat (P0449, DakoCytomation) immunoglobulin secondary antibodies were diluted 1/5000 in TBS-T 4% BSA one hour at RT.

Between each detection, the membrane was stripped by incubation with glycine 25mM/SDS 1% (pH 2) for 30min at 50°C. Every incubation was preceded by three washes with TBS Tween for 10min Immunoreactive sites were visualized using a chemiluminescence detection system (ECL Mix (1:1 mix: solution A (2,5mM Luminol, 0,4mM p-Coumarinacid in 0,1M Tris-HCl pH 8,5) and solution B (0,02% (v/v) H_2O_2 in 0,1M Tris-HCl pH 8,5)). Membranes were exposed to autoradiography film (8194540, Kodak BioMax Light Film), developed on a developer (Curix 60, Agfa) and finally scanned at 300dpi as 24bit 256 greyscale pictures on a Canon scanner (Canoscan 5000F, Canon) and compressed as jpeg files. The band intensity was measured using the AlphaEaseFC software (Alpha Innotech) for densitometry which takes into account the size and the darkness of the band. The intensity of each sample was first normalized to a standard curve loaded an each gel and then normalized to the intensity of β-actin.

2.11 Statistics

Data are presented as mean ± SEM. Comparisons between groups were performed using Mann Whitney U-test or Student's t-test. p values < 0.05 were considered significant.

3 Results

Blood pressure was measured in collaboration with K. Relle using the tail cuff method in three and nine months old animals. Physiological investigations were performed in collaboration with Bayer Schering Pharma in the four genotypes, both males and females. These experiments revealed that ET+/+eNOS-/- and eNOS-/- mice develop high blood pressure compared to WT and ET+/+ mice. Most importantly, eNOS-/- mice, but not ET+/+eNOS-/-, are characterized by left ventricular diastolic dysfunctions. In order to understand the morphological and molecular changes leading to this phenotype, the following experiments have been undertaken in the four genotypes (WT, ET+/+, eNOS-/- and ET+/+eNOS-/- mice):

- qRT-PCR analysis revealed the ET-1 gene expression pattern in the heart of nine months animals. ETAR and ETBR gene expression were analyzed by *in situ* hybridization.
- Western blot analyses were used to quantify the cardiac protein expression level of ETAR and ETBR as well as eNOS and iNOS in both three and nine months old animals.
- Aortic functions of ET+/+eNOS-/- mice have been precisely described previously.[114] Using qRT-PCR and WB, the gene expression and protein level of endothelin system components, eNOS and iNOS were analyzed in aortic tissue from nine months old male mice.
- Cardiac histological study of nine months old animals has been performed by K. Relle and is described in details in her doctoral thesis. To analyze the age-related mechanisms, cardiac morphology and histology of three months old male and female mice were investigated here.
- The expression pattern of cardiac components of the extracellular matrix (metalloproteases and collagens) has been revealed by immunohistochemistry in nine months old animals.
- Finally, in order to define the early molecular mechanisms leading to the phenotype observed in nine months old animals, a cardiac proteomics study has been undertaken in three months old male and female animals. The results of the proteomics study have been confirmed and further investigated in more details with one and two dimensional western blot analyses for some proteins of particular interest.

3.1 Quantitative RT-PCR

3.1.1 Cardiac tissue

For the relative quantification of the gene expression of the endogenous as well as the transgenic ET-1, specific primers were designed for the murine and human preproendothelin-1 cDNAs (mPPET-1 and hPPET-1) and primers binding to both cDNAs (PPET1). Amplification of genomic DNA was avoided by choosing intron spanning primers. The specificity of the primers has been verified by loading the PCR products on agarose gels (figure 3). Moreover, the dissociation curves of real time amplification using the PPET-1 primers showed two peacks, indicating that these primers bind to both cDNAs. In WT and eNOS-/- animals, amplifications with mPPET1 and PPET1 primers were similar. No amplification was observed with the hPPET1 primers in WT and eNOS-/- mice. In ET+/+ and ET+/+eNOS-/- mice, both mPPET1 and hPPET1 cDNAs were amplified with the respective primers or both together with PPET1 primers (figure 4).

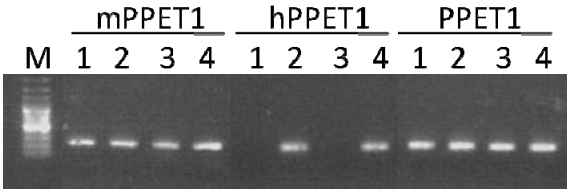

Figure 3: PCR amplification product on agarose gel using the mouse and human PPET1 specific primers and primers binding to both cDNA. (1: WT; 2: ET+/+; 3: eNOS-/-; 4: ET+/+eNOS-/-)

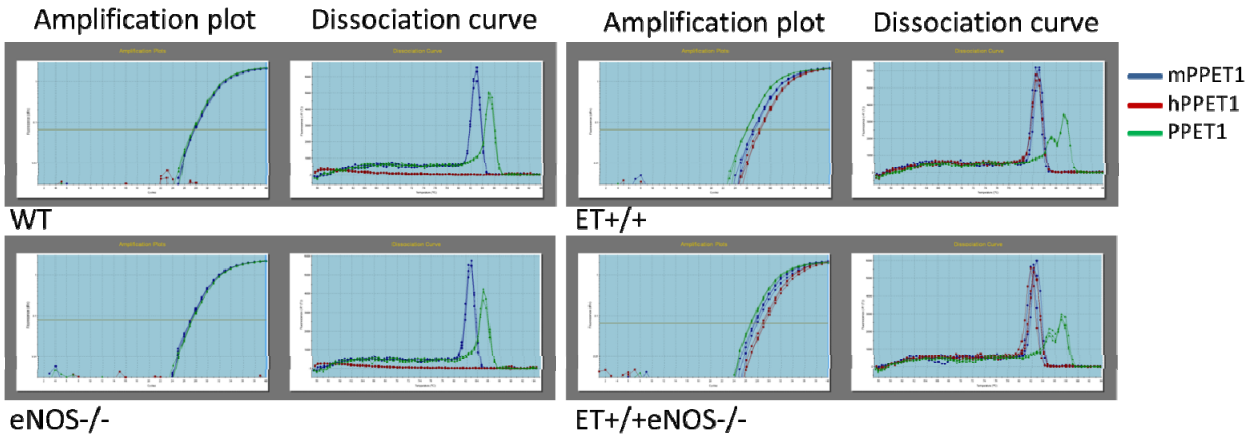

Figure 4: Representative amplification plots and dissociation curves after qRT-PCR using the mouse and human PPET1 specific primers and the primers binding to both cDNAs in WT, ET+/+, eNOS-/- and ET+/+eNOS-/- mice.

In ET+/+, eNOS-/- and ET+/+eNOS-/- male mice, total ET-1 expression was elevated twofold compared to WT. In females, only ET+/+ mice have an elevated ET-1 expression (1.8-fold). Difference between total and murine ET-1 expression indicated that the human transgene expression participated in 18 to 32% of total ET-1 expression in the transgenic animals. The level of transgene expression was similar in male ET+/+ and ET+/+eNOS-/-. In female ET+/+eNOS-/- mice, the level of transgene expression was the half of its level in ET+/+ mice (table 6).

	WT		ET+/+		eNOS-/-		ET+/+eNOS-/-	
	male	female	male	female	male	female	male	female
n	6	6	5	5	6	5	5	5
ET-1	1.0 ± 0.08	1.0 ± 0.09	2.0 ± 0.07 **	1.8 ± 0.28	2.3 ± 0.44 *	0.8 ± 0.10 §	2.0 ± 0.19 **	1.0 ± 0.06
mET-1	1.0 ± 0.18	1.0 ± 0.14	1.4 ± 0.15	1.3 ± 0.14	2.3 ± 0.33 **	1.0 ± 0.16	1.5 ± 0.07 *	0.8 ± 0.23
hET-1	n/a	n/a	1.0 ± 0.11	1.0 ± 0.11	n/a	n/a	0.8 ± 0.08	0.5 ± 0.07 §

Table 6: Cardiac gene expression of total ET-1, endogenous mouse ET-1 and transgene human ET-1 obtained by qRT-PCR in nine months old female and male mice. Data are means ± SEM. Mann Whitney's U-test: * $p<0.05$ vs. WT; ** $p<0.01$ vs. WT; § $p<0.05$ vs. ET+/+. n/a: not applicable.

3.1.2 Aortic tissue

Because of the contribution of the aorta to maintain cardiovascular functions, gene expression of transgenic human ET-1 as well as endogenous murine ET-1, ETAR and ETBR receptors, ECE, iNOS, and eNOS was assessed in aortic tissue of nine months old male mice using qRT-PCR. Results are illustrated in table 7. Whereas no significant differences regarding all of these parameters between ET+/+ and WT mice were detected, both groups that carried an eNOS knock-out (eNOS-/- and ET+/+eNOS-/-) exhibited a significantly enhanced iNOS gene expression when compared with WT mice. In crossbred mice, expression of all parameters related to the endothelin system was markedly upregulated when compared with WT controls: Endogenous murine ET-1 as well as transgenic human ET-1 (compared with ET+/+ mice), ECE, ETAR and ETBR (Table 7).

	WT	ET+/+	eNOS-/-	ET+/+eNOS-/-
n	6	6	6	5
ETAR	1.00 ± 0.25	0.54 ± 0.11	0.95 ± 0.24	5.36 ± 0,91 *,§,†
ETBR	1.00 ± 0.18	0.56 ± 0.10	0.74 ± 0.21	2.65 ± 0,73 *,§,†
eNOS	1.00 ± 0.19	0.58 ± 0.07	n/a	n/a
iNOS	1.00 ± 0.14	0.75 ± 0.04	2.45 ± 0,35 *,§§	3.93 ± 0,76 *,§§
mET-1	1.00 ± 0.46	0.86 ± 0.22	1.78 ± 0.66	6.59 ± 1,1 **,§§,†
hET-1	n/a	1.00 ± 0.35	n/a	4.26 ± 1,1 §
ECE-1	1.00 ± 0.07	0.82 ± 0.11	1.33 ± 0,12 *,§	1.45 ± 0,15 *,§

Table 7: Aortic gene expression of ETAR, ETBR, eNOS, iNOS, mET-1, hET-1 and ECE-1 obtained by qRT-PCR in nine months old male mice. Data are means ± SEM. Mann Whitney's U-test: * $p<0.05$ vs. WT; ** $p<0.01$ vs. WT; § $p<0.05$, §§ $p<0.01$ vs. ET+/+, † $p<0.05$ vs. eNOS-/-. n/a: not applicable.

3.2 In situ hybridization

The technique of *in situ* hybridization permits the localization of mRNA on tissue slides. Analyses of digital images of the slides with the program ImageJ allowed additionally the relative quantification of the signal corresponding to ETAR and ETBR mRNA expression in the myocardium of nine months old animals. *In situ* hybridization was performed in male WT and ET+/+eNOS-/- mice.

The two endothelin receptors were found to be typically expressed in cardiomyocytes as well as in the cardiac vessels (figure 5). No differences were observed concerning the localization of ETAR and ETBR between the groups. Relative quantification of the signal showed that ETBR, but not ETAR, was less expressed in the myocardium of ET+/+eNOS-/- mice compared to WT mice (figure 5B). In the vessels however, it appeared that ETBR expression was similar in both groups (Figure 5B). A negative control omitting the RNA probe confirmed the specificity of the staining.

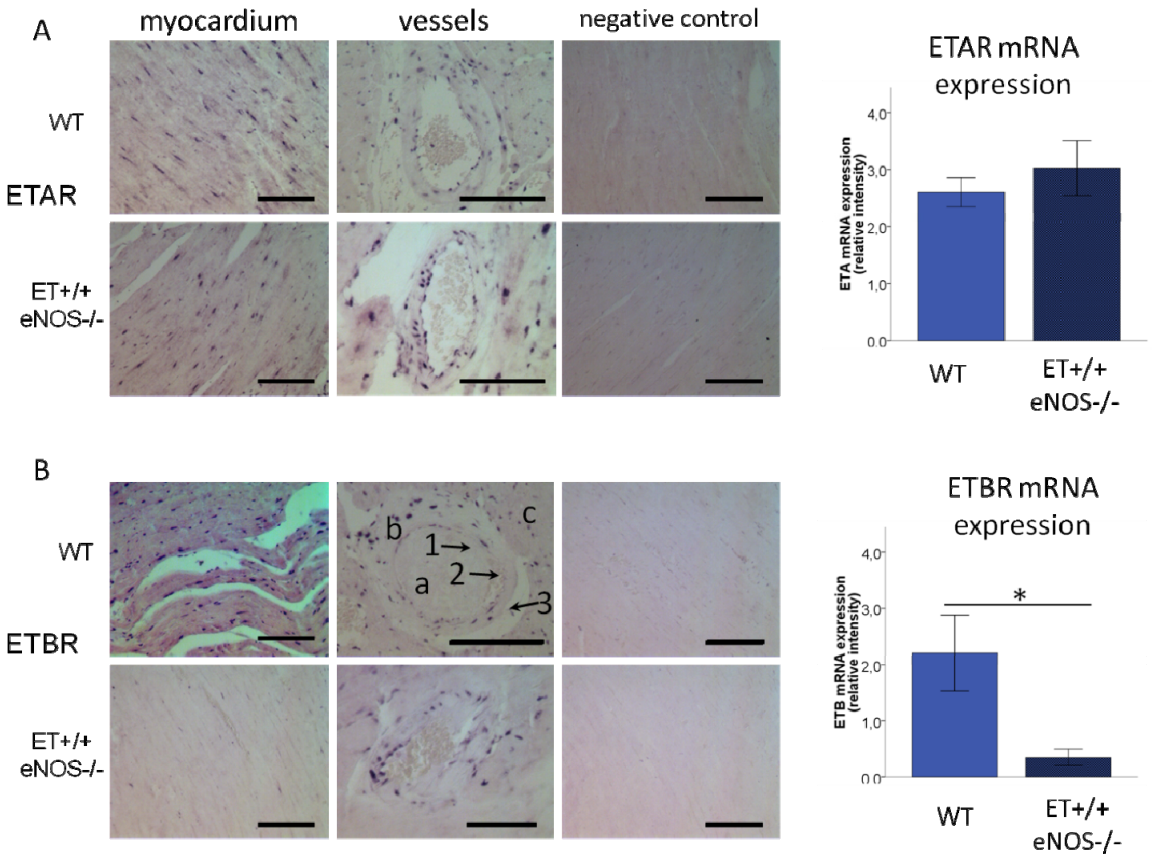

Figure 5. *In situ* hybridization analysis of ETAR (A) and ETBR (B) mRNA expression in cardiac tissue of nine months old WT (n=5) and ET+/+eNOS-/- (n=4) male mice. Left panel: myocardium; middle panel cardiac vessels; right panel: negative control. Bar 100µm. a: lumen area, b: media area, c: myocardium. 1: intima (endothelium), 2: media (smooth muscle), 3: adventia (connective tissue). Quantification of the signal in the myocardium is shown. Mann-Whitney U-test: * $p<0.05$.

3.3 Western Blot of ETAR, ETBR, eNOS and iNOS

3.3.1 Cardiac tissue

Expression levels of ETAR, ETBR, eNOS and iNOS have been analyzed by semiquantitative immunoblotting in cardiac tissue in both three and nine months old groups, in both male and female mice. In three months old animals, ETAR and ETBR were more abundant in ET+/+ male mice compared to WT and ET+/+eNOS-/- mice. In female mice, ETAR and ETBR protein level was more abundant in eNOS-/- mice. In nine months old animals, ETAR expression was similar between the groups (figure 6A) while ETBR expression was reduced in both eNOS-/- and

ET+/+eNOS-/- mice independently from sex (figure 6B). In males, ETBR was reduced significantly in ET+/+ and eNOS-/- mice; in female, however, only in ET+/+eNOS-/- mice (figure 6B).

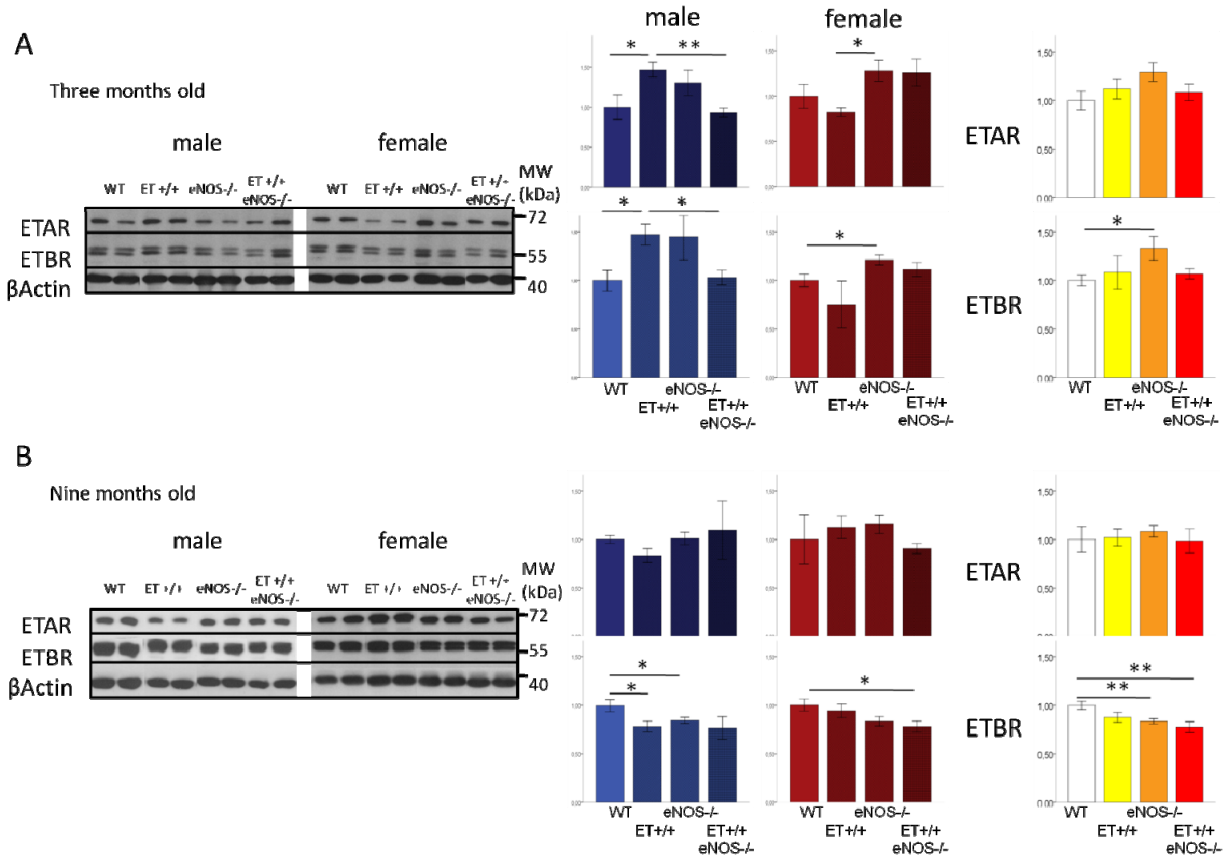

Figure 6: WB analysis of ETAR and ETBR in WT, ET+/+, eNOS-/- and ET+/+eNOS-/- male and female three (A) and nine (B) months old mice. Diagrams show quantification of the intensity of the bands normalized to β-actin. n=6-8. Values are given as mean±SEM. Mann Whitney U-test: * $p<0.05$, ** $p<0.01$.

Western Blot analysis proved the absence of eNOS at the protein level in all eNOS-/- mice groups (figure 7A). In nine months old animals, eNOS was less abundant in ET+/+ mice compared to WT, while iNOS was more abundant, without reaching significance though. iNOS was found to be less abundant in ET+/+eNOS-/- mice compared to ET+/+ and WT, or ET+/+ only depending on the age (three months old and nine months old, respectively) (figure 7B).

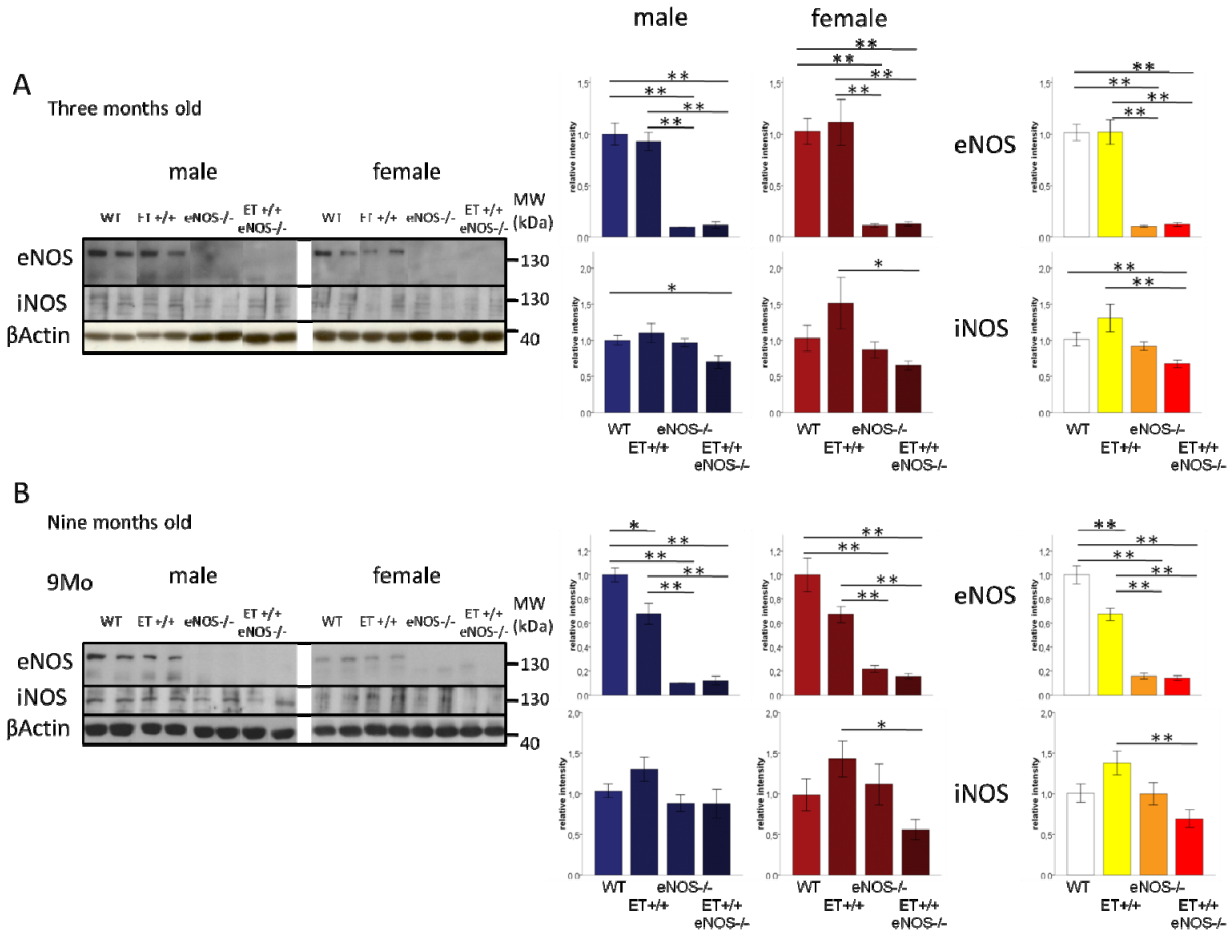

Figure 7: WB analysis of eNOS and iNOS in WT, ET+/+, eNOS-/- and ET+/+eNOS-/- male and female three (A) and nine (B) months old mice. Diagrams show quantification of the intensity of the bands normalized to β-actin. n=6-8. Values are given as mean±SEM. Mann Whitney U-test: * p<0.05, ** p<0.01.

3.3.2 Aortic tissue

Aortic protein expression of ETAR, ETBR, eNOS and iNOS was analyzed in nine months old male mice of the four genotypes. In ET+/+ mice, ETAR protein expression was not significantly altered as compared with WT mice. In eNOS-/- mice, ETAR expression was reduced, whereas in ET+/+NOS-/- mice, ETAR protein expression was significantly increased (figure 8A). In addition, ETBR was markedly overexpressed at the protein level in ET+/+eNOS-/- mice compared to WT mice (figure 8B). eNOS Western blotting confirmed the absence of eNOS protein in eNOS-/- mice, whereas eNOS protein expression in ET+/+ mice was not significantly altered (figure 8C). In ET+/+ mice, iNOS protein level was significantly increased. Knock-out of eNOS did not significantly alter iNOS protein expression (figure 8D).

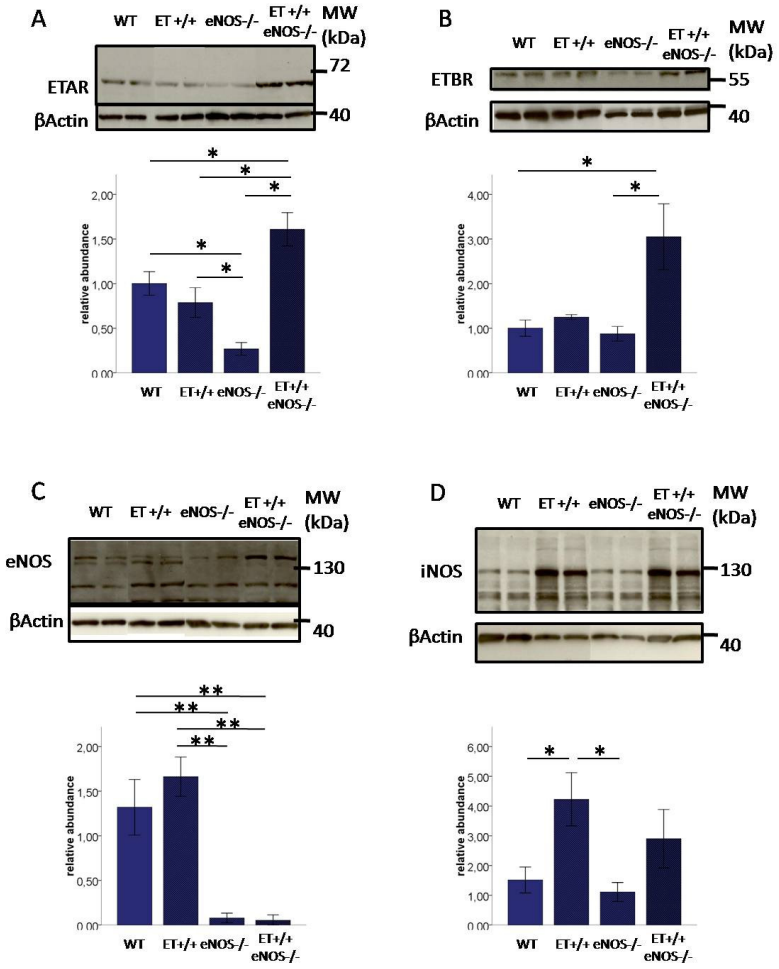

Figure 8: WB analysis of ETAR (A), ETBR (B), iNOS (C) and eNOS (D) in aortic tissue of WT, ET+/+, eNOS-/- and ET+/+eNOS-/- nine months old male mice. The diagrams show the quantification of the band intensity normalized to β-actin. n=5-6. Data are means ± SEM. Mann Whitney U-test: * $p<0.05$; ** $p<0.01$.

3.4 Histology

3.4.1 Cardiac interstitial and perivascular ECM deposition

Total ECM deposition in the cardiac muscle was measured after Sirius red staining in three months old mice. Sirius red binds unspecifically to extracellular matrix proteins and gives therefore indications on the fibrotic state of the tissue. The role of the cardiac extracellular matrix is mainly to preserve elasticity of the muscle. Its composition is therefore relevant for the function of the cardiac muscle. Similarly, the composition of the perivascular matrix has a direct effect on the ability of the vessel to contract and dilate.

Male ET+/+, eNOS-/- and ET+/+eNOS-/- mice developed cardiac interstitial fibrosis compared to WT. This was more pronounced in ET+/+eNOS-/- mice (figure 9). In female mice, there was no difference between the genotypes. ECM protein deposition was higher in WT and ET+/+ female mice compared to male littermate, but not in eNOS-/- and ET+/+eNOS-/- mice. Male and female mice taken together, both ET+/+ and ET+/+eNOS-/- mice developed interstitial cardiac fibrosis compared to WT (figure 9). The same pattern was observed for the perivascular fibrosis. In that case, the female ET+/+, eNOS-/- and ET+/+eNOS-/-, however, developed perivascular fibrosis compared to WT but not males. Similarly to interstitial fibrosis in males, perivascular fibrosis was more pronounced in crossbred female mice than in ET+/+ and eNOS-/- female mice (figure 10).

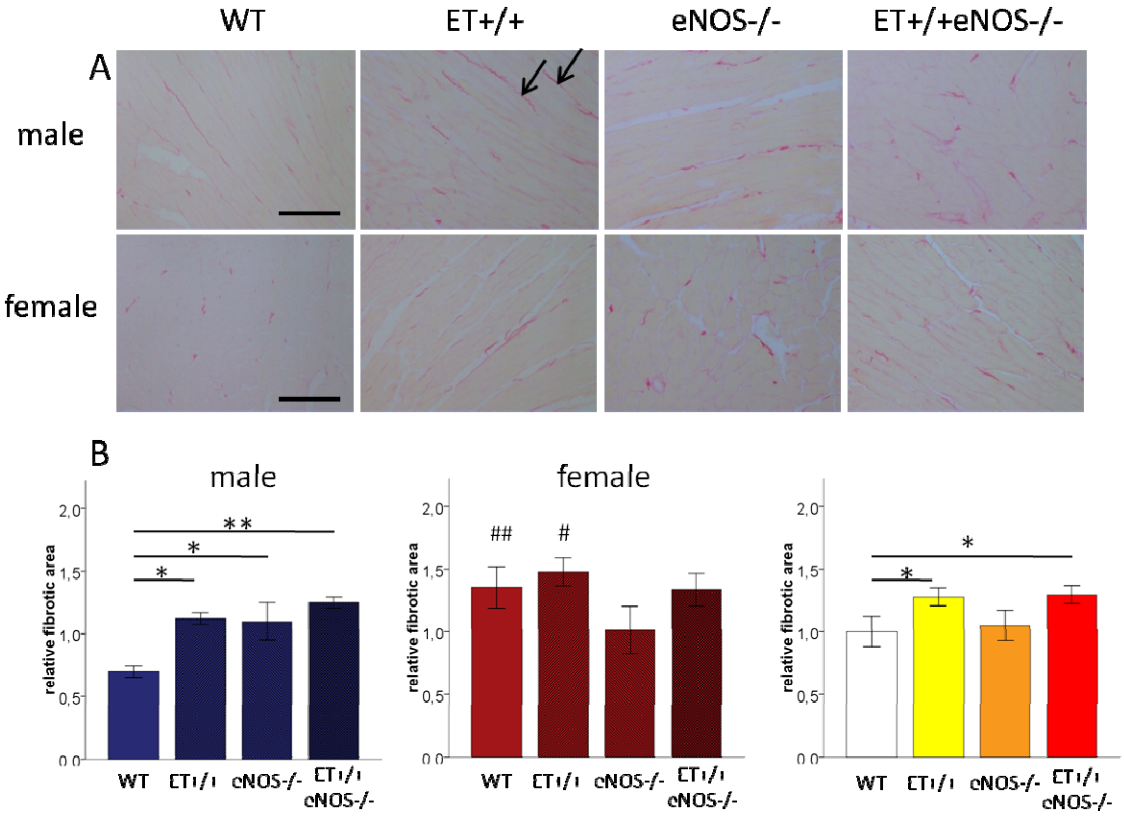

Figure 9: Interstitial ECM protein deposition. (A) Typical pictures of cardiac sections from WT, ET+/+, eNOS-/- and ET+/+eNOS-/- male and female three months old mice. Sirius red staining (bar ≙ 100µm, arrows show ECM protein deposition, (B) Quantification of the signal. n=5-7. Data are means ± SEM. Mann Whitney U-test: * p<0.05, ** p<0.01; # p<0.05, ## p<0.01 vs. male same genotype.

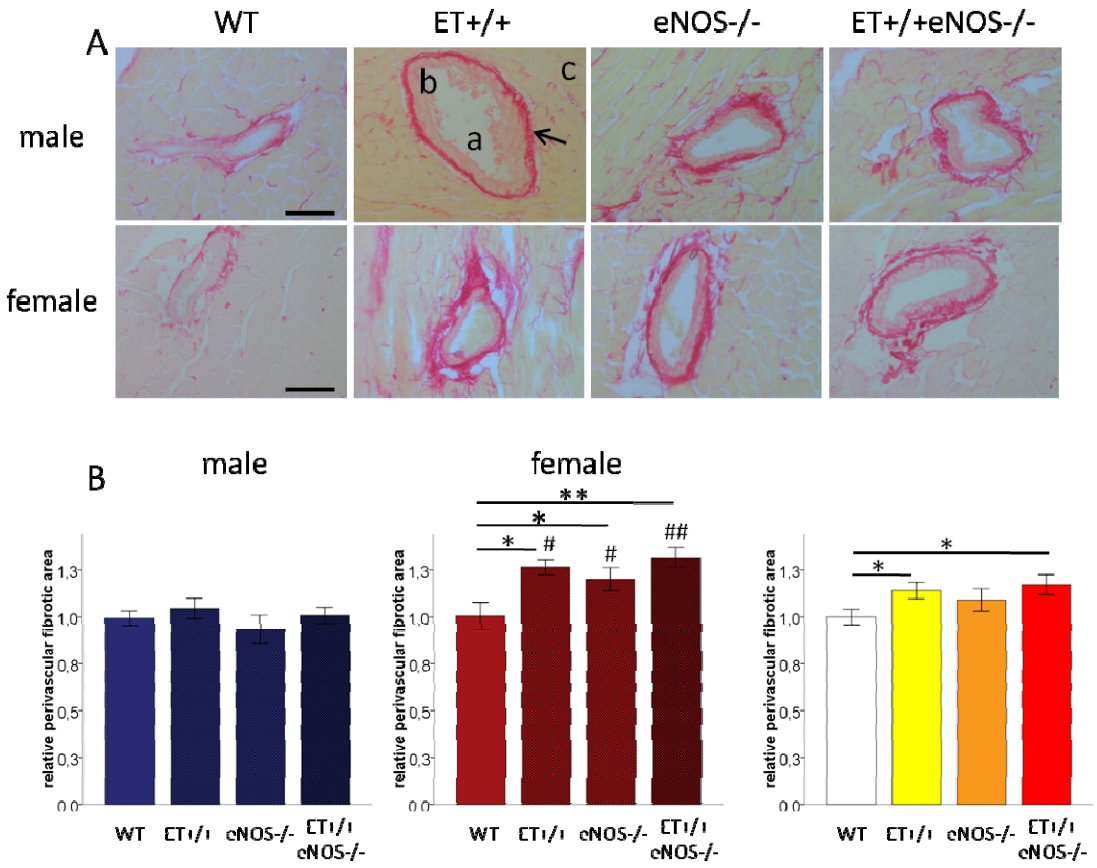

Figure 10: Perivascular ECM protein deposition. (A) Typical pictures of cardiac sections from WT, ET+/+, eNOS-/- and ET+/+eNOS-/- male and female three months old mice. Sirius red staining; bar ≙ 50µm; a: lumen area, b: media area, c: myocardium, arrows show ECM protein deposition, (B) Quantification of the signal. n=5-7. Data are means ± SEM. Mann Whitney U-test: * p<0.05, ** p<0.01; # p<0.05, ## p<0.01 vs. male same genotype.

3.4.2 Cardiomyocyte diameter

Myocyte diameter was assessed using HE staining. Cardiomyocyte diameter is an indicator for cardiac hypertrophy and is therefore pathophysiologically relevant. In three months old animals, the ET+/+eNOS-/- mice had enlarged myocytes compared to WT and ET+/+ mice independently from sex. In eNOS-/- mice, cardiomyocyte diameter was larger in males than in females (figure 11).

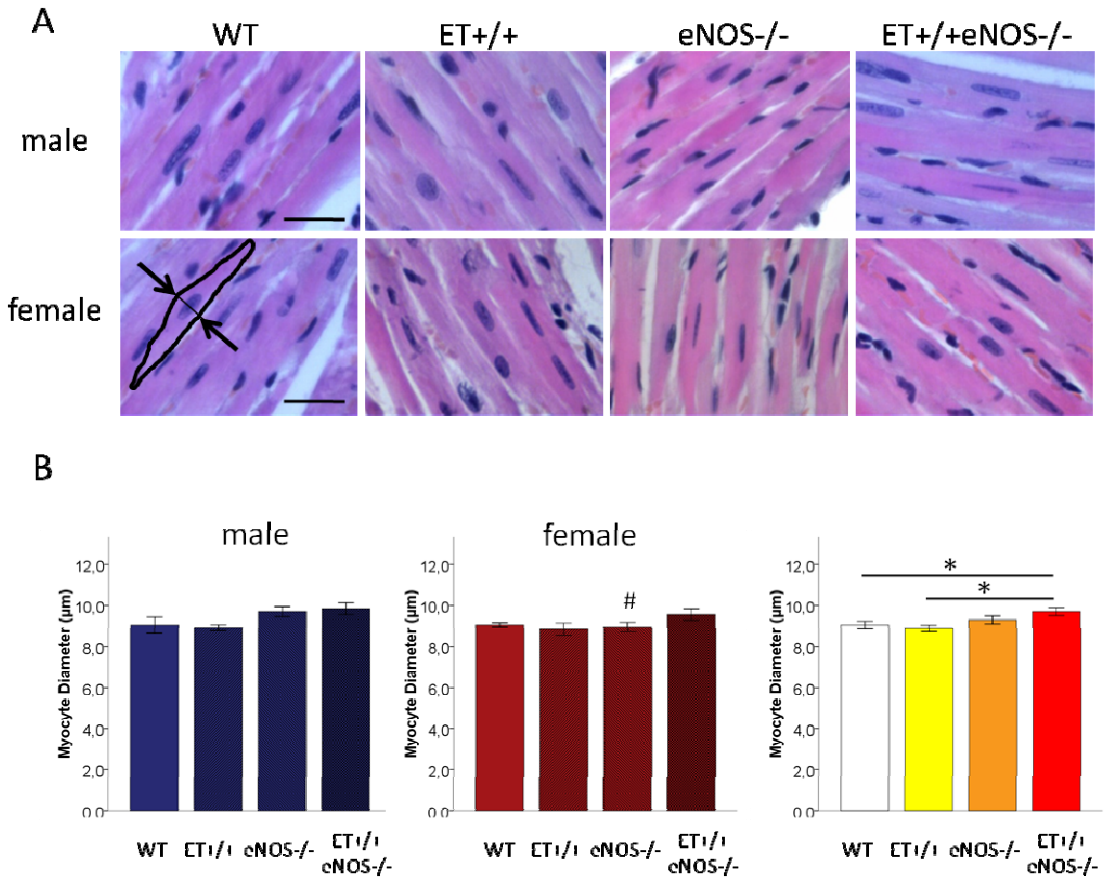

Figure 11: Cardiomyocyte diameter. (A) Typical pictures of cardiac sections from WT, ET+/+, eNOS-/- and ET+/+eNOS-/- male and female three months old mice. HE staining: nucleus in blue, cytoplasm in bluish-pink; bar ≙ 10µm; Arrows show the diameter of an encircled cardiomyocyte. (B) Quantification is shown in the diagrams. n=5-7. Data are means ± SEM. Mann Whitney U-test: * $p<0.05$; # $p<0.05$ vs. male same genotype.

3.4.3 Cardiac arteriole morphology

The areas of both the lumen and the media of vessels give an indication on the level of dilation. These parameters are important for the apprehension of vascular functions, in particular resistance and blood flow. In three months old ET+/+eNOS-/- male mice, the media area of small cardiac arteries were smaller than in ET+/+ mice and, by consequence, media-to-lumen ratio was bigger. In ET+/+ female mice, media area was bigger and media-to-lumen ratio was smaller than in WT. Male and female taken together, lumen area was bigger in ET+/+ mice compared to WT and eNOS-/- mice; media-to-lumen ratio was smaller in ET+/+ mice than in both eNOS-/- and ET+/+ eNOS-/- mice (by trend compared to WT). There were no differences between WT, eNOS-/- and ET+/+ eNOS-/- mice (figure 12).

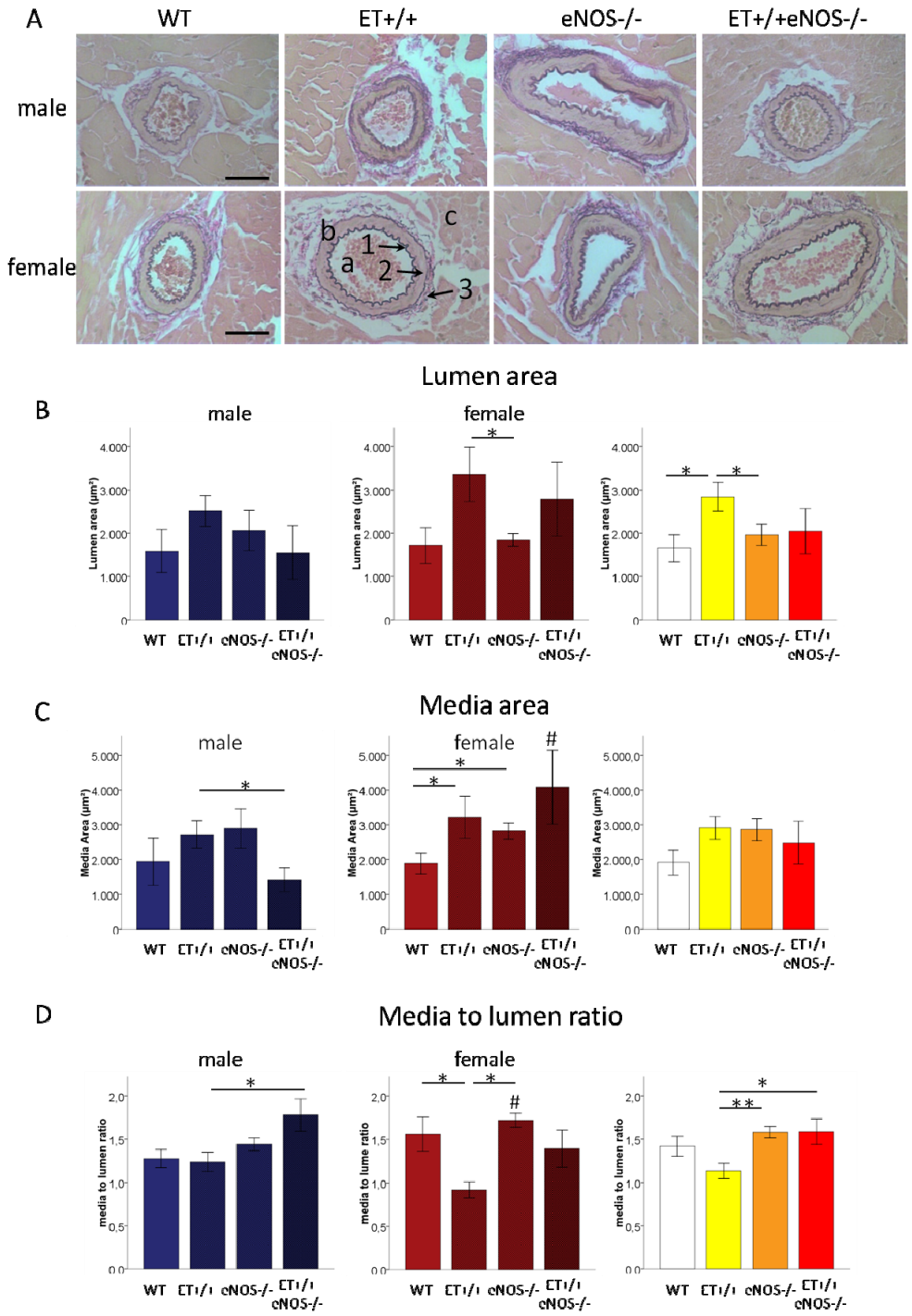

Figure 12: Cardiac arteriole morphology. (A) Typical pictures of cardiac sections from WT, ET+/+, eNOS-/- and ET+/+eNOS-/- male and female three months old mice. Elastica-van Giesson staining; bar ≙ 50µm; a: lumen area, b: media area, c: myocardium. In the vessel wall: 1: intima (endothelium), 2: media (smooth muscle), 3: adventia (connective tissue). Quantification is shown in the diagrams: (B) lumen area, (C) media area, (C) media to lumen ratio. n=5-7. Data are means ± SEM. Mann Whitney U-test: * $p<0.05$, ** $p<0.01$; # $p<0.05$ vs. male same genotype.

3.5 Immunohistochemistry

To understand the molecular mechanisms involved in cardiac fibrosis in nine months old animals, it was important to analyze some important components of the extracellular matrix. This was achieved by employing immunohistochemistry using specific antibodies against metalloprotease 2 (MMP2), metalloprotease 9 (MMP9), collagen I (Col I), collagen III (Col III).

MMP2 and MMP9 expression were similar between the four genotypes. Interestingly, both eNOS-/- and ET+/+eNOS-/- females expressed less MMP9 than the male littermates (figure 13). In females, but not in males, collagen I was up regulated in ET+/+eNOS-/- in comparison to WT. WT females expressed less collagen I than WT males, this relation was inverse in ET+/+eNOS-/-. Collagen III was moderately but significantly upregulated in ET+/+eNOS-/- independently from sex (figure 14).

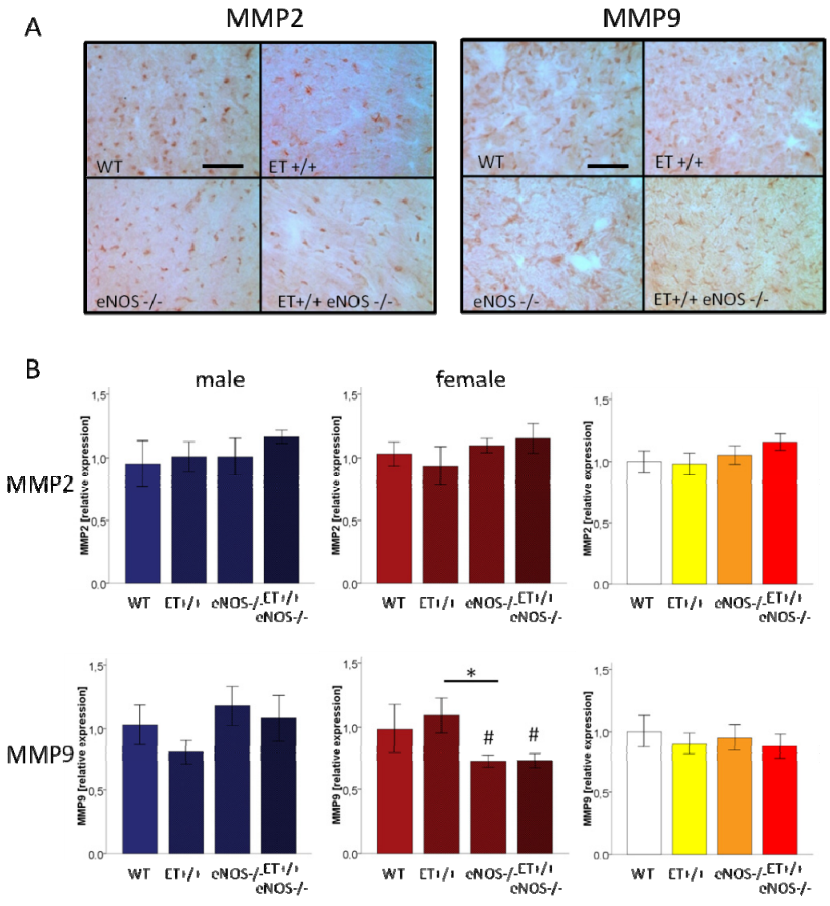

Figure 13: MMP2 and MMP9 protein expression in myocardium of nine months old WT, ET+/+, eNOS-/- and ET+/+eNOS-/- mice. (A) Typical pictures of immunohistochemistry. Bar ≙ 100µm. (B) Diagrams show the relative signal intensity. n=5-6. Data are means ± SEM. Mann Whitney U-test: * $p<0.05$, # $p<0.05$ vs. male same genotype.

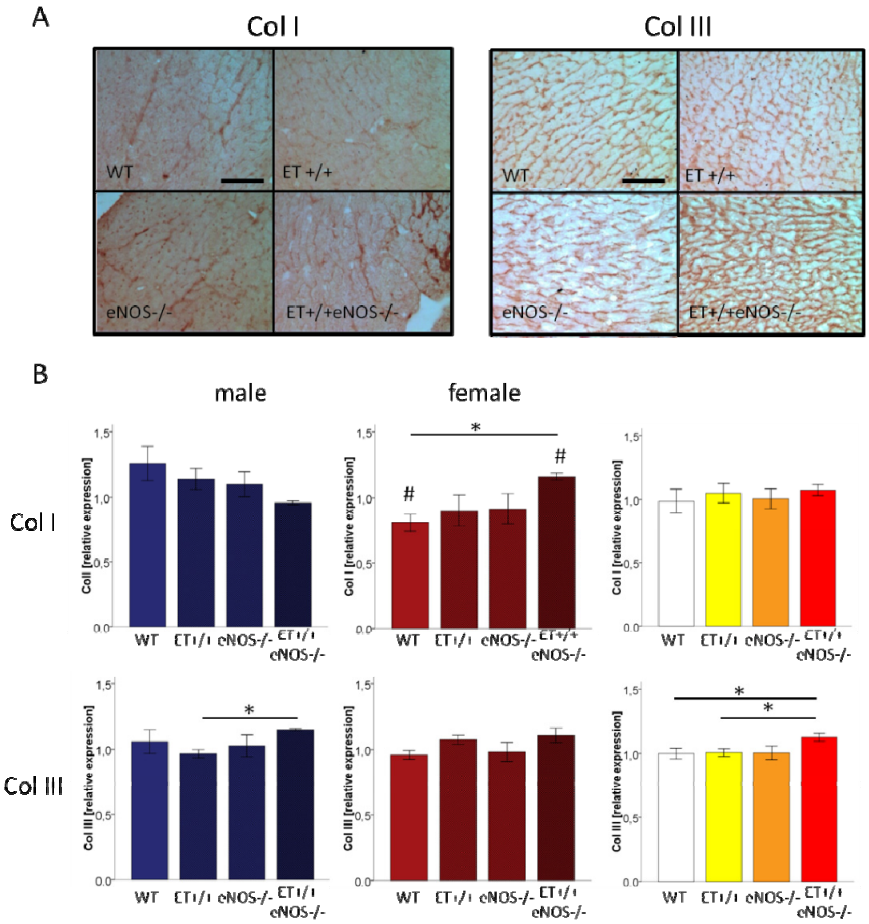

Figure 14: Col I and Col III protein expression in myocardium of nine months old WT, ET+/+, eNOS-/- and ET+/+eNOS-/- mice. (A) Typical pictures of immunohistochemistry. Bar ≙ 100µm. (B) Diagrams show the relative signal intensity. n=5-6. Data are means ± SEM. Mann Whitney U-test: * p<0.05, # p<0.05 vs. male same genotype.

3.6 Proteomics

In order to identify proteins that are differentially abundant between the groups, the cardiac proteome of three months old animals were analyzed using large scale 2DE coupled to ESI/MS. In this study, the cardiac proteome of each genetically modified mice strain (ET+/+, eNOS+/+ and ET+/+eNOS-/- mice) was compared with WT mice. Males and females were analyzed separately. Direct comparisons between males and females of the same genotype or between the transgenic and knock-out animals against each other would have been possible but are not the object of this thesis. Only for the selected spots analyzed in details in the section "3.6.6. Validation", each group was compared statistically to one another.

3.6.1 2DE: characteristics and reproducibility

On an analytical silver stained 2DE gel, around 1300 protein spots were detected by the software. The spots were well separated and covered the whole pH (2-11) as well as molecular weight (10-200kDa) range.

Every step of protein separation was standardized; every solution was produced in sufficient quantity for the complete procedure and aliquoted. This ensured a good technical reproducibility. The biological variability was assessed by comparing the normalized matched spot intensity between animals from the same genotype. A strong linear correlation was observed between the biological samples as shown by the values of correlation coefficient (R^2) of around 0.9 (figure 15).

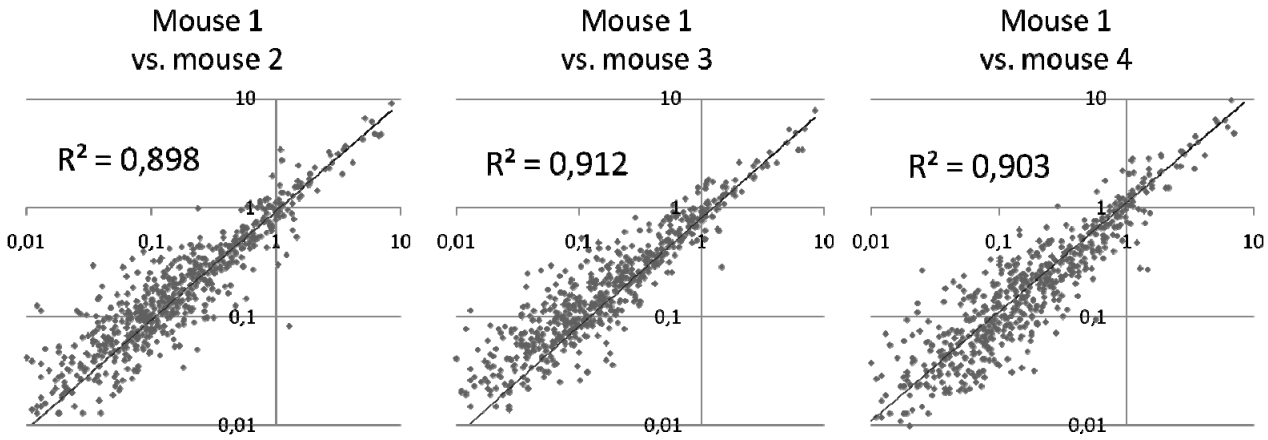

Figure 15: Evaluation of biological variability. Exemples of correlation analysis of normalized intensities of matched spots in four WT mice.

3.6.2 Number of differentially expressed spots

In total, 128 protein spots (79 in the males, 61 in the females) have been found to be differentially abundant in the three different genotypes compared to WT. They were distributed between the groups as shown in the following Venn diagrams (figure 16). Except for ET+/+ male, the number of more abundant protein species compared to WT was always higher than the number of less abundant protein species (figure 17).

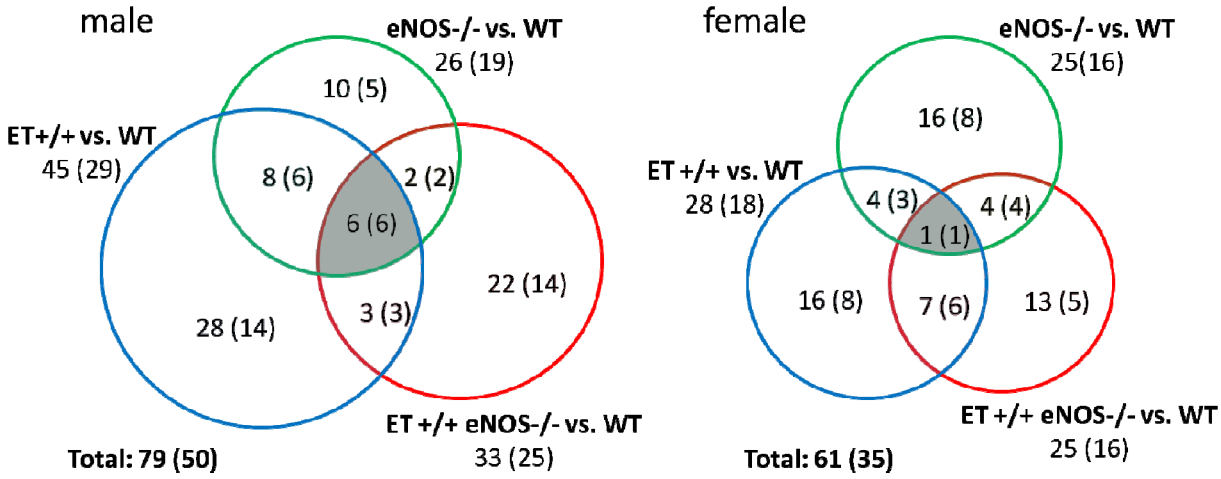

Figure 16: Venn diagrams showing the number of differentially abundant protein species in ET+/+, eNOS-/- and ET+/+eNOS-/- male (left) and female (right) mice compared to WT (n=6-9). Size of the circle is proportional to the number of protein species. The numbers in parentheses indicate the number of protein species identified by ESI/MS.

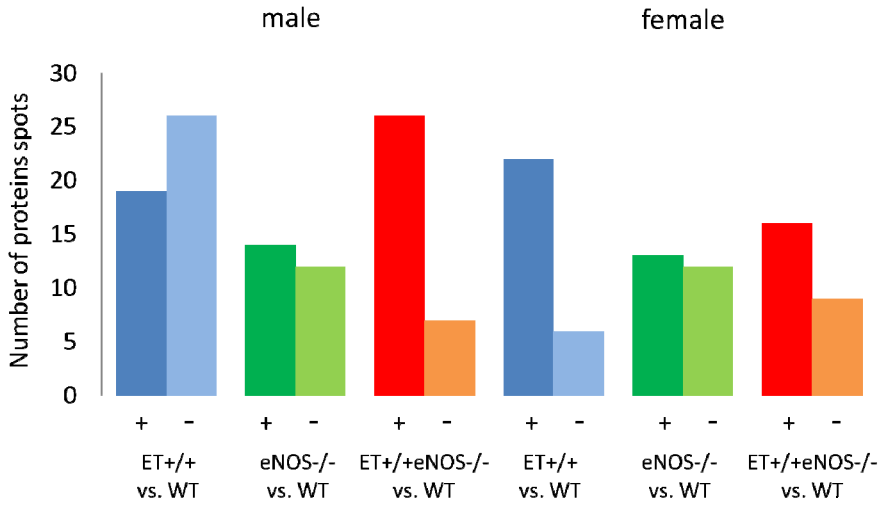

Figure 17: Distribution of the differentially abundant protein species in comparison to WT between the groups. + means more abundant, - means less abundant compared to WT.

3.6.3 Spot identification

77 protein spots have been identified by ESI/MS (50 in the males, 35 in the females). These spots are highlighted and numbered in the figure 18. In order to achieve better sequence coverage and thus reveal post-translational modifications, some spots of particular interest were reanalyzed by MS. An example of an MS output is represented in the figure 19.

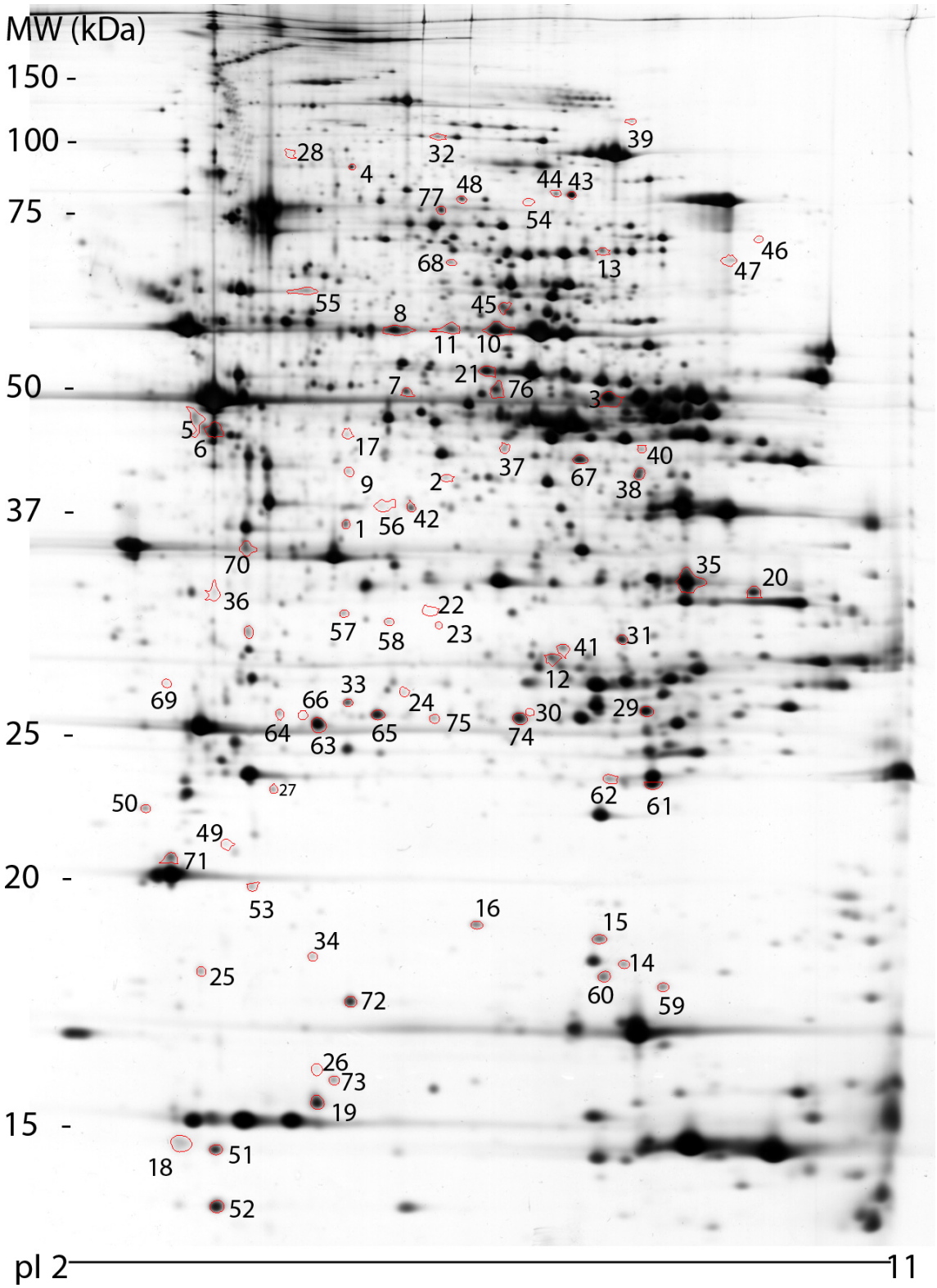

Figure 18: A typical silver stained 2DE gel of the cardiac proteome of mice. 100µg protein have been loaded on the gel. The differentially abundant protein spots successfully identified by ESI/MS are encircled and numbered from 1 to 77. MW: Molecular weight, pI: isoelectric point. The numbers correspond to the table 8.

Glycogen phosphorylase (PYGB)

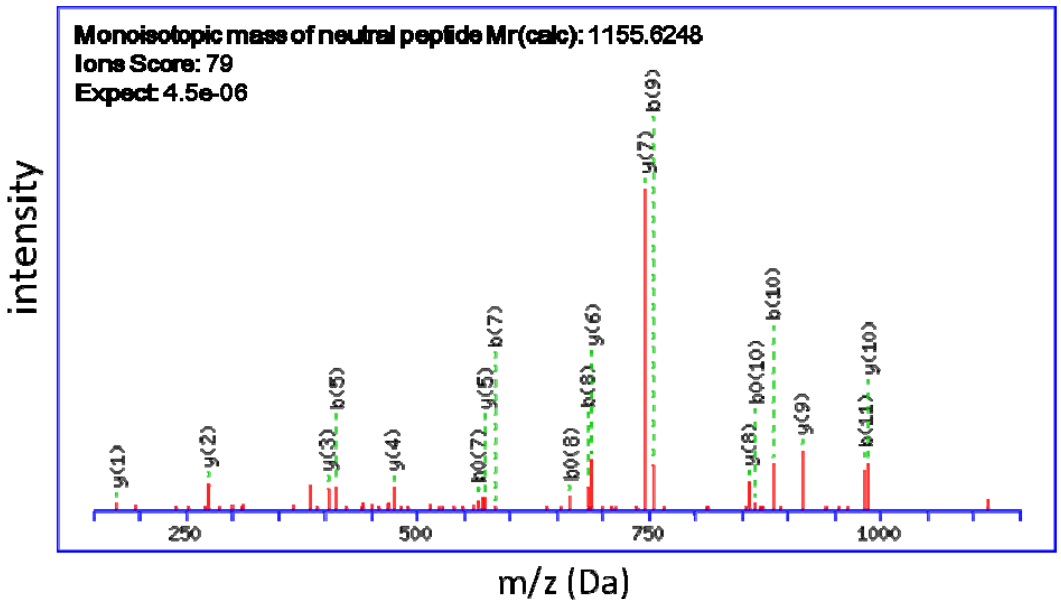

#	b	b^{++}	b^{0}	b^{0++}	Seq,	y	y^{++}	y*	y^{*++}	y^{0}	y^{0++}	#
1	580.29	295.18			G							12
2	1711.13	860.60			I	10996.11	5503.09	10825.84	5417.96	10816.00	5413.04	11
3	2421.50	1215.79			A	**9865.27**	4937.67	9695.00	4852.54	9685.16	4847.62	10
4	2991.71	1500.89			G	**9154.89**	4582.48	8984.63	4497.35	8974.79	4492.43	9
5	**4122.55**	2066.31			L	**8584.68**	4297.38	8414.41	4212.24	8404.57	4207.32	8
6	4692.77	2351.42			G	**7453.84**	3731.96	7283.57	3646.82	7273.73	3641.90	7
7	**5843.04**	2926.56	**5662.93**	2836.50	D	**6883.62**	3446.85	6713.36	3361.72	6703.52	3356.80	6
8	**6833.72**	3421.90	**6653.62**	3331.85	V	**5733.36**	2871.71	5563.09	2786.58	5553.25	2781.66	5
9	**7544.09**	3777.08	7363.99	3687.03	A	**4742.67**	2376.37	4572.41	2291.24	4562.57	2286.32	4
10	**8834.52**	4422.30	**8654.41**	4332.24	E	**4032.30**	2021.19	3862.03	1936.05	3852.19	1931.13	3
11	**9825.20**	4917.64	9645.10	4827.59	V	**2741.87**	1375.97	2571.61	1290.84			2
12					R	**1751.19**	880.63	1580.92	795.50			1

Figure 19: Representative ESI/MS ion spectra peptide fragmentation of a peptide (sequence: GIAGLGDVAEVR) obtained from spot #32 (Glycogen phosphorylase). The y ions (present on peptide fragments charged on the C-terminus) and the b ions (present on peptide fragments charged on the N-terminus) are listed. Matches for this sequence are indicated in red.

3.6.4 Protein classification

The 77 identified spots represented 62 single proteins (45 in males, 30 in females). Their biological functions have been classified according to the online available Panther database (table 8). According to the number of proteins in each functional group and their relevance for cardiac functions, proteins were assigned to the following groups:

- Eight proteins played a role in the regulation of oxidative stress (PRDX1, PRDX3, PRDX6, SODC, HSPB7, ALDH2, GSTM1 and GSTM2); these proteins were more abundant in genetically modified animals than in WT.
- Twelve proteins were part of the contractile machinery (ACTA, ACTC, MLRA, GELS, MLRV, MYL3, DEST, COF1, COF2, SRCA, MYPC3, LDB3).
- Six proteins were involved in fatty acid metabolism (THIM, CACP, FABPH, HCDH, ECHA, and PECI); these proteins were mainly less abundant in the transgenic and knock-out animals than in WT.
- Four proteins were involved in glucose metabolism (TPIS, G3P, PYGB and ODPB).
- Six enzymes belonged to the tricarboxylic cycle and the mitochondrial respiratory chain (MDHC, IDH3A, Q3UQ73, QCR6, COX5B, ATPA).
- Other metabolisms were represented by the following proteins (MCCA, PSDE, SAHH, ALDH2, ACY1, CAH2, BDH, DHB8, ETHE1, HCDH, MMSA, NIT2, PSA5).

Table 8: List of the differentially abundant protein spots identified by ESI/MS

spot #	accesion number		name	abv.	regulation in male vs. WT			regulation in female vs.WT			
	GeneID NCBI	Swiss Prot			ET+/+	eNOS-/-	ET+/+ eNOS-/-	ET+/+	eNOS-/-	ET+/+ eNOS-/-	Biological function
1	59029	O35593	26S proteasome non-ATPase regulatory subunit 14	PSDE		+	+				Protein metabolism and modification
2	227095	Q8QZS1	3-hydroxyisobutyryl-CoA hydrolase, mitochondrial	HIBCH			+				Carbohydrate metabolism, Fatty acid beta-oxidation, Coenzyme metabolism, Vitamin biosynthesis
3	52538	Q8BWT1	3-ketoacyl-CoA thiolase, mitochondrial	THIM			-				Other protein metabolism
4	171210	Q99NB1	Acetyl-coenzyme A synthetase 2-like	ACS2L	+						Fatty acid metabolism, Coenzyme metabolism
5	11475	P62737	Actin, alpha 2, smooth muscle, aorta	ACTA			+	+			Exocytosis, Endocytosis, Transport, Cytokinesis, Cell structure
6	11464	P68033	Actin, alpha cardiac muscle 1	ACTC			+				Exocytosis, Endocytosis, Transport, Cytokinesis, Cell structure
7	269378	P50247	Adenosylhomocysteinase	SAHH					-		Purine metabolism
8	11669	P47738	Aldehyde dehydrogenase, mitochondrial	ALDH2	-		-			-	Other carbon metabolism
9	109652	Q99JW2	Aminoacylase-1	ACY1			+				Amino acid biosynthesis
10	11946	Q03265	ATP synthase subunit alpha, mitochondrial precursor	ATPA	-	-	-				unclassified
11	11946	Q03265	ATP synthase subunit alpha, mitochondrial precursor	ATPA	-	-	-				unclassified
12	12349	P00920	Carbonic anhydrase 2	CAH2				-		-	Other carbon metabolism
13	12908	P47934	Carnitine O-acetyltransferase	CACP		-					Fatty acid metabolism, Amino acid metabolism
14	56431	Q9R0P5	Destrin	DEST		+	+		+		Cell structure
15	12631	P18760	Cofilin-1	COF1		+					Cell structure
16	12632	P45591	Cofilin-2	COF2		+					Cell structure
17	26754	O35864	COP9 signalosome complex subunit 5	CSN5	-						mRNA transcription
18	66576	P99028	Cytochrome b-c1 complex subunit 6, mitochondrial	QCR6				+			Oxidative phosphorylation
19	12859	P19536	Cytochrome c oxidase subunit 5B, mitochondrial precursor	COX5B	+						Oxidative phosphorylation
20	71911	Q80XN0	D-beta-hydroxybutyrate dehydrogenase, mitochondrial	BDH					+	+	Other metabolism
21	13806	P17182	Alpha-Enolase	ENOA	-						Glycolysis
22	14979	P50171	Estradiol 17-beta-dehydrogenase 8	DHB8				+	+		Androgen/estrogene/progesterone biosynthesis
23	14979	P50171	Estradiol 17-beta-dehydrogenase 8	DHB8			+				Androgen/estrogene/progesterone biosynthesis
24	66071	Q9DCM0	Protein ETHE1, mitochondrial	ETHE1		-					Other carbon metabolism
25	276770	P63242	Eukaryotic translation initiation factor 5A-1	IF5A1	+	+					Protein biosynthesis
26	14077	P11404	Fatty acid-binding protein, heart	FABPH	+	+					Lipid and fatty acid transport, Lipid and fatty acid binding, Vitamin/cofactor transport, Steroid hormone-mediated signaling
27	14325	P29391	Ferritin light chain 1	FRIL1			+				Cation transport, Other homeostasis activities
28	227753	P13020	Gelsolin	GELS				+	+		Non-motor actin binding protein
29	14862	P10649	Glutathione S-transferase Mu 1	GSTM1	+						Detoxification

Table 8: List of the differentially abundant protein spots identified by ESI/MS (continued)

spot #	accesion number		name	abv.	regulation in male vs. WT			regulation in female vs.WT			
	GeneID NCBI	Swiss Prot			ET+/+	eNOS-/-	ET+/+ eNOS-/-	ET+/+	eNOS-/-	ET+/+ eNOS-/-	Biological function
30	14863	P15626	Glutathione S-transferase Mu 2	GSTM2	+		+	+		+	Antioxidation and free radical removal
31	14433	P16858	Glyceraldehyde-3-phosphate dehydrogenase	G3P				+			unclassified
32	110078	Q8CI94	Glycogen phosphorylase, brain form	PYGB			+				Glycogen metabolism
33	15507	P14602	Heat shock protein beta-1	HSPB1					+	+	Stress response
34	29818	P35385	Heat shock protein beta-7	HSPB7				+		+	Stress response
35	15107	Q61425	Hydroxyacyl-coenzyme A dehydrogenase, mitochondrial	HCDH						-	Protein metabolism and modification, Amino acid activation, Fatty acid beta-oxidation, Carbohydrate metabolism
36	67834	Q9D6R2	Isocitrate dehydrogenase [NAD] subunit alpha, mitochondrial	IDH3A			+				Tricarboxylic acid pathway
37	56357	Q9JHI5	Isovaleryl-CoA dehydrogenase, mitochondrial	IVD	-						Acyl-CoA metabolism, Electron transport
38	24131	Q9JKS4-5	LIM domain-binding protein 3 (isoform 5)	LDB3			+				Muscle development, Heart development, Cell structure, Cell motility
39	24131	Q9JKS4-1	LIM domain-binding protein 3 (isoform 1)	LDB3				+		+	Muscle development, Heart development, Cell structure, Cell motility
40	24131	Q9JKS4-1	LIM domain-binding protein 3 (isoform 1)	LDB3						+	Muscle development, Heart development, Cell structure, Cell motility
41	17449	P14152	Malate dehydrogenase, cytoplasmic	MDHC			+				Tricarboxylic acid pathway
42	17448	P08249	Malate dehydrogenase, mitochondrial	MDHM	-	-					Tricarboxylic acid pathway
43	72039	Q99MR8	Methylcrotonoyl CoA carboxylase subunit alpha, mitochondrial	MCCA		-			-		Gluconeogenesis
44	72039	Q99MR8	Methylcrotonoyl CoA carboxylase subunit alpha, mitochondrial	MCCA	-	-			-		Gluconeogenesis
45	104776	Q9EQ20	Methylmalonate-semialdehyde dehydrogenase [acylating], mitochondrial	MMSA	-	-					Amino acid metabolism, Pyrimidine metabolism
46	97212	Q8BMS1	Trifunctional protein subunit alpha, mitochondrial	ECHA				+	+		Carbohydrate metabolism, Fatty acid beta-oxidation, Amino acid activation
47	97212	Q8BMS1	Trifunctional protein subunit alpha, mitochondrial	ECHA						-	Carbohydrate metabolism, Fatty acid beta-oxidation, Amino acid activation
48	17698	P26041	Moesin	MOES	-						Cell structure
49	17897	P09542	Myosin light chain 3	MYL3	+						Muscle contraction
50	17898	Q9QVP4	Myosin regulatory light chain 2, atrial isoform	MLRA					+		Muscle contraction
51	17906	P51667	Myosin regulatory light chain 2, ventricular/cardiac muscle isoform	MLRV				+			Muscle contraction, Muscle development, Cell structure and motility
52	17906	P51667	Myosin regulatory light chain 2, ventricular/cardiac muscle isoform	MLRV				+			Muscle contraction, Muscle development, Cell structure and motility
53	17906	P51667	Myosin regulatory light chain 2, ventricular/cardiac muscle isoform	MLRV						+	Muscle development, Heart development, Cell structure, Cell motility
54	17868	O70468	Myosin-binding protein C, cardiac type	MYPC3				+			Muscle contraction
55	227197	Q3UQ73	NADH-ubiquinone oxidoreductase 75 kDa subunit	Q3UQ73	-						Electron transport

Table 8: List of the differentially abundant protein spots identified by ESI/MS (continued)

spot #	accesion number		name	abv.	regulation in male vs. WT			regulation in female vs.WT			
	GeneID NCBI	Swiss Prot			ET+/+	eNOS-/-	ET+/+ eNOS-/-	ET+/+	eNOS-/-	ET+/+ eNOS-/-	Biological function
56	227197	Q3UQ73	NADH-ubiquinone oxidoreductase 75 kDa subunit	Q3UQ73			+				Electron transport
57	52633	Q9JHW2	Nitrilase homolog 2	NIT2				-			Other carbon metabolism
58	52633	Q9JHW2	Nitrilase homolog 2	NIT2			+				Other carbon metabolism
59	268373	P17742	Peptidyl-prolyl cis-trans isomerase A	PPIA	+	+	+				Protein folding, Nuclear transport, Immunity and defense
60	268373	P17742	Peptidyl-prolyl cis-trans isomerase A	PPIA	+	+	+				Protein folding, Nuclear transport, Immunity and defense
61	18477	P35700	Peroxiredoxin-1	PRDX1	+	+	+		+		Antioxidation and free radical removal
62	18477	P35700	Peroxiredoxin-1	PRDX1				+	+		Antioxidation and free radical removal
63	11757	P20108	Peroxiredoxin-3	PRDX3		+					Antioxidation and free radical removal
64	11757	P20108	Peroxiredoxin-3	PRDX3				+			Antioxidation and free radical removal
65	11758	O08709	Peroxiredoxin-6	PRDX6	-		-	-		-	Antioxidation and free radical removal
66	11758	O08709	Peroxiredoxin-6	PRDX6	+	+	+	+	+	+	Antioxidation and free radical removal
67	10455	Q9WUR2	Peroxisomal 3,2-trans-enoyl-CoA isomerase	PECI	-		-	-		-	Fatty acid metabolism
68	226041	Q8BZF8	Phosphoglucomutase-like protein 5	PGM5	-						Monosaccharide
69	26442	Q9Z2U1	Proteasome subunit alpha type-5	PSA5					+	+	Proteolysis
70	68263	Q9D051	Pyruvate dehydrogenase E1	ODPB			+				Carbohydrate metabolism
71	106393	Q7TQ48	Sarcalumenin	SRCA					-		Muscle contraction, Muscle development
72	20655	P08228	Superoxide dismutase [Cu-Zn]	SODC	+						Immunity and defense
73	22139	P07309	Transthyretin	TTHY	+	+					unclassified
74	21991	P17751	Triosephosphate isomerase	TPIS	+						Glycolysis
75	21991	P17751	Triosephosphate isomerase	TPIS					+	+	Glycolysis
76	233870	Q8BFR5	Elongation factor Tu, mitochondrial	EFTU	-						Protein biosynthesis
77	22388	O88342	WD repeat-containing protein 1	WDR1					-		Cell motility

Table 8: List of the differentially abundant protein spots successfully identified by ESI/MS in ET+/+, eNOS-/- and ET+/+eNOS-/- male and female three months old mice versus WT. The spot numbers refer to the figure 18. The NCBI gene ID, Swiss Prot protein ID, full name, abbreviation (abv.) are shown. + means an elevated abundance versus WT of at least 1.6 fold. – means a reduced abundance versus WT of at least 0.625 fold. All results are significant: Student's t-test $p<0.05$. The respective biological functions are shown as given by the classification system Panther.

3.6.5 Observed post-translational modifications

Virtually all proteins are post-translationally modified. Numerous organic residues can be bound on specific sites of the proteins. In many cases, these modifications play a major role in the function, three dimensional structure and localization of proteins. They are therefore of high biological relevance. ESI/MS technology in combination with specialized protein databases is

able to predict modifications by comparison between the observed and theoretical peptide mass and in function of the mass of the residues (figure 20).

A MS/MS Fragmentation of **MVNPTVFFDITADDEPLGR**
Found in **PPIA_MOUSE**, (spot #59)

Monoisotopic mass of neutral peptide Mr(calc): 2016.9899
Variable modifications: N-term : Met-loss+Acetyl (Protein N-term M)
Ions Score: 77 Expect: 1.7e-07

#	b	Seq.	y	#
1	43,0179	M		19
2	142,0863	V	2005,9865	18
3	256,1292	N	1906,9181	17
4	353,1820	P	1792,8752	16
5	454,2296	T	1695,8224	15
6	553,2981	V	1594,7748	14
7	700,3665	F	1495,7064	13
8	847,4349	F	1348,6379	12
9	962,4618	D	1201,5695	11
10	1075,5459	I	1086,5426	10
11	1176,5936	T	973,4585	9
12	1247,6307	A	872,4108	8
13	1362,6576	D	801,3737	7
14	1477,6846	D	686,3468	6
15	1606,7272	E	571,3198	5
16	1703,7799	P	442,2772	4
17	1816,8640	L	345,2245	3
18	1873,8855	G	232,1404	2
19		R	175,1190	1

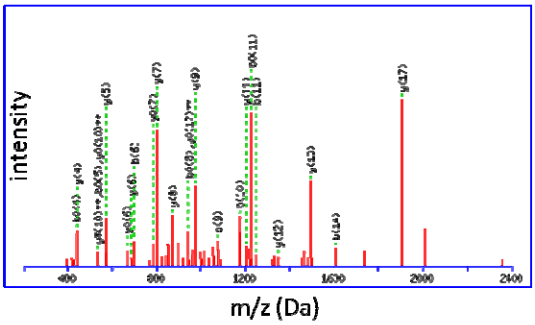

B MS/MS Fragmentation of **MVNPTVFFDITADDEPLGR**
Found in **PPIA_MOUSE**, (spot #60)

Monoisotopic mass of neutral peptide Mr(calc): 2001.9793
Variable modifications: N-term : Met-loss (Protein N-term M)
Ions Score: 79 Expect: 5.3e-08

#	b	Seq.	y	#
1	1,0073	M		19
2	100,0757	V	2005,9865	18
3	214,1186	N	1906,9181	17
4	311,1714	P	1792,8752	16
5	412,2191	T	1695,8224	15
6	511,2875	V	1594,7748	14
7	658,3559	F	1495,7064	13
8	805,4243	F	1348,6379	12
9	920,4513	D	1201,5695	11
10	1033,5353	I	1086,5426	10
11	1134,5830	T	973,4585	9
12	1205,6201	A	872,4108	8
13	1320,6471	D	801,3737	7
14	1435,6740	D	686,3468	6
15	1564,7166	E	571,3198	5
16	1661,7694	P	442,2772	4
17	1774,8534	L	345,2245	3
18	1831,8749	G	232,1404	2
19		R	175,1190	1

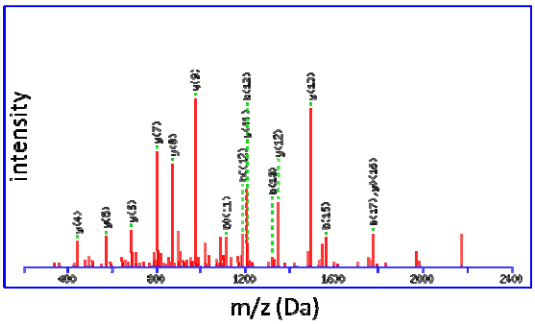

Figure 20: Comparison of the N-terminal peptides from two spots identified as Peptidyl-prolyl cis-trans isomerase A (spots #59 and #60). The mass of the y ions (peptide fragment charged on the C-terminus), are the same in both spots, the b ions (peptide fragment charged on the N-terminus) are all 42 Da heavier in the spot #59 (A) than in the spot #60 (B), suggesting the presence of an acetyl group at the N-terminus. Both peptides lack the initial methionine.

Analyses of mass spectra revealed post-translational modifications on the following fifteen protein spots (table 9):

spot #	protein	modification	residue
10	ATPA	methylation	S483
15	COF1	triacetylation	N-terminal
16	COF2	triacetylation	N-terminal
24	ETHE1	ADP-ribosylation	S14
29	GSTM1	M1 loss; acetylation	N-terminal
37	IVD	O-linked glycosylation	S32
38	LDB3	M1 loss; acylation	N-terminal
39	LDB3	M1 loss; acylation	N-terminal
40	LDB3	degradation	
46	ECHA	oxidation	D482
47	ECHA	oxidation	D482
51	MLRV	degradation	
52	MLRV	degradation	
59	PPIA	M1 loss; acetylation	N-terminal
60	PPIA	M1 loss	N-terminal

Table 9: Post-translational modifications observed in the differentially abundant proteins. ADP: adenosine phosphate, M1: initial methionine.

Please note that this list is not exhaustive since the sequence coverage of the proteins is never complete being between 20% and 60%. The size of the protein on the gels was for MLRV (spot #51 and #52) and LDB3 (spot #40) smaller than the expected size; the sequencing coverage indicated that these spots represented degradation products of the protein.

3.6.6 Validation

In this final section of the results, particular attention has been given to a series of proteins selected for the importance of their functions (oxidative stress, contractibility, and metabolism) and their particular pattern on 2DE gels (isoelectric shift, molecular weight shift, and additional spots). By the use of specific antibodies on 2D and 1D Western Blot, I sought to clarify, confirm and specify some findings from the proteomics study.

3.6.6.1 Oxidative stress

3.6.6.1.1 Peroxiredoxin-6 (PRDX6)

PRDX6 was found in two different spots (spot #65 and #66) with same molecular weight but different isoelectric points. The basic form was found only in WT and eNOS-/- mice whereas the acidic form was found in ET+/+, eNOS-/- and ET+/+eNOS-/- mice but not in WT (figure 21A). Despite the change in isoelectronic point of PRDX6 between the two spots, no differences were found comparing the corresponding mass spectra.

Moreover, 2D Western Blot using a specific anti-PRDX6 antibody confirmed the presence of both spots in eNOS-/- mice, the presence of the acidic form only in both ET+/+ and ET+/+eNOS-/- mice. In WT mice, beside the basic form, the acidic form was also visible; this is probably due to the higher sensitivity of immunoblotting technology compared to silver staining (figure 21B). 2D-WB using an antibody specific for the overoxidized forms of PRDX6 (PRDX6-SO3) demonstrated that these two spots did not represent overoxidized PRDX6. However, the presence of two additional spots of higher molecular weight in ET+/+, eNOS-/- and ET+/+eNOS-/- mice, but not in WT, were detected using the PRDX6-SO3 antibody. The total amount of PRDX6 (the sum of both spots intensity) was higher in ET+/+, eNOS-/- and ET+/+eNOS-/- male mice (figure 21A). These results were confirmed by 1D-WB at least by trend, except for male ET+/+eNOS-/- mice. 1D-WB in nine months old animals revealed the age-related expression pattern of PRDX6. At this age, PRDX6 was still more abundant in ET+/+ mice compared to WT (figure 21C).

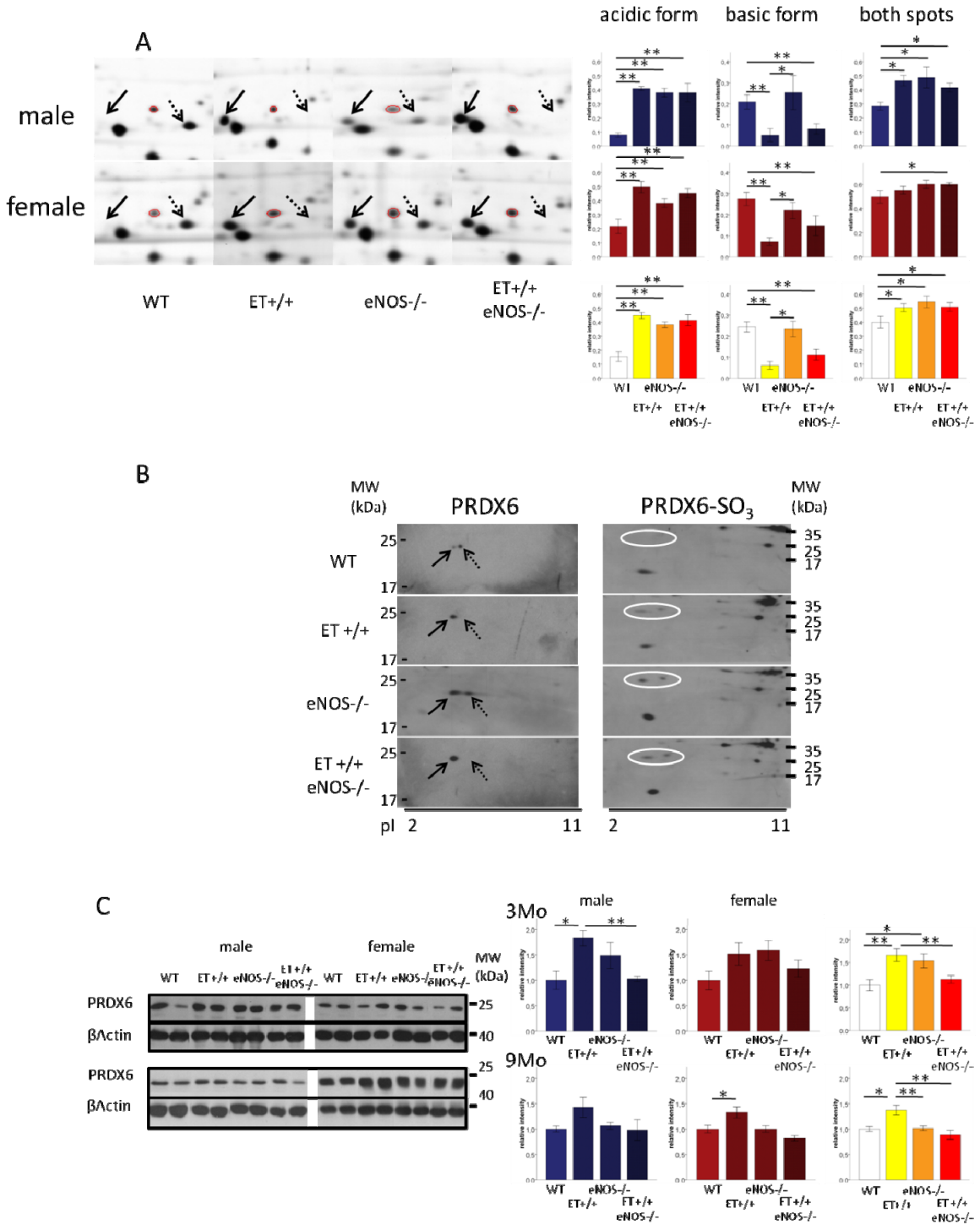

Figure 21: (A) Two dimensional gel pictures of the spots identified as PRDX6 (spot #65 and #66) in the heart of three months old male and female mice. For each group, a typical picture from one heart is shown. The solid arrow show the acidic form of PRDX6 (only in ET+/+, eNOS-/- and ET+/+eNOS-/- mice), the doted arrow shows the basic form of PRDX6 (only in WT and eNOS-/- mice). The diagrams show the relative intensity of the acidic and basic spots as well as the sum of both. Mann Whitney U-test: * $p<0.05$, ** $p<0.01$. (B) (left) Confirmation of the presence of two spots on 2D WB using an antibody

against PRDX6. The solid arrow show the acidic form of PRDX6, the doted arrow shows the basic form of PRDX6 (only in WT and eNOS-/- mice). (right) 2D-WB using an antibody against the overoxidized forms of PRDX6 (PRDX6-SO3). The two additional spots observed in ET+/+, eNOS-/- and ET+/+eNOS-/- mice are in white circles. (C) 1D-WB analysis of PRDX6 protein abundance in the heart of WT, ET+/+, eNOS-/- and ET+/+eNOS-/-, male and female three (3Mo) and nine months (9Mo) old mice. The diagrams show the quantification of the band intensity normalized to β-actin. n=6. Mann Whitney U-test: * $p<0.05$, ** $p<0.01$.

3.6.6.1.2 Peroxiredoxin-1 (PRDX1)

PRDX1 was also found in two different spots (spot #61 and #62). In males, the basic form was more abundant in ET+/+, eNOS-/- and ET+/+eNOS-/- than in WT mice. In females, the acidic form was more abundant in ET+/+ and eNOS-/- mice; the basic form was more abundant in eNOS-/- female mice only (figure 22A).

The total amount of PRDX1 (sum of both spots) was also higher in ET+/+, eNOS-/- and ET+/+eNOS-/- than in WT male mice and was higher in eNOS-/- and ET+/+eNOS-/- than in WT female mice (figure 22A). Western blot analyses confirmed these results, at least by trend, except, like PRDX6, for male ET+/+eNOS-/- mice (figure 22B). Western blot analyses showed additionally that in nine months old ET+/+, eNOS-/- and ET+/+eNOS-/- female, PRDX1 abundance was reduced compared to WT, while no change were observed in male mice (figure 22B).

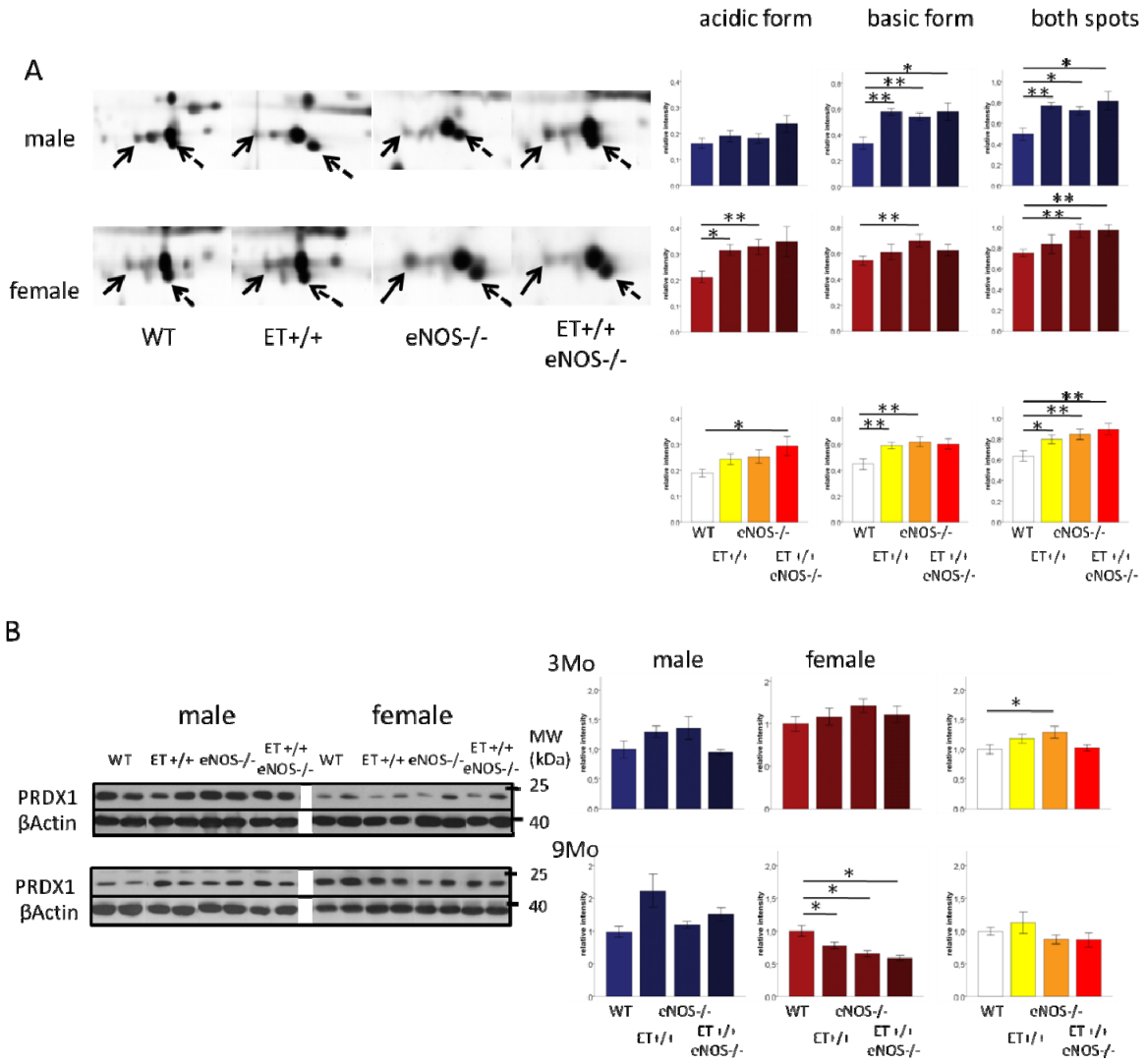

Figure 22:(A) Two dimensional gel pictures of the spots identified as PRDX1 (spot #61 and #62) in the heart of three months old male and female mice. For each group, a typical picture from one heart is shown. The solid arrow show the acidic form of PRDX1, the doted arrow shows the basic form of PRDX1. The diagrams show the relative intensity of the acidic and basic spots as well as the sum of both. Mann Whitney U-test: * $p<0.05$, ** $p<0.01$. (B) 1D-WB analysis of PRDX1 protein abundance in the heart of WT, ET+/+, eNOS-/- and ET+/+eNOS-/-, male and female three and nine months old mice. The diagrams on the right show the quantification of the band intensity normalized to β-actin. n=6. Mann Whitney U-test: * $p<0.05$, ** $p<0.01$.

3.6.6.1.3 Superoxide dismutase [Cu-Zn] (SODC)

2DE analysis showed that SODC (spot #72) was more abundant in ET+/+ mice than in WT (figure 23A). 1D Western Blot analysis confirmed this and confirmed that SODC was less abundant in ET+/+eNOS-/- than in ET+/+ male mice (figure 23B). In nine months old ET+/+ and ET+/+eNOS-/- male mice, SODC was more abundant than in WT and eNOS-/-. In females, SODC was less abundant in the three transgenic and knock-out mice compared to WT (figure 23B).

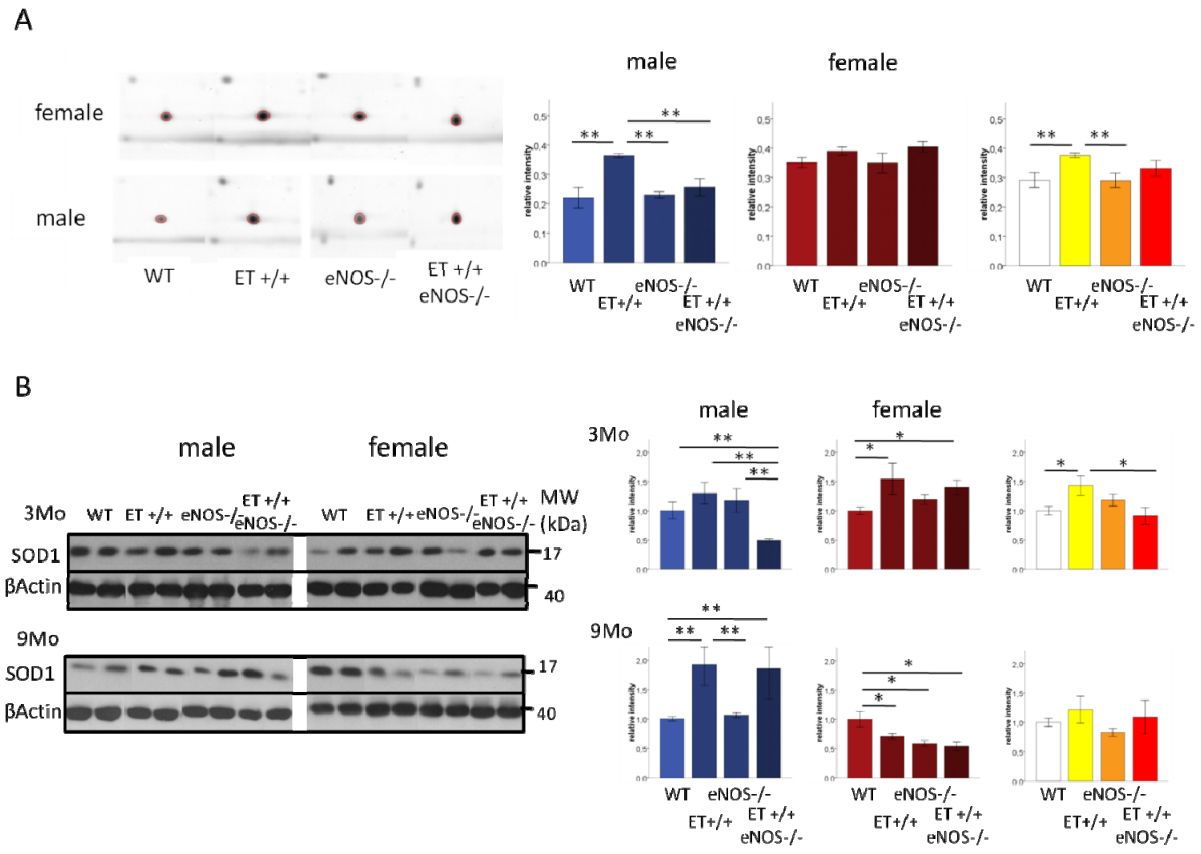

Figure 23: (A) Two dimensional gel pictures of the spots identified as SODC (spot #72) in the heart of three months old male and female mice. For each group, a typical picture from one heart is shown. The diagrams show the relative intensity of the spots. Mann Whitney U-test: * p<0.05, ** p<0.01. (B) 1D-WB analysis of SODC protein abundance in the heart of WT, ET+/+, eNOS-/- and ET+/+eNOS-/-, male and female three and nine months old mice. The diagrams show the quantification of the band intensity normalized to β-actin. n=6. Mann Whitney U-test: * p<0.05, ** p<0.01.

3.6.6.1.4 Glutathione S transferase Mu 2 (GSTM2)

An additional spot identified as GSTM2 (spot #30), an antioxidant enzyme, was found in ET+/+ and ET+/+eNOS-/- male and female mice (figure 24), which was not visible in WT.

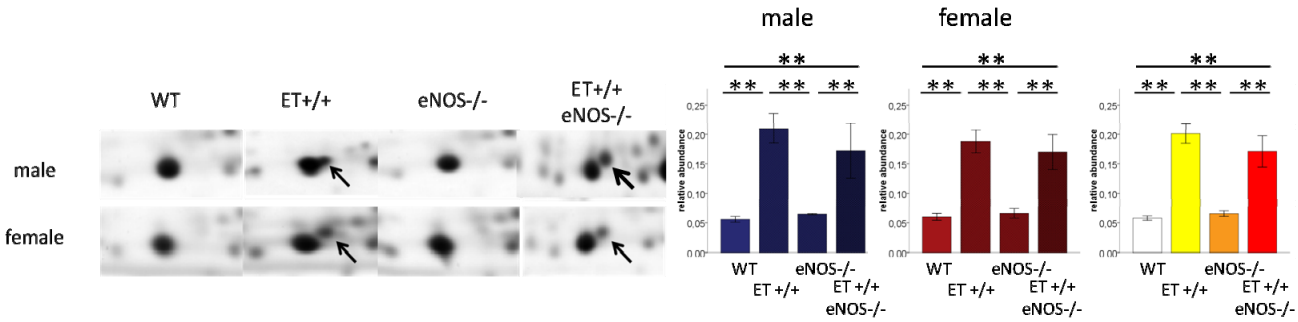

Figure 24: Two dimensional gel pictures of the spot identified as GSTM2 (spot #30, arrow) in the heart of three months old male and female mice. For each group, a typical picture from one heart is shown. The diagrams show the quantification of the spot intensity. Mann Whitney U-test: ** $p<0.01$.

3.6.6.2 Contractile machinery

3.6.6.2.1 Myosin regulatory light chain 2, ventricular/cardiac muscle isoform (MLRV)

Three spots have been identified as MLRV. One was at the expected size, 20kDa (spot #53). The spots #51 and #52 were found below 15kDa indicating degraded forms of the protein. The sequence coverage of the MS indicated that these spots correspond to the N-terminal half of MLRV (figure 25A). These two forms were more abundant in female ET+/+ mice compared to WT and ET+/+eNOS-/- mice (figure 25A). 1D-WB using an antibody against the N-terminal part of MLRV showed that the 20kDa protein was more abundant in eNOS-/- male and female mice, as well as in ET+/+eNOS-/- female mice, compared to WT (figure 25B).

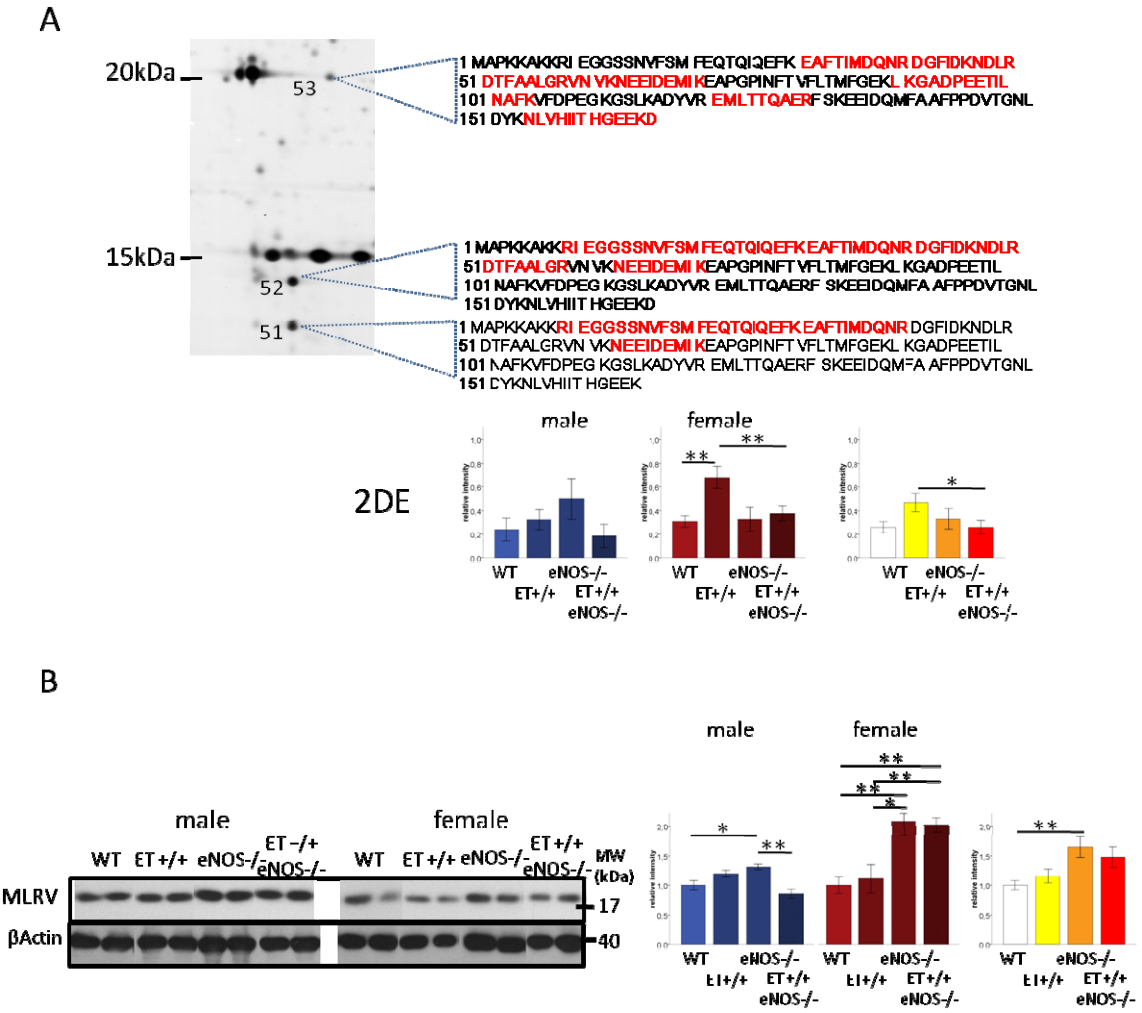

Figure 25: (A) Representative two dimensional gel picture of the spots identified as MRLV (spots 51, #52, #53) in the heart of three months old mice and the corresponding sequencing coverage in red. The diagrams show the relative intensity of the sum of both spots corresponding to the degraded forms (<15kDa) in male and female three months old mice. Mann Whitney U-test: * p<0.05, ** p<0.01. (B) 1D-WB analysis of MRLV protein abundance in the heart of WT, ET+/+, eNOS-/- and ET+/+eNOS-/-, male and female three months old mice. The diagrams show the quantification of the band intensity normalized to β-actin. n=6. Mann Whitney U-test: * p<0.05, ** p<0.01.

3.6.6.3 Metabolic proteins

3.6.6.3.1 3-methylcrotonyl-CoA carboxylase alpha subunit (MCCA)

MCCA was found in two spots (spots #43 and #44). Only in eNOS-/- mice, both male and female, were both spots less abundant than in WT (figure 26A). 2D Western Blot using a specific antibody against MCCA revealed the presence of four different isoforms. In eNOS-/- mice, two additional more basic spots were visible (figure 26B).

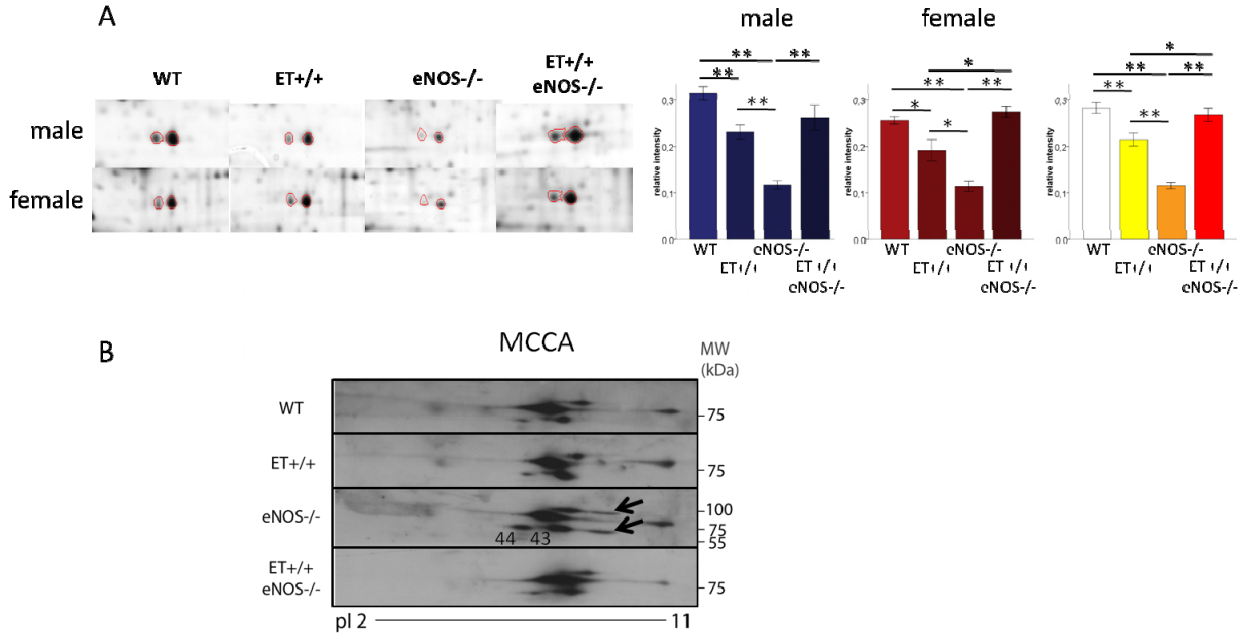

Figure 26: (A) Two dimensional gel pictures of the spots identified as MCCA (spots #43 and #44) in the heart of three months old male and female mice. For each group, a typical picture from one heart is shown. The diagrams on the right show the relative intensity of the sum of both spots. Mann Whitney U-test: * $p<0.05$, ** $p<0.01$. (B) 2D-WB analysis of MCCA in the heart of WT, ET+/+, eNOS-/- and ET+/+eNOS-/- three months old mice. The arrows show the additional spots observed in eNOS-/- mice. The corresponding spots #43 and #44 are indicated.

4 Discussion

The starting point of the project, even before the crossbreeding of the ET+/+ and eNOS-/- mice, was the will to elucidate the physiological and molecular mechanisms preventing ET+/+ mice to suffer from elevation of blood pressure. Because of the recognized potent vasoconstrictive properties of ET-1, Theuring *et al.*, the initiators of the project in the early 1990s, had expected an elevation of blood pressure in these mice. Because the endothelin receptors reorganization, at least in lungs[60] and kidneys,[88] was not sufficient to explain the lack of hypertension, attention has been paid to probable compensatory effects mediated by molecules from outside the endothelin system. Representing a reported natural functional antagonist of ET-1, NO was first assumed to compensate ET-1 actions. In fact, following works on ET+/+ mice demonstrated that iNOS expression was enhanced in the vasculature and NO bioavailability was elevated in the kidney and in the vasculature. Most importantly, at the systemic level, elevation of blood pressure after intravenous injection of L-NAME was more pronounced in ET+/+ mice than WT.[87-89] The equilibrium between NO and ET-1 seemed to be preserved in ET+/+ mice but at a higher level. Therefore, the additional inactivation of eNOS, the most important source of NO, in ET+/+ mice was thought to unmask the pure ET+/+ induced phenotype and should have consequently worsen the cardiac phenotype. To test this hypothesis, ET+/+ mice have been crossbred with eNOS-/- mice. The four resulting genotypes, WT, ET+/+, eNOS-/- and ET+/+eNOS-/- mice, were studied by employing physiological, histological and molecular techniques.

Heart catheterization procedure revealed that, while eNOS-/- mice developed diastolic dysfunctions, ET+/+eNOS-/- mice did not. The left ventricle dysfunctions in eNOS-/- mice were characterized by a reduced velocity of pressure fall, an elevated left ventricular end diastolic blood pressure (LVEDP), and a slower cardiac relaxation as shown by reduced relaxation constant Tau depicting an enhanced heart stiffness. Heart stiffness and high LVEDP are two symptoms of diastolic dysfunctions, i.e. a reduced ability of the heart to correctly fill because of defect in relaxing. All these parameters went back to WT level in ET+/+eNOS-/- mice and relaxation constant Tau was even better in ET+/+ than WT mice. These findings did not only invalidate the primary hypothesis but strongly suggested that overexpression of ET-1 could be beneficial for cardiac functions, even in absence of eNOS.

An eventuality would be that a natural selection over the generations provided the ET+/+eNOS-/- mice with a natal predisposition for a better cardiac phenotype. However, systolic blood pressure was elevated in both eNOS-/- and ET+/+eNOS-/- mice but when blood pressure kept on increasing with age in eNOS-/- mice, this did not happen in ET+/+eNOS-/- mice suggesting that protective mechanisms took place during the life of the animals.

Kalk *et al.* previously demonstrated a similar functional effect in ET+/+ mice lacking the inducible NOS (ET+/+iNOS-/-). These mice are characterized by a better heart stiffness constant than ET+/+ mice and a lower LVEDP than both ET+/+ and iNOS-/- mice.[89]

Analysis performed in Prof. Hocher's laboratory showed that brain natriuretic peptide (BNP) serum level was elevated in both ET+/+ and ET+/+eNOS-/- mice, but not in eNOS-/-. BNP, clinically considered as a biomarker for cardiovascular disease, acts as a vasodilator through the activation of cGMP production. Cardioprotective effects of BNP can be stimulated by ET-1.[154]

This could only in part explain why ET+/+eNOS-/- mice displayed better cardiac functions than eNOS-/- mice. My research aimed at answering this question by exploring the underlying molecular mechanisms, using particularly a proteomics approach. The results are now being discussed.

4.1 Expression of ET components

In this thesis, the cardiac expression pattern of ET-1 was first analyzed at the mRNA level by qRT-PCR. ET receptors expression was analyzed at the mRNA and protein level, by *in situ* hybridization and WB, respectively.

In ET+/+ and ET+/+eNOS-/- nine months old male mice, total cardiac ET-1 expression was enhanced twofold compared to WT (table 6). The expression of the human transgene was moderate and participated in 18% to 32% of total ET-1 expression depending on the groups (table 6). ET-1 playing an important role in development,[155] a too high level of ET-1 transgenic expression could have been lethal at birth. In eNOS-/- male mice, endogenous ET-1 was also more expressed depicting here again the negative feedback of NO on ET-1 expression and confirming that elevation of ET-1 expression could participate in hypertension in eNOS-/- mice, as previously suggested by Labonté *et al.*.[99] Thus, at the age of nine months, ET-1 expression levels were similar between eNOS-/- and ET+/+eNOS-/- mice; however, one should be aware

that chronic transgenic overexpression of ET-1 must have conditioned both ET+/+ and ET+/+eNOS-/- mice, but not eNOS-/-. Taking into account the proteome plasticity, this phenomenon must have physiological consequences. Moreover, mRNA expression does not reflect necessarily protein level and processing of big ET-1 can be different between the groups.

In female eNOS-/- and ET+/+eNOS-/- mice, ET-1 was less expressed than in males (table 6). This could reflect the less pronounced cardiac dysfunctions and hypertrophy observed in female eNOS-/- mice than in males.[95] Moreover nNOS and iNOS expressions are enhanced in eNOS-/- females but not in males, suggesting that females can better compensate eNOS deficiency than males. nNOS and iNOS derived NO could thus repress ET-1 production in female eNOS-/- mice.[95]

In situ hybridization revealed that cardiac expression of ETAR was unchanged in nine months old crossbred male animals. ETBR mRNA expression, however, was reduced in this group compared to WT (figure 5), illustrating the higher responsiveness of ETBR than ETAR to stress.[156] At the protein level, WB analysis confirmed these results. ETBR was additionally reduced in eNOS-/- mice to a similar extent (figure 6). This is in line with previous observations by Labonté *et al.*, who showed a reduced ETBR expression and limited response to a selective ETBR antagonist in the heart of eNOS-/- mice.[98, 99] ETBR being responsible for ET-1 clearance, the reduced ETBR expression in eNOS-/- mice could lead to an elevated responsiveness of ETAR to circulating ET-1. This question could be clarified by a pharmacological approach using ETBR and ETAR specific antagonists.

To summarize, expression of ET-1 and its receptors was similar between eNOS-/- and ET+/+eNOS-/- nine months old mice. Molecular mechanisms induced by the transgenic overexpression of ET-1 and taking place over time should therefore be responsible for the physiological differences between these two groups.

4.2 Histology

4.2.1 Interstitium

4.2.1.1 Matrix protein expression

Because the interstitial extracellular matrix plays a major role in the elasticity of the myocardium, its composition is closely related to cardiac functions. The analysis of ECM composition in the different groups brought therefore insights into the molecular mechanisms.

Sirius red staining analyses showed that all three transgenic, knock-out and crossbred male mice had a stronger ECM protein deposition in the cardiac interstitium than WT mice, when the female had not (figure 9). Both sexes taken together, ET-1 overexpression promoted ECM proteins accumulation. This is in line with the potent profibrotic effects of ET-1.[60] In nine months old animals, only ET+/+eNOS-/- mice displayed an elevated matrix protein expression, which can be explained by the counterregulation of NO on ET-1 profibrotic effects.[157]

Despite of all this, at this age, cardiac functions were reduced only in eNOS-/- mice. Fibrillar collagen deposition is responsible for diastolic and systolic dysfunctions,[158, 159] and myocardial stiffening.[160] Collagen I and III, the two most important components of the extracellular matrix, belong to the fibrillar type of ECM proteins. Expression of these two types of collagen remained however unchanged in older male mice (figure 14). Collagen I was, nevertheless, more abundant in female ET+/+eNOS-/- mice compared to WT. The other constituents of the matrix are proteoglycans and basement membrane proteins (e.g. laminin, fibronectin). In males, these other ECM proteins may play a role in fibrosis without necessarily affecting cardiac functions: indeed, elevation in laminin expression, but not collagen I, has been reported in cardiac interstitium of ET+/+ twelve months old male mice.[82]

4.2.1.2 Metalloprotease expression

MMPs participate in the breakdown of collagens and their deregulation can lead to collagen accumulation and matrix restructuration both leading to cardiac dysfunction.[161] MMP2 and MMP9 are the most relevant proteases in the myocardium and were therefore investigated in this study. Both sexes taken together, MMP2 and MMP9 expression was similar between the genotypes of nine months old mice (figure 13).

In female eNOS-/- and ET+/+eNOS-/- mice, MMP9 expression was reduced compared to males. The sex hormone 17ß-estradiol activates eNOS induced MMP9 expression.[162] The greater amount of estradiol production by females could thus explain the greater effect of eNOS deficiency on MMP9 expression and fibrosis development. Moreover, in case of myocardial infarction, MMP9 is less expressed in female than in male mice.[163] In smooth muscle cells, the activity of MMP9 can be however reduced by eNOS.[164] These conflicting results underline the non linear relationship between MMP expression and activity. Indeed, MMP2 activity but not expression is reduced after an L-NAME treatment induced NOS inhibition in rat cardiac tissue.[165] This could additionally suggest that, in the eNOS-/- mice, MMP2 activity was reduced if not its expression level. To get better insights in these mechanisms, further investigations would require the measurement of the activity of both MMP2 and MMP9 by applying zymography.

Fibrosis is a highly dynamic process; advanced fibrosis, particularly characterized by a reduction of fibrillar collagen crosslinking, has a deleterious impact on cardiac stiffness and functions.[166, 167] The data on fibrotic components described here, put on perspective with the cardiac physiology in the corresponding groups, suggest that the development of fibrosis observed in ET+/+eNOS-/- mice was not advanced enough to alter cardiac function. This may explain the dissociation between ECM deposition and diastolic function in this group.

4.2.2 Perivascular area

Perivascular fibrosis is an indicator for vascular dysfunction; it was thus important to take a closer look at ECM protein deposition in the perivascular area of small intracardiac arterioles. At the age of three months, perivascular fibrosis affected female ET+/+, eNOS-/- and ET+/+eNOS-/- mice, but not males (figure 10). As already shown in the interstitium, differential collagen deposition occurred between males and females and this could also happen in the vasculature. Immunostaining technique used here was unfortunately unsuitable for quantification of the different collagens in the perivascular area because of the heterogeneity of vessel size and number on the slides between the groups. Perivascular fibrosis is closely related to inflammation induced macrophage infiltration.[168] Moreover, inflammatory responses are known to be regulated by female sex hormones.[169] This can therefore explain the more prominent

perivascular ECM proteins deposition in females than in males. Because of these findings, the inflammatory status should be closely investigated in the different genetic groups of mice.

4.2.3 Cardiomyocyte diameter

An elevated myocyte diameter is an indication for cardiac hypertrophy, which is an important cardiovascular risk factor.[170] At the age of three months, eNOS-/- mice showed cardiomyocyte diameter similar to WT mice, but developed hypertrophy at the age of nine months. This age-related development is in line with the deterioration of cardiac functions in eNOS-/- mice. In crossbred animals, a cardiomyocyte enlargement was observed at three months of age (figure 11), but this hypertrophy was abolished at the age of nine months. One could postulate this reduction of cardiomyocyte size to be the result of a selective loss of hypertrophied myocytes by apoptosis. This is however questionable because the age-related loss of cardiomyocytes is responsible for the hypertrophy of the remaining myocytes.[171] Moreover, ET-1 exerts rather strong antiapoptotic effects on cardiomyocytes *in vivo*.[172] On the other hand, the molecular pathways implicated in the hypertrophic effects of ET-1 in cardiomyocytes have been described in details.[173] Therefore these findings corroborate the hypothesis that, in contrast to eNOS-/- mice, ET+/+ and ET+/+eNOS-/- mice developed mechanisms preventing cardiac hypertrophy and thus function in an age dependent manner. ET-1 is indeed necessary not only for cardiomyocyte survival but also for normal cardiac function during aging.[174]

Interestingly, in both age groups, female eNOS-/- mice had smaller cardiomyocyte diameter than males. This confirmed the previous observations by Li *et al.* describing a strong age-related cardiac hypertrophy in eNOS-/- male mice but not female.[95]

4.2.4 Cardiac arteriole morphology

ET-1 overexpression dilated small cardiac arterioles (figure 12). Whereas, at the age of three months, ET+/+ mice only displayed dilated arterioles, K. Relle showed that, in both ET+/+ and ET+/+eNOS-/- nine months old mice, lumen and media area were bigger than in WT and eNOS-/- mice. ET-1 participates in coronary vasculature tone and exerts in this vascular bed a constrictive effect.[175] On the other hand, an ET-1 induced vasodilation of the coronary

vasculature has already been observed in rodents.[176] Moreover, the coronary vasculature can regulate its morphology as reaction to changes in cardiac conditions.[177] In particular, an elevated cardiac contraction leads to coronary vasodilation.[178] Coronary vasodilation improves coronary blood flow and consequently cardiac functions.[179] Dilation of arterioles in ET-1 overexpressing mice can be seen as a regulatory mechanism; ET+/+ mice exhibited indeed a higher cardiac pulsation rate as shown by heart catheterization experiments. The consequent reduced resistance and enhanced coronary blood flow could participate in the improved cardiac functions observed in both ET+/+ and ET+/+eNOS-/- compared to eNOS-/- mice.

4.3 Proteomics

Histological investigations could only in part elucidate the cardiac physiology of ET+/+, eNOS-/- and ET+/+eNOS-/- mice. In order to get more insight into the early cardiac alteration in protein abundance explaining the phenotype observed in nine months old ET+/+eNOS-/- mice, particularly the restored cardiac functions compared to eNOS-/- mice, and to identify the underlying molecular mechanisms, the cardiac proteome of three months old animals was analyzed by using a hypothesis-free technique: Two Dimensional Electrophoresis coupled to Mass Spectrometry. In regard to the age-related pattern observed at the histological level, in particular concerning the cardiomyocyte enlargement, the molecular changes preventing the crossbred animals to develop diastolic dysfunctions should have already been initiated at the age of three months. A proteomics study in old animals would have shown the molecular consequences of the process, the present study aimed however at depicting the causes.

The method of protein separation applied here offered many advantages. First, the highly detergent buffer used for protein preparation permitted to collect cytosolic, nuclear as well as membrane proteins. Secondly, the size of the gels allows the separation of up to 2000 protein species. More than 1300 protein spots could be visualized after silver staining (figure 18). Finally, the standardization of the protocol afforded a good technical reproducibility. Moreover, biological variability within the groups was low (figure 15). On a silver stained gel, protein species with an abundance of at least 100pg per spot can be visualized. This staining shows a dynamic range of only two orders of magnitude.[180] Very low abundant proteins are therefore

not necessary visible and this is one limitation of this staining technique. However, the above listed characteristics of protein separation and staining together with the compatibility with mass spectrometry made this protocol convenient. Last but not least, because of its higher sensitivity and broader dynamic range compared to MALDI/MS, ESI/MS allowed a good identification rate of low abundant protein spots because of their enrichment in the ion trap.[181]
The primary focus was thus the comparison of eNOS-/- and ET+/+eNOS-/- mice, since these two lines were functionally clearly different. In this way, the priority was given to the analysis of the consequences of ET-1 transgenic overexpression on an eNOS-/- background. After identification and according to their biological functions, the differentially abundant proteins were grouped in the following four categories representing important biological systems playing a major role in cardiac functions: oxidative stress, contractibility, hypertrophy, and metabolism (energy and other metabolisms).

4.3.1 Oxidative stress

Reactive oxygen species (ROS) are produced principally as byproducts of aerobic respiration in the mitochondria.[182] ROS are mainly hydrogen peroxide (H_2O_2), superoxide (O_{2-}) and peroxynitrite (ONOO-). At physiological levels, ROS are believed to participate in controlling the activity of enzymes through site specific post-translational modifications.[183] In pathophysiological situations, the excessive production of ROS and the inability of the cells to reduce them via specific enzymes result in oxidative stress; ROS then damage DNA, proteins and lipids by oxidation. Oxidative stress occurs in numerous cardiovascular pathologies like hypertension,[184] heart failure,[185] and artherosclerosis.[77] The control of ROS abundance is therefore of high clinical relevance.
Peroxiredoxins form a family of six recently discovered antioxidant enzymes. They share a common domain containing an active cysteine, which can be oxidized while peroxide is reduced. They are then reduced back to the active form by specific thioredoxin reductases. By this way, they catalyze the reduction of hydrogen peroxide to water and oxygen (figure 27).[186, 187]
Peroxiredoxin-6 (PRDX6) was identified in two spots. The basic form (spot #65) was present in wild type mice but was not found in ET+/+ and ET+/+eNOS-/- mice. In these groups, only a more acidic form (spot #66) was observed. In eNOS-/- mice, both spots were present (figure 21A). 2D-

WB analysis confirmed these observations using a specific anti-PRDX6 antibody (figure 21B). Peroxiredoxin-6 exists in different states of oxidation.[188-190] According to these studies, the acidic form would correspond to an irreversibly inactive form of the enzyme after overoxidation of the cysteine 47 at the active site (sulphinic (Cys-SO_2) or sulphonic (Cys-SO_3) acid) by superoxide-derived hydrogen peroxide and appears in case of oxidative stress,[190] while the more basic protein species would represent a reduced form of peroxiredoxin-6 (Cys-SOH) (figure 27). The careful analysis of the spectra didn't reveal any difference in the mass of the peptide containing the cysteine 47, even by adding iodoacetamide to the IEF incubation solution, which protects oxidized sites from reaction with acrylamide. Others could not directly detect oxidation on the acidic form of PRDX6 either.[188, 190] Moreover, using an antibody against the overoxidized forms of PRDX6 (Cys-SO_2 and Cys-SO_3) on 2D-WB showed that none of these spots correspond to the overoxidized form (confirming the MS data) but revealed the presence of two spots present in all genetically modified animals but not in WT (figure 21B). The overoxidized forms of PRDX6 are present in case of an elevated cellular concentration of hydrogen peroxide, suggesting nevertheless an oxidative stress situation in the genetic modified animals. This assumption is supported by the fact that transgenic overexpression of ET-1 restricted to the vasculature, and eNOS deficiency as well as L-NAME induced NOS inhibition increase oxidative stress in mice.[85, 191, 192]

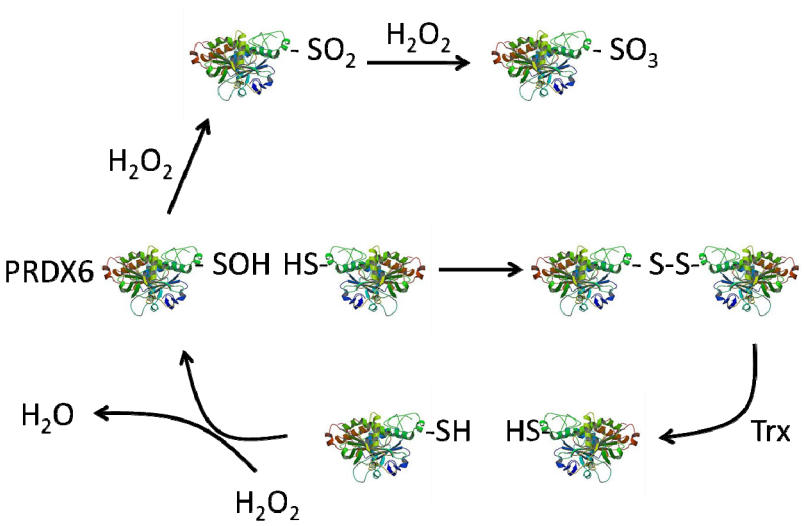

Figure 27: Enzymatic activity of PRDX6. PRDX6-SH: reduced active form. PRDX6-SOH: oxidized form. PRDX6-SO_2 and -SO_3: irreversibly inactive overoxidized forms. H_2O_2: hydrogen peroxide, Trx: thioredoxin reductase.

If the acidic form represents still a modified but reversible form due to oxidative stress, e.g. single oxidation (Cys-SOH, sulfenic acid, see figure 27),[193] the fact that in eNOS-/- mice both forms are still present could be interpreted as a reduced effectiveness of PRDX6 to scavenge peroxide.

Indeed, glutathionylation catalyzed by glutathione S-transferases seems to be required for PRDX6 activation.[194] A spot identified as glutathione S-transferase mu 2 (GSTM2, spot #30) was detected in ET+/+ and ET+/+eNOS-/- male and female mice, but not in WT and eNOS-/- mice (figure 24). Moreover, glutathione S-transferases act as antioxidant enzymes by reducing the fatty acid hydroperoxides.[195] In spontaneously hypertensive rats, GSTM2 is down regulated while oxidative stress is increased.[196]

In addition, the small heat shock protein beta 7 (HSPB7, spot #34), also known as cardiovascular heat shock protein, limits oxidative stress induced cell damage by chaperoning denatured proteins. Elevation in HSPB7 production is therefore considered as an auto-protective mechanism in cardiac tissue in response to oxidative stress.[197, 198] HSPB7 was more abundant in both ET+/+ and ET+/+eNOS-/- female mice compared to WT, but not in eNOS-/- mice (table 8).

Finally, the proteomics study revealed that superoxide dismutase-1 (SODC, spot #72) was more abundant in ET+/+ than in WT mice (figure 23A). Western Blot analysis in nine months old male mice showed an elevated abundance of SODC in both ET+/+ and ET+/+eNOS-/- mice compared to WT and eNOS-/- mice (figure 23B). Chronic overexpression of ET-1 seemed therefore to activate SODC expression and promote the reduction of superoxide.

On the other hand, aldehyde dehydrogenase 2 (ALDH2, spot #8) was less abundant in both ET+/+ and ET+/+eNOS-/- male mice (table 8). Acetaldehyde is cardiotoxic; ALDH2 is responsible for aldehyde oxidation and protects thereby from cardiac hypertrophy and contractile dysfunction.[199] Nevertheless, because acetaldehyde is a byproduct of oxidative stress, the reduced abundance of ALDH2 induced by transgenic overexpression of ET-1 may be a hint for a limited oxidative stress in these groups compared to eNOS-/- mice.

All of this suggests that, even though the three genetic modifications seemed to enhance oxidative stress, ET+/+ and ET+/+eNOS-/- mice developed stress induced molecular mechanisms to limit oxidative damages, that the eNOS-/- mice did not.

Hocher *et al.* showed previously that NO production is elevated in ET+/+ mice and that this could be beneficial by normalizing blood pressure in these mice.[88] The ambivalent role of NO has been however extensively documented.[76-78] NO can indeed react with superoxide to form peroxynitrite. Moreover, in pathological situations, uncoupled eNOS produces preferentially superoxide rather than NO.[79] Kalk *et al.* already suspected iNOS derived NO to be deleterious in aged ET+/+ mice.[89] On the other hand, acute treatment with ET-1 is known to increase production of superoxide through the activation of NADPH oxidase in cardiomyocytes.[200]

The potential reduced production of NO and eNOS derived cytotoxic products due to additional lack of eNOS in ET+/+ mice together with the protective mechanisms developed by ET+/+ and ET+/+eNOS-/- mice, as proven by the proteomics analysis, could therefore explain the restored cardiac functions in ET+/+eNOS-/- compared to eNOS-/- mice. The cytoprotective role of ET-1 in case of oxidative stress has already been mentioned recently.[43] Particularly, the activation of calcineurin by ET-1 protects against oxidative stress induced apoptosis.[201]

To confirm the relevance of oxidative stress in the genetic models presented here, it would be of interest in further investigations to test the reversibility of hypertension and the improvement of cardiac functions in eNOS-/- mice e.g. after a treatment with the ROS scavenger n-acetylcysteine[202] or with melatonin, known for its strong antioxidant properties in the cardiovascular system.[203]

4.3.2 Contractile machinery

In striated muscle, the basic contractile unit is the sarcomere built up of thick and thin filaments composed of myosin and actin, respectively. Increased intracellular calcium induces interaction between the filaments using ATP hydrolysis as energy source and triggers thereby contraction. The thin filament is primarily composed of actin, nebulin, tropomyosin, and troponin. In the thick filament, myosin is associated with myosin regulatory light chains, myosin binding proteins and others (figure 28). Changes in the expression or the post-translational state of any of these proteins can have functional consequences on the contractibility of the muscle.

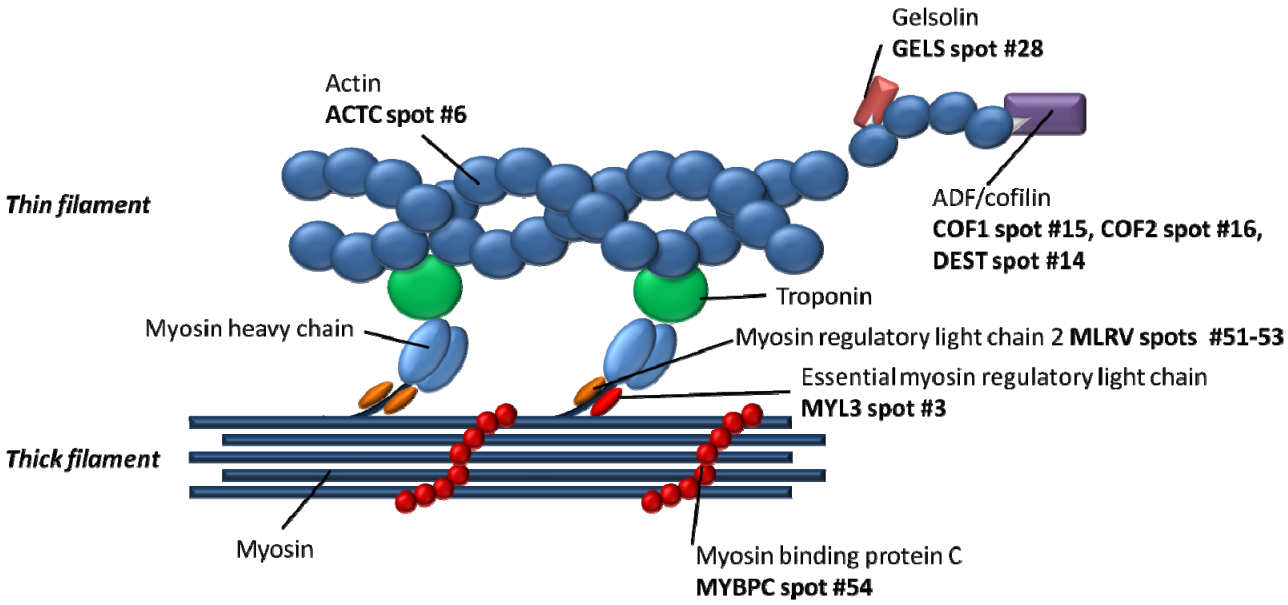

Figure 28: Schematic representation of the sarcomere. The proteins found to be differentially abundant are highlighted.

Myosin regulatory light chain 2 (MLRV) is a crucial member of the contractile machinery in myocytes. It stabilizes heavy chain myosin of the thick filament and supports the myosin neck region. MLRV is therefore essential for myofibril assembly and cardiomyocytes contractibility (figure 28).[204-206] In opposition to the essential myosin regulatory light chain (MYL3), MLRV can be phosphorylated by the myosin light chain kinase after Ca^{2+} stimulation.[207, 208] Phosphorylation of MLRV reduces time of skeletal muscle relaxation.[209] In the heart, MLRV phosphorylation increases tension production and decreases stretch activation response of cardiomyocytes.[210] Whereas its exact role is still disputed, evidences show that a mutation of the gene coding for MLRV induces cardiac myopathies.[211]

MLRV has been found in three spots (spots #51-53). Two of them represented degradation products of the protein (spots #51 and #52). These C-terminal parts of MLRV was more abundant in ET+/+ mice (figure 25A). This indicates that, added to phosphorylation, post-translational regulation of MLRV function includes degradation. The severed form of MLRV is unlikely to bind myosin and may lose its function. The presence of degradation products of sarcomeric proteins (troponin I and MYL3) has been proven in cardiac tissue after ischemia/reperfusion, particularly.[212] A proteomics study on ET-1 treated cardiomyocytes *in vitro* indicates the presence of probable breakdown products of MLRV. In this study, an acute

ET-1 treatment leads to myocyte hypertrophy and a reduced abundance of the full length MLRV.[213] A truncated form of MLRV, missing the 14 N-terminal aa, has been observed in the myocardium of rabbit after ischemia/reperfusion; this proteolysis is suspected to participate in the reduced cardiac functions.[214] It is remarkable that, in the ET+/+ mice, the proteolysis at the C-terminus did not alter cardiac functions at the age of nine months. However, in contrast to an acute ET-1 treatment,[213] ET-1 transgenic overexpression did not lead to myocyte hypertrophy. Moreover, as revealed by WB analysis using an antibody directed against the N-terminus of MLRV, MLRV is more abundant in eNOS-/- mice, both sexes, and in ET+/+eNOS-/- females but not in ET+/+ mice (figure 25B) suggesting a possible correlation between MLRV abundance and development of cardiac dysfunction. Additionally, the essential myosin regulatory chain (MYL3, spot #49) was more abundant in ET+/+ male mice (table 8). However, it has been shown that an acute ET-1 treatment does not change MYL3 abundance in cultivated cardiomyocytes.[213]
To summarize, these observations brought to light the role of ET-1 and NO in controlling myosin light chains abundance and post-translational modifications but, at the same time, revealed the discrepancy between the acute and chronic effects of ET-1 on this system.

The three actin-depolymerizing factor(ADF)/cofilin family members, destrin (DEST, spot #14), cofilin-1 and 2 (COF1, spot #15 and COF2, spot #16) were more abundant in eNOS-/- male mice. DEST and, by trend, COF2 were also more abundant in eNOS-/- females compared to WT (table 8). These proteins are actin binding proteins, which twist actin filaments in a way that prevents phalloidin to bind to actin and sever actin with concomitant generation of free ends; these processes destabilize actin filaments and enhance actin turnover, respectively (figure 28).[215] The inactive form of cofilins is phosphorylated on serine 3 by the Lim kinase.[216] The mass spectra indicated that the protein spots for COF1 and COF2 corresponded to the active non-phosphorylated form (the protein spot for phospho-COF2 has been identified somewhere else on the 2DE gels but was not differentially abundant). The role of cofilins in sarcomere disassembly and consequent contractile dysfunction in rat cardiomyocytes has been shown in primary cell culture.[206, 217] This could therefore explain the slower left ventricle relaxation in eNOS-/- mice compared to the others groups. Moreover, the activation of cofilins through

dephosphorylation by the protein phosphatase slingshot is enhanced by reactive oxygen species,[218] which was assumed to be more abundant in eNOS-/- mice (see above).

Destrin (spot #14) was additionally more abundant in ET+/+eNOS-/- mice. Its role in cardiac tissue is however less understood so far.

Finally, myosin binding protein C (MYPC3, spot #54), an essential component of the sarcomere, permits the stabilization of the thick filament and regulates myosin function during contraction.[219] MYPC3 phosphorylation accelerates myocardium stretch, improves cardiac functions[220] and plays a positive role in heart stiffness.[221] Its greater abundance in ET+/+ female mice could in part explain the reduced time of relaxation and increased contractility observed in this group.

Sarcalumenin (SRCA) is not a part of the sarcomere but is responsible for Ca^{2+} buffering in sarcoplasmic reticulum, which is essential for contraction of the cardiac muscle. SRCA (spot #71) was less abundant in female eNOS-/- mice than in WT. SRCA deficient mice develop, like eNOS-/- mice, cardiac dysfunctions characterized by longer cardiac relaxation time tau and reduced cardiomyocytes contractibility.[222]

In summary, the abundance of several proteins involved in myocyte contractibility is modulated by ET-1 and NO. Diastolic dysfunction in eNOS-/- mice might be a consequence of an elevated abundance of proteins from the ADF/cofilin family. Additional transgenic overexpression of ET-1 may restore these changes.

4.3.3 Hypertrophy

The three months old crossbred animals displayed a light cardiomyocyte hypertrophy (figure 11). At the age of nine months, however, this evolution was abolished but a moderate cardiomyocyte hypertrophy was measured in eNOS-/- mice, only. In this respect, this observations are in line with the diastolic dysfunction observed in nine months old eNOS-/- mice, since cardiac hypertrophy is a risk factor for diastolic dysfunction.[223] On the other hand, ET-1 is known to induce myocyte hypertrophy and this effect is antagonized by NO.[42] The fact that, over time, ET+/+ and ET+/+eNOS-/- mice did not develop hypertrophy could indicate that protective mechanisms mediated by ET-1 took place.

LIM domain-binding protein 3 (LDB3) is a LIM and PDZ domain containing protein with six isoforms produced by alternative splicing.[224] In ET+/+eNOS-/- male mice, LDB3 (isoform 5, spot

#38) was more abundant; in ET+/+eNOS-/- female, the isoform 1 (spot #39) and in both ET+/+ and ET+/+eNOS-/- female mice a post-translationally cleaved part of isoform 1 (spot #40) were more abundant. LDB3 plays a crucial role in the structure and function of the Z-lines in cardiomyocytes, which link the sarcomeres to one another. Mutations of LDB3 are associated with cardiac myopathies in human[225] and its cardiac specific genetic deletion in mouse causes dramatic cardiac dilation.[226] Carbonic anhydrase 2 (CAH2, spot #12) catalyses the hydration of carbon dioxide and plays a role in cardiomyocyte growth in a mechanism implicating among others the ET-1/Protein Kinase C pathway; moreover the inhibition of CAH2 reduces and prevents myocyte hypertrophy in primary mouse cell culture.[227]

The reduced abundance of CAH2 observed in ET+/+ and ET+/+eNOS-/- female mice as well as the greater abundance of LDB3 could be interpreted as protective mechanisms to prevent cardiomyocyte hypertrophy, which did not take place in eNOS-/- mice.

4.3.4 Metabolism

The maintaining of cardiac function is extremely energy consuming. Mitochondrial activity and thus energy production have logically tremendous consequences on cardiac function. The heart produces around 70% of its energy from fatty acid metabolism. Depending on the substrate availability, energy needs and pathophysiological situations, the heart can switch to glucose metabolism.[228] A switch from fatty acid, low oxygen consuming, to glucose, high oxygen consuming, metabolism is considered as cardioprotective.[229, 230] This switch is complex and can have functional consequences.[231]

The respective roles of ET-1 and NO in energy metabolism have been less investigated in comparison to their roles in cardiovascular functions and are therefore not clear. Nonetheless, evidences indicate that NOS inhibition contributes to glucose oxidation at the expense of fatty acid metabolism.[232] Other studies demonstrate, however, no effects of NO on substrate utilization in the heart even if NOS blockade enhances oxygen consumption.[233] This same study indicates that both ET-1 treatment and blockade do not change substrate utilization, but ET-1 increases oxygen consumption. Using isolated hearts from salt sensitive rats, others show increased oxygen consumption after ET receptor blockade.[234]

The current study demonstrated that proteins involved in both fatty acid and glucose metabolism are differentially abundant in the transgenic, knock-out and crossbred mice.

4.3.4.1 Fatty acid metabolism

The fatty acid β-oxidation consists of a series of four consecutive catalytic steps: dehydrogenation, hydration, NAD+-linked dehydrogenation and thiolysis (figure 29). The degradation of fatty acyl-CoA results in production of acetyl-CoA which enters the tricarboxylic acid (TCA) cycle. Each step is realized by different enzymes accordingly to the length of the carbon chain. Some enzymes are monofunctional; others are multifunctional, which means that they are composed of different subunits, each of them catalyzing different steps.

The proteomics study revealed that six differentially abundant proteins play a role in fatty acid metabolism (THIM, spot #3; CACP, spot#13; FABPH, spot #26; HCDH spot #35; ECHA, spots #46 and #47 and PECI, spot #67) (table 8 and figure 29). The genes coding for all these proteins are targets of the transcription factor peroxisome proliferator-activated receptor alpha (PPARα).[235, 236] PPARα is indeed a strong activator of fatty acid β-oxidation. The role of both ET-1 and NO in the modulation of PPARα effects has been shown in several studies. NO contributes to the protective effects of PPARα after myocardial infarction.[237] PPARα can inhibit ET-1 expression, independently from NO or through the NO-Protein Kinase C pathway.[237-239] In general, the activation of PPARα correlates with a reduction of ET-1 expression and elevation of NO. Interestingly, in ET+/+eNOS-/- mice, the four differentially abundant PPARα targets are all less abundant than in WT, suggesting an inhibition of PPARα and consequent reduction of the fatty acid β-oxidation in this group.

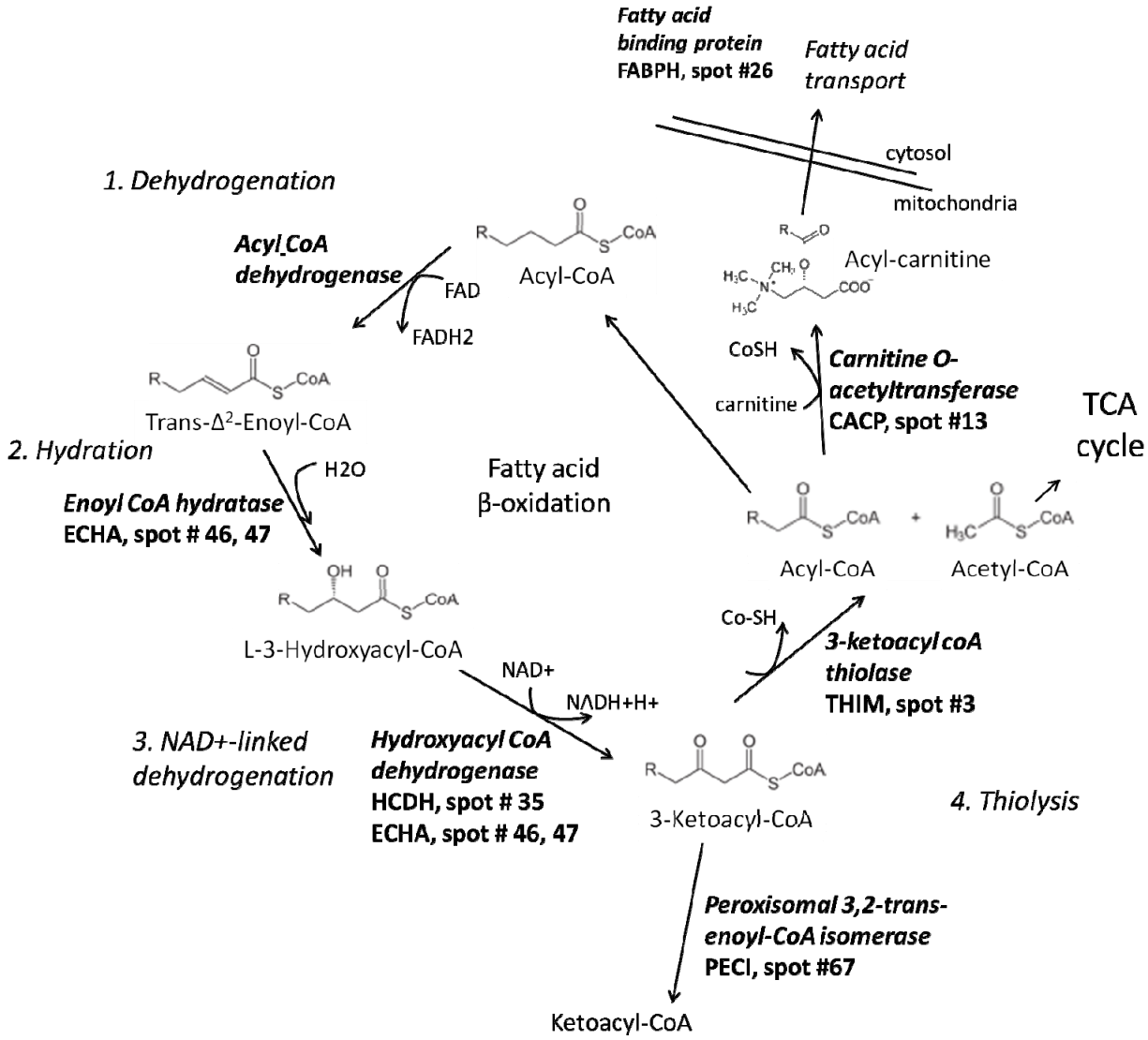

Figure 29: Schematic representation of the fatty acid β-oxidation. The enzymes found to be differentially abundant are highlighted.

In ET+/+eNOS-/- female mice, the short chain 3-hydroxyacyl-CoA dehydrogenase (HCDH) was less abundant than in WT. 3-hydroxyacyl-CoA dehydrogenases catalyze the third step of fatty acid oxidation.[240] The trifunctional enzyme subunit alpha (ECHA), which includes the long-chain enoyl-CoA hydratase and long chain 3-hydroxyacyl-CoA dehydrogenase domains (second and third steps of fatty acid oxidation, respectively) was also less abundant in ET+/+eNOS-/- female mice but more abundant in eNOS-/-. In ET+/+eNOS-/- male mice, 3-ketoacyl coenzyme A thiolase (THIM), the enzyme involved in the last step of β-oxidation, was less abundant than in WT (figure 29).

Peroxisomal 3,2-trans-enoyl-CoA isomerase (PECI), essential for unsaturated fatty acid β-oxidation in the peroxisome but also in the mitochondria,[241] was less abundant in ET+/+ and ET+/+eNOS-/- male and female mice compared to WT, but not in eNOS-/-.

On the other hand, carnitine O-acetyltransferase (CACP) abundance was reduced in eNOS-/- mice. Carnitine is essential for the mitochondrial fatty acid oxidation, particularly in the myocardium, because acyl-carnitine, the product of CACP, is the form of transport of fatty acids through the different cellular compartments (figure 29). Nevertheless, CACP abundance and activity is reduced in a model for pulmonary hypertension – where the NO system is compromised – and is associated with a reduced mitochondrial function[242] which can be responsible for reduced heart functions.[243] Most interestingly, carnitine and acyl-carnitine have antioxidant effects on the cardiovascular system, by reducing lipid peroxide formation.[244, 245] It was suggested above that eNOS-/- mice showed a reduced ability to scavenge peroxide.

Taken together, these data would indicate that fatty acid metabolism is refrained in the ET+/+eNOS-/- mice compared to the other groups, particularly compared to eNOS-/- mice. Because cardiac functions were maintained in ET+/+eNOS-/- mice, one could expect that the reduced utilization of fatty acid had for consequences a higher glucose metabolism, which is cardioprotective; this will be discussed in the next paragraph.

4.3.4.2 Glucose metabolism

The myocardium produces only 30% of its energy from glucose but in pathological situations this metabolism is preferred because of its better efficiency.

Four proteins involved in glucose metabolism were more abundant in the different genetic models: TPIS (spots #74) und G3P (spot #31) in ET+/+ male and female, respectively; TPIS (spot #75) in eNOS-/- female; and PYGB (spot #32), ODPB (spot #70) and TPIS (spot #75) in ET+/+eNOS-/- male and female respectively (table 8 and figure 30).

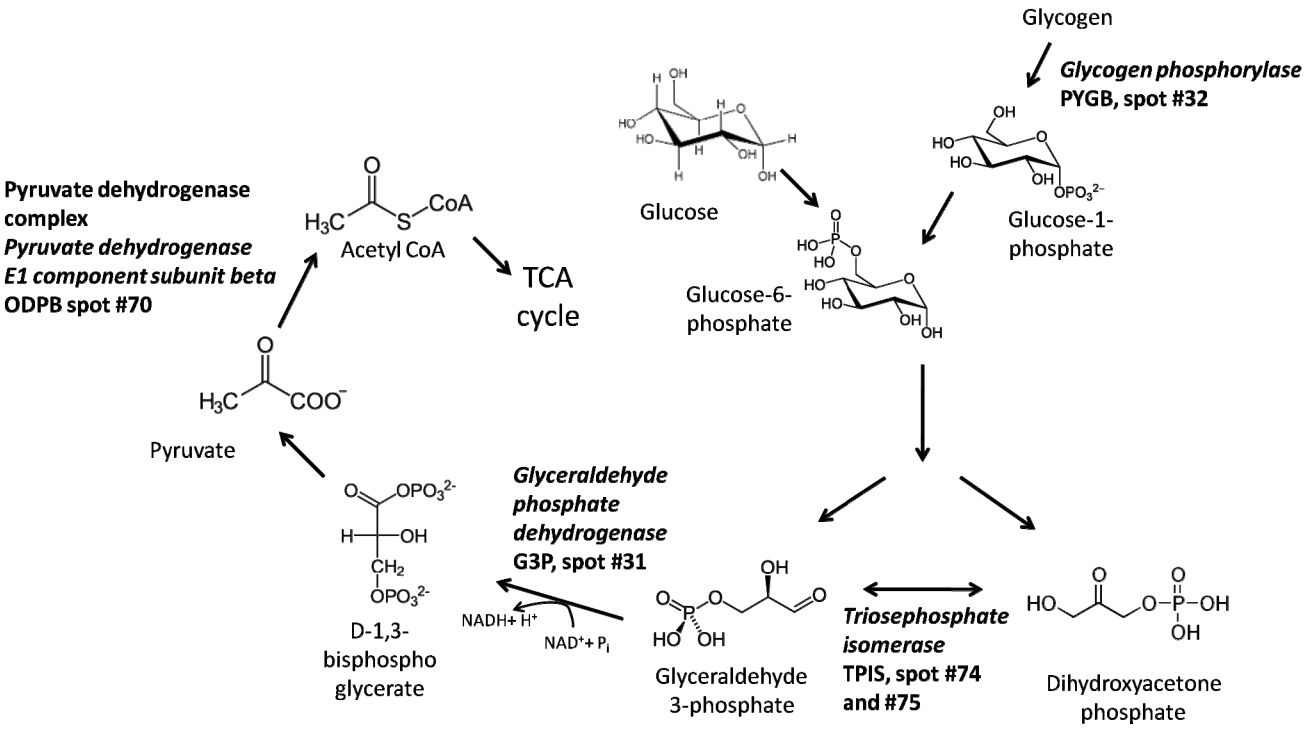

Figure 30: Schematic representation of the glycolysis. The proteins found to be differentially abundant are highlighted.

In ET+/+eNOS-/- mice, three enzymes responsible for glucose metabolism were thus more abundant, in eNOS-/- mice only one.

ODPB is a subunit of the pyruvate dehydrogenase complex (PDH), which catalyses the last step of glycolysis before acetyl CoA enters the TCA cycle (figure 30). Activation of PDH enhances glucose oxidation and consequently improves cardiac function.[246] ODPB has been shown to be repressed by NO.[247] In addition, glycolysis correlates positively with ET-1 expression.[248] In ET+/+eNOS-/- male mice ODPB is indeed more abundant.

Triosephosphate isomerase (TPIS) was more abundant in ET+/+ male and in both eNOS-/- and ET+/+eNOS-/- female mice compared to WT. TPIS facilitates glycolysis by converting dihydroxyacetone phosphate into glyceraldehyde-3-phosphate and is therefore important for an efficient energy production (figure 30). ET-1 overexpression additionally enhanced the abundance of G3P, promoting this way glycolysis.

Finally, glycogen phosphorylase (PYGB), more abundant in ET+/+eNOS-/- mice, catalyses the first step of glycogenolysis (figure 30). Chronic pharmacological eNOS blockade leads to a

reduction in glycogen phosphorylase activity in the myocardium,[249] however ET-1 is capable of activating glycogen phosphorylase and therefore promotes glycogenolysis.[250]

In 12 months old eNOS-/- mice, a microarray study revealed that several genes involved in glycolysis are overexpressed while genes coding for enzymes responsible for fatty acid metabolism are repressed compared to WT mice.[103] A similar effect was observed in the present study but to a lesser extent, most probably because the mice analyzed in the proteomics study were younger.

Many studies describe a positive correlation between cardiac glucose metabolism and ET-1 gene expression and plasma levels in cardiovascular diseases. These studies often define ET-1 as an agent promoting, or at least participating in the pathology.[248, 251-253] In ET+/+eNOS-/- mice, relatively to the restored cardiac functions compared to eNOS-/- mice, one would rather consider ET-1 as a factor favoring glycolysis, and therefore contributing to a better energy efficiency and consequent improvement of cardiac functions.

Indeed, in pathological situations, the cardiac muscle switches to a glucose metabolism because of its greater efficiency compared to fatty acid metabolism. This phenomenon prevents from cardiac dysfunctions. Many classes of drugs targeting the energy metabolism are under investigations in several cardiovascular applications. The aim of this therapeutic approach is to reduce fatty acid metabolism and simultaneously enhance glycolysis. For example, dichloroacetate, a drug which promotes glycolysis, can be beneficial for cardiac functions after ischemia/reperfusion.[246] In patients with heart failure, a class of 3-ketoacyl coenzyme A thiolase (THIM) inhibitors enhances left ventricular function by favoring glucose metabolism.[254] Malonyl CoA reduces cardiac fatty acid β-oxidation, through the inhibition of carnitine palmitoyltransferase 1 (CAT), the enzyme responsible for the transit of fatty acids into the mitochondria. Agents which either enhance malonyl CoA concentration or directly inhibit CAT can be beneficial in models of cardiac ischemia/reperfusion.[255]

In ET+/+eNOS-/- mice, glycolysis was favored, which was not the case, or at least to a lesser extent, in eNOS-/- mice. In conclusion, these findings might contribute to the restored cardiac functions in the crossbred animals compared to eNOS-/- mice.

In order to confirm these conclusions, it would be of interest to target pharmacologically enzymes of the fatty acid and glucose metabolism. One hypothesis would be that inhibition of THIM by a trimetazidine treatment could be beneficial for cardiac functions in eNOS-/- mice. An improvement of cardiac functions in eNOS-/- mice after treatment with dichloroacetate, an activator of the mitochondrial PDH complex, which is more abundant in ET+/+eNOS-/- mice, would also confirm these observations.

4.3.4.3 TCA cycle and oxidative phosphorylation

The glucose and fatty acid metabolic pathways converge both to the TCA cycle. The TCA cycle produces a form of usable energy, NADH, from the acetyl-CoA synthesized during glycolysis and fatty acid β-oxidation. The TCA cycle is followed by the oxidative phosphorylation, which produces ATP using NADH as electron donor (figure 31).

Malate dehydrogenase, (MDHC, spot #41) and the alpha subunit of isocitrate dehydrogenase (IDH3A, spot #36), two enzymes of the TCA cycle, were more abundant in ET+/+eNOS-/- male mice, suggesting a higher energy production in this group compared to WT.

The oxidative phosphorylation is carried out by five complexes of enzymes (complexes I-V) schematically represented in the figure 31. The complex I subunit NADH-ubiquinone oxidoreductase 75kDa (Q3UQ73, spot#55) was less abundant in male ET+/+ but more abundant in ET+/+eNOS-/- male mice (spot #56), the complex III subunit QCR6 (spot #18) and complex IV subunit COX5B (spot #19) were also more abundant in ET+/+ mice, females and males, respectively. ATP synthase subunit alpha (ATPA spots #10 and #11), however, was less abundant in all three male ET+/+, eNOS-/- and ET+/+eNOS-/- mice (table 8 and figure 31).

In an acute model for heart failure, ETAR blockade has been shown to increase activity of complex III and V of the respiratory chain, thus improving mitochondrial function.[256] Moreover, ET-1 potentiates mitochondrial dysfunction in an *in vitro* model, but ET-1 alone does not decrease mitochondrial activity.

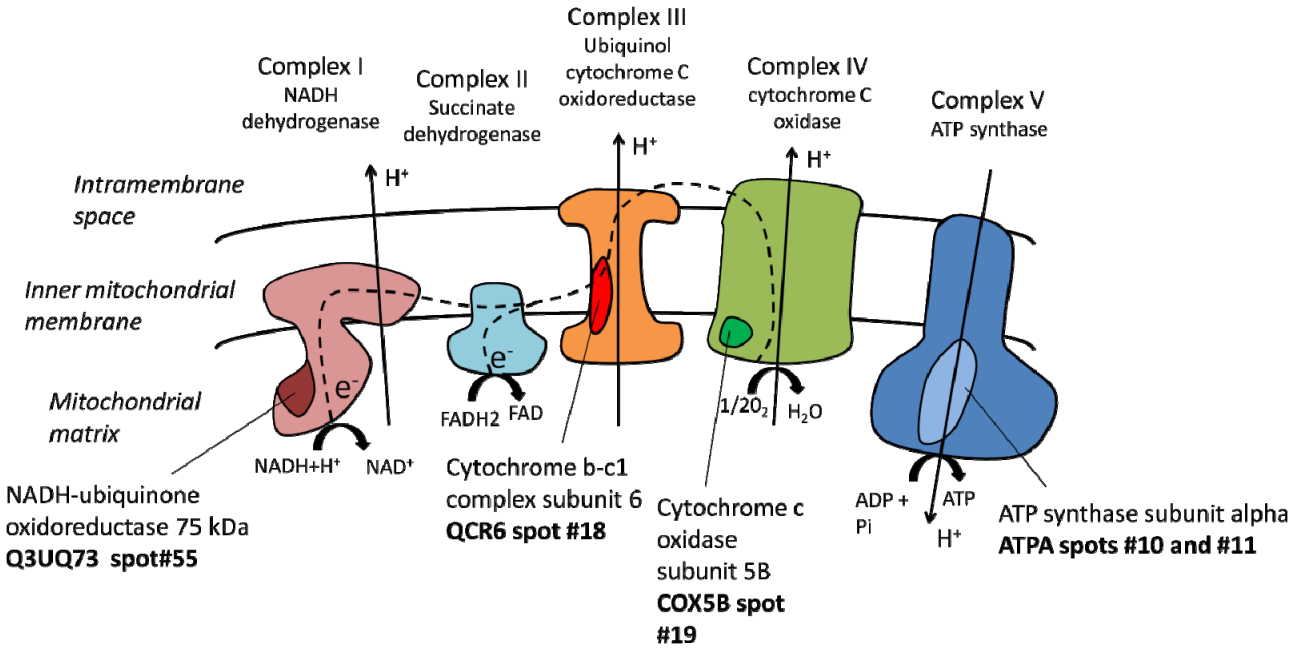

Figure 31: Schematic representation of the mitochondrial oxidative phosphorylation. Proteins found to be differentially abundant are highlighted.

On the other hand, in the same study, glucose uptake is dramatically enhanced by ET-1.[257] Finally, another study reveals that ET-1-induced protection of apoptosis is not due to an improvement of oxidative phosphorylation in cardiomyocytes.[258]

The role of NO on cardiac mitochondrial respiration is at least as controversial as ET-1's. NO can inhibit directly different enzymes of the respiratory chain by competing with oxygen and could therefore participate in a tonic control of the respiratory chain.[259] However, in the isolated mouse heart, a bradikinin-induced fivefold elevation in eNOS activity does not alter oxygen consumption.[260] Others showed that bradikinin reduces oxygen consumption in the isolated mouse heart and this effect is blunted in the heart from eNOS-/- mice, even though they observe no differences in oxygen consumption between eNOS-/- and WT mice.[261]

From these data, it becomes evident that ET-1 and NO play a role in controlling energy metabolism. The discrepancies between the studies must depend on the animal model used, the pathological situation, and ET-1 and NO doses. The data presented here demonstrated that ET-1 overexpression mostly enhanced the abundance of proteins involved in TCA cycle and oxidative phosphorylation, even in the absence of eNOS. The gross effects on ATP production

and oxygen consumption as well as the enzymatic activity of the respiratory chain remain to be investigated.

4.3.4.4 Other metabolisms

Beside energy metabolism, the proteomics study revealed changes in the abundance of proteins participating in various other metabolisms. In this last section, some examples likely to explain the functional differences between eNOS-/- and ET+/+eNOS-/- mice on the bases of their relevance in cardiovascular pathology will be described in more details.

Methylcrotonoyl CoA carboxylase subunit alpha (MCCA) participates in the catabolic process of the essential amino acid leucine. MCCA was found in two spots (spots #43 and #44). Only in eNOS-/- mice both spots were less abundant than in WT (figure 26A). Clinical studies proved the link between MCCA deficiency and cardiomyopathy, which is moreover associated with carnitine deficiency.[262] 2D-WB using an anti-MCCA antibody revealed the presence of two additional isoforms in eNOS-/- mice only, suggesting that rather the post-translational state than the amount of MCCA is modified (figure 26B). Immunoblotting is a much more sensitive method than silver staining, explaining why these additional spots were not seen on the large 2DE gels. Mass spectrometric analysis of the correspond region of the gel revealed however a low abundance of MCCA. The low sequence coverage unfortunately did not allow the identification of differential post-translational modifications compared to the other spots.

The adenosine synthase adenosylhomocysteinase (SAHH, spot #7) was less abundant in eNOS-/- female mice. Being a precursor of ATP synthesis, adenosine can prevent cardiac dysfunction through an amelioration of energy production.[263] Additionally, adenosine reduces free radical production and is for this reason also cardioprotective;[264] as already shown above, eNOS-/- mice may be less capable to scavenge free radicals.

Protein ETHE1 (ETHE1, spot #24) is a mitochondrial sulfur dioxygenase, for which a physiological relevance is not well established yet. ETHE1 genetic deficiency in mice is however toxic because of a sulfide accumulation in muscle.[265] Moreover ETHE1 expression positively correlates with oxygen consumption in human skeletal muscle.[266] ETHE1 was less abundant in eNOS-/- male mice. This is another indirect argument in favor of a limited energy production in this group.

These observations would indicate that amino acid, purine and sulfur metabolisms were differently affected in eNOS-/- mice compared to WT and that overexpression of ET-1 restored

these changes in ET+/+eNOS-/- mice. Once again, these data are indications for the understanding of the molecular mechanisms involved in the improvement of cardiac functions observed in ET+/+eNOS-/- mice compared to eNOS-/-.

4.4 Conclusions

The study of vasoactive substances and their roles in maintaining cardiovascular functions is of prime importance to further understand pathophysiological situations. Animal models are important tools to dissect the molecular processes involved in pathological developments *in vivo*. Therefore, in this study, the role of ET-1 and NO on cardiovascular functions have been investigated using genetically manipulated mice.

At the morphological and molecular level, this study showed that transgenic overexpression of ET-1 can drive processes which protect from development of cardiac dysfunctions, even in absence of eNOS. Dilation of coronary arterioles and prevention of myocyte hypertrophy as well as a better reduction of oxidative stress and switch from fatty acid to glucose metabolism are the main mechanisms explaining the improved left ventricular diastolic functions measured in ET+/+eNOS-/- mice, compared to eNOS-/- mice. Even if elevated concentration of ET-1 is often associated with cardiovascular disease, the fact that transgenic mice are constantly exposed to higher level of ET-1 apparently led them to develop protective compensatory mechanisms. This phenomenon describes the plasticity of the proteome and the importance of ET-1 in the homeostatic control.

These observations may not be restricted to cardiac tissue. Experiments currently ongoing in Prof. Hocher's laboratory showed that transgenic overexpression of ET-1 on an eNOS-/- background also ameliorates kidney functions, even though the renal phenotype of ET+/+ mice is severe.

The study of the ET+/+eNOS-/- mice, brought to light novel mechanisms involving ET-1 on the control of cardiovascular functions. The cardioprotective effects of ET-1 described here may explain the moderate clinical benefit of ET antagonists in heart failure.

5 Summary

The hormone Endothelin-1 (ET-1) exerts vasoconstrictive, inotropic, fibrotic and mitogenic effects on the cardiovascular system through the activation of ET receptor A. On the other hand, activation of ET receptor B stimulates the endothelial nitric oxide synthase (eNOS); NO presents strong vasodilative and cardioprotective properties and represses ET-1 expression. The clinical relevance of this delicate interplay has been acknowledged because of its implication in many cardiovascular diseases, such as pulmonary arterial hypertension, systemic hypertension, and coronary artery disease. However, the underlying molecular mechanisms remain to be fully clarified.

ET-1 transgenic (ET+/+) mice develop pulmonary, cardiac and renal fibrosis, glomerulosclerosis and decreased glomerular filtration rate. However, in spite of the strong vasoconstrictive feature of ET-1, ET+/+ mice remain normotensive. The natural functional antagonist of ET-1, NO, was assumed to counteract the ET-1 effect on blood pressure in ET+/+ mice. To test this hypothesis *in vivo*, ET+/+ mice were crossbred with eNOS knock-out (eNOS-/-) mice. Similar to the eNOS-/- model, the ET+/+eNOS-/- mice develop high blood pressure compared to wild type (WT) and ET+/+ animals. However, at the age of nine months, the eNOS-/-, but not ET+/+eNOS-/- mice, are characterized by diastolic dysfunction. These findings suggested that transgenic overexpression of ET-1 on an eNOS-/- background could be beneficial for diastolic functions.

In this thesis, it is shown that cardiac ET-1 gene expression was elevated in both eNOS-/- and ET+/+eNOS-/- mice compared to WT at the age of nine months with no significant difference between these groups. This suggests that the functional differences observed between eNOS-/- and eNOS-/-ET+/+ animals are due to the chronic overexpression of ET-1 mediated by the transgene, which may have conditioned ET+/+eNOS-/- animals over time to prevent the development of diastolic dysfunction. In line with this, eNOS-/- animals displayed normal cardiomyocyte diameters at the age of three months, but developed cardiac hypertrophy at the age of nine months, whereas ET+/+eNOS-/- mice showed enlarged cardiomyocytes at the age of three months that were not detectable in animals nine months of age. Histological analysis showed that cardiac arterioles were dilated in both ET+/+ and ET+/+eNOS-/- mice compared to WT and eNOS-/- mice. By enhancing blood flow, this could be beneficial for cardiac functions.

In order to dissect the molecular changes underlying this phenomenon, the cardiac proteome of the different genotypes were compared to WT using two-dimensional electrophoresis coupled to mass spectrometry. Because these changes may take place early in the life of the animals, three months old animals were analyzed. The proteomics study revealed that transgenic overexpression of ET-1, with or without eNOS, led to a higher abundance of proteins regulating oxidative stress indicating that, in contrast to eNOS-/- animals, ET+/+ and ET+/+eNOS-/- mice developed molecular mechanisms limiting oxidative damages. Moreover, diastolic dysfunction observed in eNOS-/- mice may be explained by the differential abundance of proteins involved in the contractile machinery. Overexpression of ET-1 in eNOS-/- mice restored these changes and may have thereby benefited the cardiac functions. Finally, this study indicated that a shift from fatty acid to glucose metabolism, considered as cardioprotective, may have occurred to a greater extent in crossbred animals than in eNOS-/- mice.

Taken together, this study showed that transgenic overexpression of ET-1 in mice can have beneficial effects on cardiac function, even in the absence of eNOS, by modulating various systems (oxidative stress, contractile machinery, and energy metabolism). The clinical relevance of these findings should be confirmed by analyzing the impact of a pharmacological interference with these systems on cardiac function. Finally, the fact that additional overexpression of ET-1 restored the deleterious effect of eNOS deficiency underlines the importance of the interplay between the two systems in the heart of mice.

6 Zusammenfassung

Endothelin-1 (ET-1) ist ein Peptidhormon, das durch Aktivierung des ET-1 Rezeptors A vasokonstriktorische, inotrope, fibrotische und mitogene Effekte im kardiovaskulären System vermittelt. Gleichzeitig stimuliert Aktivierung des ET-1 Rezeptors B die endotheliale Stickstoffmonoxid-Synthase (eNOS), wobei NO starke vasodilatative and kardioprotektive Eigenschaften aufweist und die ET-1 Expression hemmt. Aufgrund seines wesentlichen Einflusses auf zahlreiche Erkrankungen des kardiovaskulären Systems wie zum Beispiel die pulmonal-arterielle und systemische Hypertonie oder die koronare Herzerkrankung ist dieses fein abgestimmte Gleichgewicht von erheblicher klinischer Relevanz; die zugrundeliegenden molekularen Mechanismen konnten bislang jedoch nur unvollständig identifiziert werden.

In vorangegangenen Arbeiten konnte gezeigt werden, dass transgene Mäuse mit einer ET-1 Überexpression eine pulmonale, kardiale und renale Fibrose sowie eine Glomerulosklerose mit verminderter glomerulärer Filtrationsrate entwickeln. Interessanterweise zeigen diese Tiere jedoch trotz der bekannten vasokonstriktorischen Effekte von ET-1 keine Hypertonie. Um die Hypothese, dass dies auf eine Antagonisierung der ET-1 Wirkung durch NO zurückzuführen ist, in einem *in vivo* System zu überprüfen, wurden ET+/+ Mäuse mit eNOS knock-out Tieren (eNOS-/-) gekreuzt. Analog zum Phänotyp der eNOS-/- Tiere zeigte sich in diesem kombinierten ET+/+eNOS-/- Modell eine arterielle Hypertonie. Während eNOS-/- Mäuse jedoch im Alter von neun Monaten eine diastolische Dysfunktion entwickelten, waren diese Veränderungen im kombinierten ET+/+eNOS-/- Modell nicht nachzuweisen, so dass sich damit Hinweise für einen möglichen protektiven Effekt der ET-1 Überexpression auf die diastolische Funktion ergaben.

In der vorliegenden Arbeit wird gezeigt, dass sowohl eNOS-/- als auch ET+/+eNOS-/- Tiere im Alter von neun Monaten eine im Vergleich zu Wildtypkontrollen erhöhte ET-1 Expression zeigen, die sich zwischen diesen Gruppen nicht signifikant unterscheidet. Dies deutet darauf hin, dass die funktionellen Unterschiede zwischen beiden Modellen darauf zurückzuführen sein könnten, dass die Expression des ET-1 Transgens in ET+/+eNOS-/- Tieren zu einer bereits früh beginnenden ET-1 Überexpression führt, während sich dies in eNOS-/- Mäusen erst im Verlauf entwickelt. Eine chronische ET-1 Überexpression könnte so im kombinierten ET+/+eNOS-/- Modell zu einer Konditionierung der Tiere führen, die im weiteren Verlauf die Entwicklung einer diastolischen Dysfunktion verhindert. Dies wird durch die Beobachtung unterstützt, dass eNOS-

/- Tiere im Alter von drei Monaten normale Kardiomyozytendurchmesser aufweisen, im Alter von neun Monaten jedoch eine kardiale Hypertrophie entwickeln, während eine im Alter von drei Monaten in ET+/+eNOS-/- Mäusen nachweisbare Vergrößerung der Kardiomyozytendurchmesser in neun Monate alten Tieren nicht mehr nachweisbar ist. Histologisch zeigte sich darüber hinaus im Vergleich zu Wildtyp-Kontrollen und eNOS-/- Tieren sowohl in ET+/+ als auch in ET+/+eNOS-/- Mäusen eine Dilatation kardialer Arteriolen, so dass eine vermehrte myokardiale Durchblutung zu den beobachteten funktionellen Unterschiede beitragen könnte.

Um die molekularen Mechanismen, die diesen Beobachtungen zugrunde liegen, zu analysieren, erfolgte ein Vergleich des kardialen Proteoms jeder Genotypen mit Wildtyp Kontrollen durch zweidimensionale Elektrophorese in Kombination mit Massenspektrometrie. Hier zeigte sich, dass die Überexpression von ET-1 sowohl im Wildtyp als auch im eNOS -/- Hintergrund zu einer höheren Expression von Proteinen der oxidativen Stressantwort führt. Dies deutet darauf hin, dass ET+/+ and ET+/+eNOS-/- Tiere im Gegensatz zu eNOS-/- Mäusen molekulare Mechanismen entwickelt haben, um Schäden durch oxidativen Stress zu limitieren. Darüberhinaus war die beobachtete diastolische Dysfunktion in eNOS-/- Mäusen mit Änderungen in der Expression von Proteinen, die bei der Regulation kontraktiler Prozesse eine Rolle spielen, assoziiert. ET-1 Überexpression führte in eNOS-/- Tieren zu einer Antagonisierung dieser Veränderungen. Schließlich zeigte sich in diesen Untersuchungen, dass im ET+/+eNOS-/- Modell im Gegensatz zu eNOS-/- Tieren in höherem Maße eine Verschiebung vom Fettsäure-Metabolismus zur vermehrten Glukose-Utilisation erfolgt, die als kardioprotektiv betrachtet wird.

Zusammenfassend wird in der vorliegenden Arbeit damit gezeigt, dass eine chronische Überexpression von ET-1 in Mäusen durch die Modulation verschiedener Systeme (oxidativer Stress, Kontraktionsprozesse, Energiemetabolismus) auch in Abwesenheit der eNOS protektive Effekte auf die kardiale Funktion haben kann. Untersuchungen zum Einfluss einer pharmakologischen Modulation dieser Systeme auf kardiale Funktionsparameter könnten dazu beitragen, die klinische Relevanz dieser Beobachtungen zu überprüfen.

7 References

(1) Yanagisawa M, Kurihara H, Kimura S et al. A novel potent vasoconstrictor peptide produced by vascular endothelial cells. *Nature* 1988 March 31;332(6163):411-5.

(2) Matsumoto H, Suzuki N, Onda H, Fujino M. Abundance of endothelin-3 in rat intestine, pituitary gland and brain. *Biochem Biophys Res Commun* 1989 October 16;164(1):74-80.

(3) Saida K, Kometani N, Uchide T, Mitsui Y. Sequence analysis and expression of the mouse full-length vasoactive intestinal contractor/endothelin-2 gene (EDN2): comparison with the endothelin-1 gene (EDN1). *Clin Sci (Lond)* 2002 August;103 Suppl 48:84S-9S.

(4) Denault JB, Claing A, Orleans-Juste P et al. Processing of proendothelin-1 by human furin convertase. *FEBS Lett* 1995 April 10;362(3):276-80.

(5) Xu D, Emoto N, Giaid A et al. ECE-1: a membrane-bound metalloprotease that catalyzes the proteolytic activation of big endothelin-1. *Cell* 1994 August 12;78(3):473-85.

(6) Nagata N, Niwa Y, Nakaya Y. A novel 31-amino-acid-length endothelin, ET-1(1-31), can act as a biologically active peptide for vascular smooth muscle cells. *Biochem Biophys Res Commun* 2000 August 28;275(2):595-600.

(7) Hemsen A, Larsson O, Lundberg JM. Characteristics of endothelin A and B binding sites and their vascular effects in pig peripheral tissues. *Eur J Pharmacol* 1991 December 12;208(4):313-22.

(8) Pacher R, Stanek B, Hulsmann M et al. Prognostic impact of big endothelin-1 plasma concentrations compared with invasive hemodynamic evaluation in severe heart failure. *J Am Coll Cardiol* 1996 March 1;27(3):633-41.

(9) Hulsmann M, Stanek B, Frey B et al. Value of cardiopulmonary exercise testing and big endothelin plasma levels to predict short-term prognosis of patients with chronic heart failure. *J Am Coll Cardiol* 1998 November 15;32(6):1695-700.

(10) Shichiri M, Hirata Y, Ando K et al. Plasma endothelin levels in hypertension and chronic renal failure. *Hypertension* 1990 May;15(5):493-6.

(11) Kohan DE. The renal medullary endothelin system in control of sodium and water excretion and systemic blood pressure. *Curr Opin Nephrol Hypertens* 2006 January;15(1):34-40.

(12) Suzuki T, Kumazaki T, Mitsui Y. Endothelin-1 is produced and secreted by neonatal rat cardiac myocytes in vitro. *Biochem Biophys Res Commun* 1993 March 31;191(3):823-30.

(13) Russell FD, Molenaar P. The human heart endothelin system: ET-1 synthesis, storage, release and effect. *Trends Pharmacol Sci* 2000 September;21(9):353-9.

(14) Lee ME, de la Monte SM, Ng SC, Bloch KD, Quertermous T. Expression of the potent vasoconstrictor endothelin in the human central nervous system. *J Clin Invest* 1990 July;86(1):141-7.

(15) Giaid A, Polak JM, Gaitonde V et al. Distribution of endothelin-like immunoreactivity and mRNA in the developing and adult human lung. *Am J Respir Cell Mol Biol* 1991 January;4(1):50-8.

(16) MacCumber MW, Ross CA, Glaser BM, Snyder SH. Endothelin: visualization of mRNAs by in situ hybridization provides evidence for local action. *Proc Natl Acad Sci U S A* 1989 September;86(18):7285-9.

(17) Ehrenreich H, Anderson RW, Fox CH et al. Endothelins, peptides with potent vasoactive properties, are produced by human macrophages. *J Exp Med* 1990 December 1;172(6):1741-8.

(18) Imai T, Hirata Y, Emori T, Yanagisawa M, Masaki T, Marumo F. Induction of endothelin-1 gene by angiotensin and vasopressin in endothelial cells. *Hypertension* 1992 June;19(6 Pt 2):753-7.

(19) Kohno M, Murakawa K, Yokokawa K et al. Production of endothelin by cultured porcine endothelial cells: modulation by adrenaline. *J Hypertens Suppl* 1989 December;7(6):S130-S131.

(20) Kurihara H, Yoshizumi M, Sugiyama T et al. Transforming growth factor-beta stimulates the expression of endothelin mRNA by vascular endothelial cells. *Biochem Biophys Res Commun* 1989 March 31;159(3):1435-40.

(21) Fujisaki H, Ito H, Hirata Y et al. Natriuretic peptides inhibit angiotensin II-induced proliferation of rat cardiac fibroblasts by blocking endothelin-1 gene expression. *J Clin Invest* 1995 August;96(2):1059-65.

(22) Boulanger C, Luscher TF. Release of endothelin from the porcine aorta. Inhibition by endothelium-derived nitric oxide. *J Clin Invest* 1990 February;85(2):587-90.

(23) Prins BA, Hu RM, Nazario B et al. Prostaglandin E2 and prostacyclin inhibit the production and secretion of endothelin from cultured endothelial cells. *J Biol Chem* 1994 April 22;269(16):11938-44.

(24) Arai H, Hori S, Aramori I, Ohkubo H, Nakanishi S. Cloning and expression of a cDNA encoding an endothelin receptor. *Nature* 1990 December 20;348(6303):730-2.

(25) Sakurai T, Yanagisawa M, Takuwa Y et al. Cloning of a cDNA encoding a non-isopeptide-selective subtype of the endothelin receptor. *Nature* 1990 December 20;348(6303):732-5.

(26) Watts SW. Endothelin Receptors: what's new and what do we need to know? *Am J Physiol Regul Integr Comp Physiol* 2009 November 11.

(27) Ihara M, Ishikawa K, Fukuroda T et al. In vitro biological profile of a highly potent novel endothelin (ET) antagonist BQ-123 selective for the ETA receptor. *J Cardiovasc Pharmacol* 1992;20 Suppl 12:S11-S14.

(28) Ishikawa K, Ihara M, Noguchi K et al. Biochemical and pharmacological profile of a potent and selective endothelin B-receptor antagonist, BQ-788. *Proc Natl Acad Sci U S A* 1994 May 24;91(11):4892-6.

(29) Clozel M, Breu V, Gray GA et al. Pharmacological characterization of bosentan, a new potent orally active nonpeptide endothelin receptor antagonist. *J Pharmacol Exp Ther* 1994 July;270(1):228-35.

(30) Simonson MS, Dunn MJ. Cellular signaling by peptides of the endothelin gene family. *FASEB J* 1990 September;4(12):2989-3000.

(31) Clozel M, Gray GA. Are There Different Et(B) Receptors Mediating Constriction and Relaxation. *Journal of Cardiovascular Pharmacology* 1995;26:S262-S264.

(32) Verhaar MC, Strachan FE, Newby DE et al. Endothelin-A receptor antagonist-mediated vasodilatation is attenuated by inhibition of nitric oxide synthesis and by endothelin-B receptor blockade. *Circulation* 1998 March 3;97(8):752-6.

(33) Tsukahara H, Ende H, Magazine HI, Bahou WF, Goligorsky MS. Molecular and functional characterization of the non-isopeptide-selective ETB receptor in endothelial cells. Receptor coupling to nitric oxide synthase. *J Biol Chem* 1994 August 26;269(34):21778-85.

(34) Goligorsky MS, Tsukahara H, Magazine H, Andersen TT, Malik AB, Bahou WF. Termination of endothelin signaling: role of nitric oxide. *J Cell Physiol* 1994 March;158(3):485-94.

(35) Fukuroda T, Fujikawa T, Ozaki S, Ishikawa K, Yano M, Nishikibe M. Clearance of circulating endothelin-1 by ETB receptors in rats. *Biochem Biophys Res Commun* 1994 March 30;199(3):1461-5.

(36) Ozaki S, Ohwaki K, Ihara M, Fukuroda T, Ishikawa K, Yano M. ETB-mediated regulation of extracellular levels of endothelin-1 in cultured human endothelial cells. *Biochem Biophys Res Commun* 1995 April 17;209(2):483-9.

(37) Fujitani Y, Ninomiya H, Okada T, Urade Y, Masaki T. Suppression of endothelin-1-induced mitogenic responses of human aortic smooth muscle cells by interleukin-1 beta. *J Clin Invest* 1995 June;95(6):2474-82.

(38) MacNulty EE, Plevin R, Wakelam MJ. Stimulation of the hydrolysis of phosphatidylinositol 4,5-bisphosphate and phosphatidylcholine by endothelin, a complete mitogen for Rat-1 fibroblasts. *Biochem J* 1990 December 15;272(3):761-6.

(39) Ruetten H, Thiemermann C. Endothelin-1 stimulates the biosynthesis of tumour necrosis factor in macrophages: ET-receptors, signal transduction and inhibition by dexamethasone. *J Physiol Pharmacol* 1997 December;48(4):675-88.

(40) MacCarthy PA, Grocott-Mason R, Prendergast BD, Shah AM. Contrasting inotropic effects of endogenous endothelin in the normal and failing human heart: studies with an intracoronary ET(A) receptor antagonist. *Circulation* 2000 January 18;101(2):142-7.

(41) Wada A, Tsutamoto T, Fukai D et al. Comparison of the effects of selective endothelin ETA and ETB receptor antagonists in congestive heart failure. *J Am Coll Cardiol* 1997 November 1;30(5):1385-92.

(42) Cheng TH, Shih NL, Chen SY et al. Nitric oxide inhibits endothelin-1-induced cardiomyocyte hypertrophy through cGMP-mediated suppression of extracellular-signal regulated kinase phosphorylation. *Mol Pharmacol* 2005 October;68(4):1183-92.

(43) Schorlemmer A, Matter ML, Shohet RV. Cardioprotective signaling by endothelin. *Trends Cardiovasc Med* 2008 October;18(7):233-9.

(44) Simonson MS, Dunn MJ. Endothelin-1 stimulates contraction of rat glomerular mesangial cells and potentiates beta-adrenergic-mediated cyclic adenosine monophosphate accumulation. *J Clin Invest* 1990 March;85(3):790-7.

(45) Gomez-Garre D, Ruiz-Ortega M, Ortego M et al. Effects and interactions of endothelin-1 and angiotensin II on matrix protein expression and synthesis and mesangial cell growth. *Hypertension* 1996 April;27(4):885-92.

(46) Rebibou JM, He CJ, Delarue F et al. Functional endothelin 1 receptors on human glomerular podocytes and mesangial cells. *Nephrol Dial Transplant* 1992;7(4):288-92.

(47) Yamamoto T, Hirohama T, Uemura H. Endothelin B receptor-like immunoreactivity in podocytes of the rat kidney. *Arch Histol Cytol* 2002 August;65(3):245-50.

(48) Schnermann J, Lorenz JN, Briggs JP, Keiser JA. Induction of water diuresis by endothelin in rats. *Am J Physiol* 1992 September;263(3 Pt 2):F516-F526.

(49) Guo X, Yang T. Endothelin B receptor antagonism in the rat renal medulla reduces urine flow rate and sodium excretion. *Exp Biol Med (Maywood)* 2006 June;231(6):1001-5.

(50) Plato CF, Pollock DM, Garvin JL. Endothelin inhibits thick ascending limb chloride flux via ET(B) receptor-mediated NO release. *Am J Physiol Renal Physiol* 2000 August;279(2):F326-F333.

(51) Evans RG, Bergstrom G, Cotterill E, Anderson WP. Renal haemodynamic effects of endothelin-1 and the ETA/ETB antagonist TAK-044 in anaesthetized rabbits. *J Hypertens* 1998 December;16(12 Pt 2):1897-905.

(52) Forbes JM, Leaker B, Hewitson TD, Becker GJ, Jones CL. Macrophage and myofibroblast involvement in ischemic acute renal failure is attenuated by endothelin receptor antagonists. *Kidney Int* 1999 January;55(1):198-208.

(53) Goldie RG, Grayson PS, Knott PG, Self GJ, Henry PJ. Predominance of endothelinA (ETA) receptors in ovine airway smooth muscle and their mediation of ET-1-induced contraction. *Br J Pharmacol* 1994 July;112(3):749-56.

(54) Goldie RG, D'Aprile AC, Cvetkovski R, Rigby PJ, Henry PJ. Influence of regional differences in ETA and ETB receptor subtype proportions on endothelin-1-induced contractions in porcine isolated trachea and bronchus. *Br J Pharmacol* 1996 February;117(4):736-42.

(55) Hay DW, Luttmann MA, Hubbard WC, Undem BJ. Endothelin receptor subtypes in human and guinea-pig pulmonary tissues. *Br J Pharmacol* 1993 November;110(3):1175-83.

(56) Fukuroda T, Ozaki S, Ihara M et al. Necessity of dual blockade of endothelin ETA and ETB receptor subtypes for antagonism of endothelin-1-induced contraction in human bronchi. *Br J Pharmacol* 1996 March;117(6):995-9.

(57) Stewart AG, Grigoriadis G, Harris T. Mitogenic actions of endothelin-1 and epidermal growth factor in cultured airway smooth muscle. *Clin Exp Pharmacol Physiol* 1994 April;21(4):277-85.

(58) Murlas CG, Gulati A, Singh G, Najmabadi F. Endothelin-1 stimulates proliferation of normal airway epithelial cells. *Biochem Biophys Res Commun* 1995 July 26;212(3):953-9.

(59) Takimoto M, Oda K, Sasaki Y, Okada T. Endothelin-A receptor-mediated prostanoid secretion via autocrine and deoxyribonucleic acid synthesis via paracrine signaling in human bronchial epithelial cells. *Endocrinology* 1996 November;137(11):4542-50.

(60) Hocher B, Schwarz A, Fagan KA et al. Pulmonary fibrosis and chronic lung inflammation in ET-1 transgenic mice. *Am J Respir Cell Mol Biol* 2000 July;23(1):19-26.

(61) Dashwood MR, Loesch A. Endothelin-1 as a neuropeptide: neurotransmitter or neurovascular effects? *J Cell Commun Signal* 2009 October 22.

(62) Kuwaki T, Kurihara H, Cao WH et al. Physiological role of brain endothelin in the central autonomic control: from neuron to knockout mouse. *Prog Neurobiol* 1997 April;51(5):545-79.

(63) Macrae I, Robinson M, McAuley M, Reid J, McCulloch J. Effects of intracisternal endothelin-1 injection on blood flow to the lower brain stem. *Eur J Pharmacol* 1991 October 2;203(1):85-91.

(64) Chew BH, Weaver DF, Gross PM. Dose-related potent brain stimulation by the neuropeptide endothelin-1 after intraventricular administration in conscious rats. *Pharmacol Biochem Behav* 1995 May;51(1):37-47.

(65) D'Amico M, Berrino L, Maione S, Filippelli A, de N, V, Rossi F. Endothelin-1 in periaqueductal gray area of mice induces analgesia via glutamatergic receptors. *Pain* 1996 May;65(2-3):205-9.

(66) McKelvy AD, Sweitzer SM. Endothelin-1 exposure on postnatal day 7 alters expression of the endothelin B receptor and behavioral sensitivity to endothelin-1 on postnatal day 11. *Neurosci Lett* 2009 February 13;451(1):89-93.

(67) Palmer RM, Ferrige AG, Moncada S. Nitric oxide release accounts for the biological activity of endothelium-derived relaxing factor. *Nature* 1987 June 11;327(6122):524-6.

(68) Ignarro LJ, Wood KS, Wolin MS. Activation of purified soluble guanylate cyclase by protoporphyrin IX. *Proc Natl Acad Sci U S A* 1982 May;79(9):2870-3.

(69) Ignarro LJ. Biological actions and properties of endothelium-derived nitric oxide formed and released from artery and vein. *Circ Res* 1989 July;65(1):1-21.

(70) Ayajiki K, Kindermann M, Hecker M, Fleming I, Busse R. Intracellular pH and tyrosine phosphorylation but not calcium determine shear stress-induced nitric oxide production in native endothelial cells. *Circ Res* 1996 May;78(5):750-8.

(71) Ignarro LJ, Byrns RE, Wood KS. Endothelium-dependent modulation of cGMP levels and intrinsic smooth muscle tone in isolated bovine intrapulmonary artery and vein. *Circ Res* 1987 January;60(1):82-92.

(72) Kubes P, Suzuki M, Granger DN. Nitric oxide: an endogenous modulator of leukocyte adhesion. *Proc Natl Acad Sci U S A* 1991 June 1;88(11):4651-5.

(73) Radomski MW, Palmer RM, Moncada S. Endogenous nitric oxide inhibits human platelet adhesion to vascular endothelium. *Lancet* 1987 November 7;2(8567):1057-8.

(74) Garg UC, Hassid A. Nitric oxide-generating vasodilators and 8-bromo-cyclic guanosine monophosphate inhibit mitogenesis and proliferation of cultured rat vascular smooth muscle cells. *J Clin Invest* 1989 May;83(5):1774-7.

(75) Kone BC, Baylis C. Biosynthesis and homeostatic roles of nitric oxide in the normal kidney. *Am J Physiol* 1997 May;272(5 Pt 2):F561-F578.

(76) Garcia-Estan J, Ortiz MC, Lee SS. Nitric oxide and renal and cardiac dysfunction in cirrhosis. *Clin Sci (Lond)* 2002 February;102(2):213-22.

(77) Ohara Y, Peterson TE, Harrison DG. Hypercholesterolemia increases endothelial superoxide anion production. *J Clin Invest* 1993 June;91(6):2546-51.

(78) Tschudi MR, Mesaros S, Luscher TF, Malinski T. Direct in situ measurement of nitric oxide in mesenteric resistance arteries. Increased decomposition by superoxide in hypertension. *Hypertension* 1996 January;27(1):32-5.

(79) Vasquez-Vivar J, Kalyanaraman B, Martasek P et al. Superoxide generation by endothelial nitric oxide synthase: the influence of cofactors. *Proc Natl Acad Sci U S A* 1998 August 4;95(16):9220-5.

(80) Hocher B, Thone-Reineke C, Rohmeiss P et al. Endothelin-1 transgenic mice develop glomerulosclerosis, interstitial fibrosis, and renal cysts but not hypertension. *J Clin Invest* 1997 March 15;99(6):1380-9.

(81) Theuring F, Thone-Reinecke C, Vogler H et al. Pathophysiology in endothelin-1 transgenic mice. *J Cardiovasc Pharmacol* 1998;31 Suppl 1:S489-S491.

(82) Schwarz A, Godes M, Thone-Reineke C et al. Tissue-dependent expression of matrix proteins in human endothelin-1 transgenic mice. *Clin Sci (Lond)* 2002 August;103 Suppl 48:39S-43S.

(83) Hocher B, Rohmeiss P, Thone-Reineke C et al. Apoptosis in kidneys of endothelin-1 transgenic mice. *J Cardiovasc Pharmacol* 1998;31 Suppl 1:S554-S556.

(84) Shindo T, Kurihara H, Maemura K et al. Renal damage and salt-dependent hypertension in aged transgenic mice overexpressing endothelin-1. *J Mol Med* 2002 February;80(2):105-16.

(85) Amiri F, Virdis A, Neves MF et al. Endothelium-restricted overexpression of human endothelin-1 causes vascular remodeling and endothelial dysfunction. *Circulation* 2004 October 12;110(15):2233-40.

(86) Amiri F, Paradis P, Reudelhuber TL, Schiffrin EL. Vascular inflammation in absence of blood pressure elevation in transgenic murine model overexpressing endothelin-1 in endothelial cells. *J Hypertens* 2008 June;26(6):1102-9.

(87) Quaschning T, Kocak S, Bauer C, Neumayer HH, Galle J, Hocher B. Increase in nitric oxide bioavailability improves endothelial function in endothelin-1 transgenic mice. *Nephrol Dial Transplant* 2003 March;18(3):479-83.

(88) Hocher B, Schwarz A, Slowinski T et al. In-vivo interaction of nitric oxide and endothelin. *J Hypertens* 2004 January;22(1):111-9.

(89) Kalk P, Westermann D, Herzfeld S et al. Additional lack of iNOS attenuates diastolic dysfunction in aged ET-1 transgenic mice. *Can J Physiol Pharmacol* 2008 June;86(6):353-7.

(90) Godecke A, Decking UK, Ding Z et al. Coronary hemodynamics in endothelial NO synthase knockout mice. *Circ Res* 1998 February 9;82(2):186-94.

(91) Gregg AR, Schauer A, Shi O, Liu Z, Lee CG, O'Brien WE. Limb reduction defects in endothelial nitric oxide synthase-deficient mice. *Am J Physiol* 1998 December;275(6 Pt 2):H2319-H2324.

(92) Huang PL, Huang Z, Mashimo H et al. Hypertension in mice lacking the gene for endothelial nitric oxide synthase. *Nature* 1995 September 21;377(6546):239-42.

(93) Shesely EG, Maeda N, Kim HS et al. Elevated blood pressures in mice lacking endothelial nitric oxide synthase. *Proc Natl Acad Sci U S A* 1996 November 12;93(23):13176-81.

(94) Meng W, Ma J, Ayata C et al. ACh dilates pial arterioles in endothelial and neuronal NOS knockout mice by NO-dependent mechanisms. *Am J Physiol* 1996 September;271(3 Pt 2):H1145-H1150.

(95) Li W, Mital S, Ojaimi C, Csiszar A, Kaley G, Hintze TH. Premature death and age-related cardiac dysfunction in male eNOS-knockout mice. *J Mol Cell Cardiol* 2004 September;37(3):671-80.

(96) Sharp BR, Jones SP, Rimmer DM, Lefer DJ. Differential response to myocardial reperfusion injury in eNOS-deficient mice. *Am J Physiol Heart Circ Physiol* 2002 June;282(6):H2422-H2426.

(97) Gyurko R, Kuhlencordt P, Fishman MC, Huang PL. Modulation of mouse cardiac function in vivo by eNOS and ANP. *Am J Physiol Heart Circ Physiol* 2000 March;278(3):H971-H981.

(98) Labonte J, Orleans-Juste P. Enhanced or repressed pressor responses to endothelin-1 or IRL-1620, respectively, in eNOS knockout mice. *J Cardiovasc Pharmacol* 2004 November;44 Suppl 1:S109-S112.

(99) Labonte J, Brochu I, Simard E, Orleans-Juste P. Distinct modulation of the endothelin-1 pathway in iNOS-/- and eNOS-/- mice. *Can J Physiol Pharmacol* 2008 August;86(8):516-25.

(100) Ortiz PA, Hong NJ, Wang D, Garvin JL. Gene transfer of eNOS to the thick ascending limb of eNOS-KO mice restores the effects of L-arginine on NaCl absorption. *Hypertension* 2003 October;42(4):674-9.

(101) Le GE, Jimenez M, Binnert C et al. Endothelial nitric oxide synthase (eNOS) knockout mice have defective mitochondrial beta-oxidation. *Diabetes* 2007 November;56(11):2690-6.

(102) Wadley GD, Choate J, McConell GK. NOS isoform-specific regulation of basal but not exercise-induced mitochondrial biogenesis in mouse skeletal muscle. *J Physiol* 2007 November 15;585(Pt 1):253-62.

(103) Ojaimi C, Li W, Kinugawa S et al. Transcriptional basis for exercise limitation in male eNOS-knockout mice with age: heart failure and the fetal phenotype. *Am J Physiol Heart Circ Physiol* 2005 October;289(4):H1399-H1407.

(104) Tada H, Thompson CI, Recchia FA et al. Myocardial glucose uptake is regulated by nitric oxide via endothelial nitric oxide synthase in Langendorff mouse heart. *Circ Res* 2000 February 18;86(3):270-4.

(105) Lee TC, Zhao YD, Courtman DW, Stewart DJ. Abnormal aortic valve development in mice lacking endothelial nitric oxide synthase. *Circulation* 2000 May 23;101(20):2345-8.

(106) Feng Q, Song W, Lu X et al. Development of heart failure and congenital septal defects in mice lacking endothelial nitric oxide synthase. *Circulation* 2002 August 13;106(7):873-9.

(107) Zhao X, Lu X, Feng Q. Deficiency in endothelial nitric oxide synthase impairs myocardial angiogenesis. *Am J Physiol Heart Circ Physiol* 2002 December;283(6):H2371-H2378.

(108) Luscher TF, Yang Z, Tschudi M et al. Interaction between endothelin-1 and endothelium-derived relaxing factor in human arteries and veins. *Circ Res* 1990 April;66(4):1088-94.

(109) Rossi GP, Seccia TM, Nussdorfer GG. Reciprocal regulation of endothelin-1 and nitric oxide: relevance in the physiology and pathology of the cardiovascular system. *Int Rev Cytol* 2001;209:241-72.

(110) Slowinski T, Kalk P, Christian M et al. Cell-type specific interaction of endothelin and the nitric oxide system: pattern of prepro-ET-1 expression in kidneys of L-NAME treated prepro-ET-1 promoter-lacZ-transgenic mice. *J Physiol* 2007 June 15;581(Pt 3):1173-81.

(111) Quaschning T, Voss F, Herzfeld S et al. Lack of iNOS impairs endothelial function in endothelin-1 transgenic mice. *Kidney Blood Press Res* 2008;31(2):127-34.

(112) Nussler AK, Billiar TR. Inflammation, immunoregulation, and inducible nitric oxide synthase. *J Leukoc Biol* 1993 August;54(2):171-8.

(113) Wilcox JN, Subramanian RR, Sundell CL et al. Expression of multiple isoforms of nitric oxide synthase in normal and atherosclerotic vessels. *Arterioscler Thromb Vasc Biol* 1997 November;17(11):2479-88.

(114) Quaschning T, Voss F, Relle K et al. Lack of endothelial nitric oxide synthase promotes endothelin-induced hypertension: lessons from endothelin-1 transgenic/endothelial nitric oxide synthase knockout mice. *J Am Soc Nephrol* 2007 March;18(3):730-40.

(115) Girgis RE, Champion HC, Diette GB, Johns RA, Permutt S, Sylvester JT. Decreased exhaled nitric oxide in pulmonary arterial hypertension: response to bosentan therapy. *Am J Respir Crit Care Med* 2005 August 1;172(3):352-7.

(116) Wagner FD, Buz S, Knosalla C, Hetzer R, Hocher B. Modulation of circulating endothelin-1 and big endothelin by nitric oxide inhalation following left ventricular assist device implantation. *Circulation* 2003 September 9;108 Suppl 1:II278-II284.

(117) Rabelink TJ, Bakris GL. The renin-angiotensin system in diabetic nephropathy: the endothelial connection. *Miner Electrolyte Metab* 1998;24(6):381-8.

(118) Xu M, Dai DZ, Dai Y. Normalizing NADPH Oxidase Contributes to Attenuating Diabetic Nephropathy by the Dual Endothelin Receptor Antagonist CPU0213 in Rats. *Am J Nephrol* 2008 September 19;29(3):252-6.

(119) Papalambros KE, Sigala F, Georgopoulos S et al. The relationship of endothelin-1 and inducible nitric oxide synthase at several stages of the anastomotic healing process. *Int Angiol* 2008 August;27(4):302-6.

(120) Wu YZ, Li SQ, Zu XG, Du J, Wang FF. Ginkgo biloba extract improves coronary artery circulation in patients with coronary artery disease: contribution of plasma nitric oxide and endothelin-1. *Phytother Res* 2008 June;22(6):734-9.

(121) Ohnishi M, Wada A, Tsutamoto T et al. Endothelin stimulates an endogenous nitric oxide synthase inhibitor, asymmetric dimethylarginine, in experimental heart failure. *Clin Sci (Lond)* 2002 August;103 Suppl 48:241S-4S.

(122) Baksu B, Davas I, Baksu A, Akyol A, Gulbaba G. Plasma nitric oxide, endothelin-1 and urinary nitric oxide and cyclic guanosine monophosphate levels in hypertensive pregnant women. *Int J Gynaecol Obstet* 2005 August;90(2):112-7.

(123) Taddei S, Virdis A, Ghiadoni L, Sudano I, Notari M, Salvetti A. Vasoconstriction to endogenous endothelin-1 is increased in the peripheral circulation of patients with essential hypertension. *Circulation* 1999 October 19;100(16):1680-3.

(124) Tesauro M, Schinzari F, Rovella V et al. Ghrelin restores the endothelin 1/nitric oxide balance in patients with obesity-related metabolic syndrome. *Hypertension* 2009 November;54(5):995-1000.

(125) Kurita A, Matsui T, Ishizuka T, Takase B, Satomura K. Significance of plasma nitric oxide/endothelial-1 ratio for prediction of coronary artery disease. *Angiology* 2005 May;56(3):259-64.

(126) Belik J. Riociguat, an oral soluble guanylate cyclase stimulator for the treatment of pulmonary hypertension. *Curr Opin Investig Drugs* 2009 September;10(9):971-9.

(127) O'Connor CM, Gattis WA, Adams KF, Jr. et al. Tezosentan in patients with acute heart failure and acute coronary syndromes: results of the Randomized Intravenous TeZosentan Study (RITZ-4). *J Am Coll Cardiol* 2003 May 7;41(9):1452-7.

(128) Iglarz M, Binkert C, Morrison K et al. PHARMACOLOGY OF MACITENTAN, AN ORALLY ACTIVE TISSUE TARGETING DUAL ENDOTHELIN RECEPTOR ANTAGONIST. *J Pharmacol Exp Ther* 2008 September 9.

(129) Viberti G. SPP301 (Avosentan) ASCEND Clinical Results. http://www.speedel.com/assets/2008_SPP301ASCENDStudy.pdf . 2009.

(130) SMITHIES O, POULIK MD. Two-dimensional electrophoresis of serum proteins. *Nature* 1956 June 2;177(4518):1033.

(131) RAYMOND S, WEINTRAUB L. Acrylamide gel as a supporting medium for zone electrophoresis. *Science* 1959 September 18;130:711.

(132) Laemmli UK. Cleavage of structural proteins during the assembly of the head of bacteriophage T4. *Nature* 1970 August 15;227(5259):680-5.

(133) Awdeh ZL, Williamson AR, Askonas BA. Isoelectric focusing in polyacrylamide gel and its application to immunoglobulins. *Nature* 1968 July 6;219(5149):66-7.

(134) Klose J. Protein mapping by combined isoelectric focusing and electrophoresis of mouse tissues. A novel approach to testing for induced point mutations in mammals. *Humangenetik* 1975;26(3):231-43.

(135) O'Farrell PH. High resolution two-dimensional electrophoresis of proteins. *J Biol Chem* 1975 May 25;250(10):4007-21.

(136) Klose J, Kobalz U. Two-dimensional electrophoresis of proteins: an updated protocol and implications for a functional analysis of the genome. *Electrophoresis* 1995 June;16(6):1034-59.

(137) Karas M, Hillenkamp F. Laser desorption ionization of proteins with molecular masses exceeding 10,000 daltons. *Anal Chem* 1988 October 15;60(20):2299-301.

(138) Fenn JB, Mann M, Meng CK, Wong SF, Whitehouse CM. Electrospray ionization for mass spectrometry of large biomolecules. *Science* 1989 October 6;246(4926):64-71.

(139) Sharova LV, Sharov AA, Nedorezov T, Piao Y, Shaik N, Ko MS. Database for mRNA half-life of 19 977 genes obtained by DNA microarray analysis of pluripotent and differentiating mouse embryonic stem cells. *DNA Res* 2009 February;16(1):45-58.

(140) Shao R, Yan W, Rockey DC. Regulation of endothelin-1 synthesis by endothelin-converting enzyme-1 during wound healing. *J Biol Chem* 1999 January 29;274(5):3228-34.

(141) Pickart CM, Cohen RE. Proteasomes and their kin: proteases in the machine age. *Nat Rev Mol Cell Biol* 2004 March;5(3):177-87.

(142) Rozen S, Skaletsky H. Primer3 on the WWW for general users and for biologist programmers. *Methods Mol Biol* 2000;132:365-86.

(143) Hubbard TJ, Aken BL, Ayling S et al. Ensembl 2009. *Nucleic Acids Res* 2009 January;37(Database issue):D690-D697.

(144) Johnson M, Zaretskaya I, Raytselis Y, Merezhuk Y, McGinnis S, Madden TL. NCBI BLAST: a better web interface. *Nucleic Acids Res* 2008 July 1;36(Web Server issue):W5-W9.

(145) Adur J, Takizawa S, Quan J, Uchide T, Saida K. Increased gene expression and production of murine endothelin receptors after birth. *Biochem Biophys Res Commun* 2003 June 6;305(3):700-6.

(146) Phillipson M, Henriksnas J, Holstad M, Sandler S, Holm L. Inducible nitric oxide synthase is involved in acid-induced gastric hyperemia in rats and mice. *Am J Physiol Gastrointest Liver Physiol* 2003 July;285(1):G154-G162.

(147) Stirone C, Chu Y, Sunday L, Duckles SP, Krause DN. 17 Beta-estradiol increases endothelial nitric oxide synthase mRNA copy number in cerebral blood vessels: quantification by real-time polymerase chain reaction. *Eur J Pharmacol* 2003 September 30;478(1):35-8.

(148) Petkova SB, Tanowitz HB, Magazine HI et al. Myocardial expression of endothelin-1 in murine Trypanosoma cruzi infection. *Cardiovasc Pathol* 2000 September;9(5):257-65.

(149) Aksu S, Scheler C, Focks N et al. An iterative calibration method with prediction of post-translational modifications for the construction of a two-dimensional electrophoresis database of mouse mammary gland proteins. *Proteomics* 2002 October;2(10):1452-63.

(150) Zimny-Arndt U, Schmid M, Ackermann R, Jungblut PR. Classical proteomics: two-dimensional electrophoresis/MALDI mass spectrometry. *Methods Mol Biol* 2009;492:65-91.

(151) Nebrich G, Herrmann M, Sagi D, Klose J, Giavalisco P. High MS-compatibility of silver nitrate-stained protein spots from 2-DE gels using ZipPlates and AnchorChips for successful protein identification. *Electrophoresis* 2007 May;28(10):1607-14.

(152) The universal protein resource (UniProt). *Nucleic Acids Res* 2008 January;36(Database issue):D190-D195.

(153) Thomas PD, Campbell MJ, Kejariwal A et al. PANTHER: a library of protein families and subfamilies indexed by function. *Genome Res* 2003 September;13(9):2129-41.

(154) Han B, Hasin Y. Cardiovascular effects of natriuretic peptides and their interrelation with endothelin-1. *Cardiovasc Drugs Ther* 2003 January;17(1):41-52.

(155) Kurihara Y, Kurihara H, Oda H et al. Aortic arch malformations and ventricular septal defect in mice deficient in endothelin-1. *J Clin Invest* 1995 July;96(1):293-300.

(156) Kedzierski RM, Yanagisawa M. Endothelin system: the double-edged sword in health and disease. *Annu Rev Pharmacol Toxicol* 2001;41:851-76.

(157) Dussaule JC, Tharaux PL, Boffa JJ, Fakhouri F, Ardaillou R, Chatziantoniou C. Mechanisms mediating the renal profibrotic actions of vasoactive peptides in transgenic mice. *J Am Soc Nephrol* 2000 November;11 Suppl 16:S124-S128.

(158) Zile MR, Brutsaert DL. New concepts in diastolic dysfunction and diastolic heart failure: Part II: causal mechanisms and treatment. *Circulation* 2002 March 26;105(12):1503-8.

(159) Lopez B, Gonzalez A, Querejeta R, Larman M, Diez J. Alterations in the pattern of collagen deposition may contribute to the deterioration of systolic function in hypertensive patients with heart failure. *J Am Coll Cardiol* 2006 July 4;48(1):89-96.

(160) Diez J, Querejeta R, Lopez B, Gonzalez A, Larman M, Martinez Ubago JL. Losartan-dependent regression of myocardial fibrosis is associated with reduction of left ventricular chamber stiffness in hypertensive patients. *Circulation* 2002 May 28;105(21):2512-7.

(161) Vanhoutte D, Schellings M, Pinto Y, Heymans S. Relevance of matrix metalloproteinases and their inhibitors after myocardial infarction: a temporal and spatial window. *Cardiovasc Res* 2006 February 15;69(3):604-13.

(162) Iwakura A, Shastry S, Luedemann C et al. Estradiol enhances recovery after myocardial infarction by augmenting incorporation of bone marrow-derived endothelial progenitor cells into sites of ischemia-induced neovascularization via endothelial nitric oxide synthase-mediated activation of matrix metalloproteinase-9. *Circulation* 2006 March 28;113(12):1605-14.

(163) Wang F, Keimig T, He Q et al. Augmented healing process in female mice with acute myocardial infarction. *Gend Med* 2007 September;4(3):230-47.

(164) Gurjar MV, Sharma RV, Bhalla RC. eNOS gene transfer inhibits smooth muscle cell migration and MMP-2 and MMP-9 activity. *Arterioscler Thromb Vasc Biol* 1999 December;19(12):2871-7.

(165) Spanikova A, Simoncikova P, Ravingerova T, Pechanova O, Barancik M. The effect of chronic nitric oxide synthases inhibition on regulatory proteins in rat hearts. *Mol Cell Biochem* 2008 May;312(1-2):113-20.

(166) Kato S, Spinale FG, Tanaka R, Johnson W, Cooper G, Zile MR. Inhibition of collagen cross-linking: effects on fibrillar collagen and ventricular diastolic function. *Am J Physiol* 1995 September;269(3 Pt 2):H863-H868.

(167) Shirwany A, Weber KT. Extracellular matrix remodeling in hypertensive heart disease. *J Am Coll Cardiol* 2006 July 4;48(1):97-8.

(168) Kai H, Kuwahara F, Tokuda K, Imaizumi T. Diastolic dysfunction in hypertensive hearts: roles of perivascular inflammation and reactive myocardial fibrosis. *Hypertens Res* 2005 June;28(6):483-90.

(169) Georgiadou P, Sbarouni E. Effect of hormone replacement therapy on inflammatory biomarkers. *Adv Clin Chem* 2009;47:59-93.

(170) Haider AW, Larson MG, Benjamin EJ, Levy D. Increased left ventricular mass and hypertrophy are associated with increased risk for sudden death. *J Am Coll Cardiol* 1998 November;32(5):1454-9.

(171) Zhang XP, Vatner SF, Shen YT et al. Increased apoptosis and myocyte enlargement with decreased cardiac mass; distinctive features of the aging male, but not female, monkey heart. *J Mol Cell Cardiol* 2007 October;43(4):487-91.

(172) Araki M, Hasegawa K, Iwai-Kanai E et al. Endothelin-1 as a protective factor against beta-adrenergic agonist-induced apoptosis in cardiac myocytes. *J Am Coll Cardiol* 2000 October;36(4):1411-8.

(173) Sugden PH. Signalling pathways in cardiac myocyte hypertrophy. *Ann Med* 2001 December;33(9):611-22.

(174) Zhao XS, Pan W, Bekeredjian R, Shohet RV. Endogenous endothelin-1 is required for cardiomyocyte survival in vivo. *Circulation* 2006 August 22;114(8):830-7.

(175) Berti F, Rossoni G, Della BD et al. Nitric oxide and prostacyclin influence coronary vasomotor tone in perfused rabbit heart and modulate endothelin-1 activity. *J Cardiovasc Pharmacol* 1993 August;22(2):321-6.

(176) Folta A, Joshua IG, Webb RC. Dilator actions of endothelin in coronary resistance vessels and the abdominal aorta of the guinea pig. *Life Sci* 1989;45(26):2627-35.

(177) Westerhof N, Boer C, Lamberts RR, Sipkema P. Cross-talk between cardiac muscle and coronary vasculature. *Physiol Rev* 2006 October;86(4):1263-308.

(178) Recchia FA, Senzaki H, Saeki A, Byrne BJ, Kass DA. Pulse pressure-related changes in coronary flow in vivo are modulated by nitric oxide and adenosine. *Circ Res* 1996 October;79(4):849-56.

(179) Cheng TO. Cardiovascular effects of Danshen. *Int J Cardiol* 2007 September 14;121(1):9-22.

(180) Miller I, Crawford J, Gianazza E. Protein stains for proteomic applications: which, when, why? *Proteomics* 2006 October;6(20):5385-408.

(181) Bennett P, Zhu Q, Van Horne KC, Li L, Huang Y. Is MALDI-TOF MS ready for bioanalytical analysis? *Presented at the 2008 ASMS Conference, Denver, CO, June 2008* 2008.

(182) St-Pierre J, Buckingham JA, Roebuck SJ, Brand MD. Topology of superoxide production from different sites in the mitochondrial electron transport chain. *J Biol Chem* 2002 November 22;277(47):44784-90.

(183) Foster DB, Van Eyk JE, Marban E, O'Rourke B. Redox signaling and protein phosphorylation in mitochondria: progress and prospects. *J Bioenerg Biomembr* 2009 April;41(2):159-68.

(184) Rajagopalan S, Kurz S, Munzel T et al. Angiotensin II-mediated hypertension in the rat increases vascular superoxide production via membrane NADH/NADPH oxidase activation. Contribution to alterations of vasomotor tone. *J Clin Invest* 1996 April 15;97(8):1916-23.

(185) Linke A, Adams V, Schulze PC et al. Antioxidative effects of exercise training in patients with chronic heart failure: increase in radical scavenger enzyme activity in skeletal muscle. *Circulation* 2005 April 12;111(14):1763-70.

(186) Chae HZ, Robison K, Poole LB, Church G, Storz G, Rhee SG. Cloning and sequencing of thiol-specific antioxidant from mammalian brain: alkyl hydroperoxide reductase and thiol-specific antioxidant define a large family of antioxidant enzymes. *Proc Natl Acad Sci U S A* 1994 July 19;91(15):7017-21.

(187) Chae HZ, Kim HJ, Kang SW, Rhee SG. Characterization of three isoforms of mammalian peroxiredoxin that reduce peroxides in the presence of thioredoxin. *Diabetes Res Clin Pract* 1999 September;45(2-3):101-12.

(188) Cullingford TE, Wait R, Clerk A, Sugden PH. Effects of oxidative stress on the cardiac myocyte proteome: modifications to peroxiredoxins and small heat shock proteins. *J Mol Cell Cardiol* 2006 January;40(1):157-72.

(189) Power JH, Asad S, Chataway TK et al. Peroxiredoxin 6 in human brain: molecular forms, cellular distribution and association with Alzheimer's disease pathology. *Acta Neuropathol* 2008 June;115(6):611-22.

(190) Wagner E, Luche S, Penna L et al. A method for detection of overoxidation of cysteines: peroxiredoxins are oxidized in vivo at the active-site cysteine during oxidative stress. *Biochem J* 2002 September 15;366(Pt 3):777-85.

(191) Cauwels A, Bultinck J, Brouckaert P. Dual role of endogenous nitric oxide in tumor necrosis factor shock: induced NO tempers oxidative stress. *Cell Mol Life Sci* 2005 July;62(14):1632-40.

(192) Otto A, Fontaine J, Berkenboom G. Ramipril treatment protects against nitrate-induced oxidative stress in eNOS-/- mice: An implication of the NADPH oxidase pathway. *J Cardiovasc Pharmacol* 2006 July;48(1):842-9.

(193) Choi HJ, Kang SW, Yang CH, Rhee SG, Ryu SE. Crystal structure of a novel human peroxidase enzyme at 2.0 A resolution. *Nat Struct Biol* 1998 May;5(5):400-6.

(194) Manevich Y, Feinstein SI, Fisher AB. Activation of the antioxidant enzyme 1-CYS peroxiredoxin requires glutathionylation mediated by heterodimerization with pi GST. *Proc Natl Acad Sci U S A* 2004 March 16;101(11):3780-5.

(195) Hayes JD, Flanagan JU, Jowsey IR. Glutathione transferases. *Annu Rev Pharmacol Toxicol* 2005;45:51-88.

(196) Zhou SG, Wang P, Pi RB et al. Reduced expression of GSTM2 and increased oxidative stress in spontaneously hypertensive rat. *Mol Cell Biochem* 2008 February;309(1-2):99-107.

(197) Doran P, Gannon J, O'Connell K, Ohlendieck K. Aging skeletal muscle shows a drastic increase in the small heat shock proteins alphaB-crystallin/HspB5 and cvHsp/HspB7. *Eur J Cell Biol* 2007 October;86(10):629-40.

(198) Koh TJ. Do small heat shock proteins protect skeletal muscle from injury? *Exerc Sport Sci Rev* 2002 July;30(3):117-21.

(199) Doser TA, Turdi S, Thomas DP, Epstein PN, Li SY, Ren J. Transgenic overexpression of aldehyde dehydrogenase-2 rescues chronic alcohol intake-induced myocardial hypertrophy and contractile dysfunction. *Circulation* 2009 April 14;119(14):1941-9.

(200) Zeng Q, Zhou Q, Yao F, O'Rourke ST, Sun C. Endothelin-1 regulates cardiac L-type calcium channels via NAD(P)H oxidase-derived superoxide. *J Pharmacol Exp Ther* 2008 September;326(3):732-8.

(201) Kakita T, Hasegawa K, Iwai-Kanai E et al. Calcineurin pathway is required for endothelin-1-mediated protection against oxidant stress-induced apoptosis in cardiac myocytes. *Circ Res* 2001 June 22;88(12):1239-46.

(202) Lachmanova V, Hnilickova O, Povysilova V, Hampl V, Herget J. N-acetylcysteine inhibits hypoxic pulmonary hypertension most effectively in the initial phase of chronic hypoxia. *Life Sci* 2005 May 27;77(2):175-82.

(203) Paulis L, Simko F. Blood pressure modulation and cardiovascular protection by melatonin: potential mechanisms behind. *Physiol Res* 2007;56(6):671-84.

(204) Moss RL, Fitzsimons DP. Myosin light chain 2 into the mainstream of cardiac development and contractility. *Circ Res* 2006 August 4;99(3):225-7.

(205) Rottbauer W, Wessels G, Dahme T et al. Cardiac myosin light chain-2: a novel essential component of thick-myofilament assembly and contractility of the heart. *Circ Res* 2006 August 4;99(3):323-31.

(206) Skwarek-Maruszewska A, Hotulainen P, Mattila PK, Lappalainen P. Contractility-dependent actin dynamics in cardiomyocyte sarcomeres. *J Cell Sci* 2009 June 15;122(Pt 12):2119-26.

(207) Hernandez OM, Jones M, Guzman G, Szczesna-Cordary D. Myosin essential light chain in health and disease. *Am J Physiol Heart Circ Physiol* 2007 April;292(4):H1643-H1654.

(208) Driska SP, Aksoy MO, Murphy RA. Myosin light chain phosphorylation associated with contraction in arterial smooth muscle. *Am J Physiol* 1981 May;240(5):C222-C233.

(209) Patel JR, Diffee GM, Huang XP, Moss RL. Phosphorylation of myosin regulatory light chain eliminates force-dependent changes in relaxation rates in skeletal muscle. *Biophys J* 1998 January;74(1):360-8.

(210) Davis JS, Hassanzadeh S, Winitsky S et al. The overall pattern of cardiac contraction depends on a spatial gradient of myosin regulatory light chain phosphorylation. *Cell* 2001 November 30;107(5):631-41.

(211) Poetter K, Jiang H, Hassanzadeh S et al. Mutations in either the essential or regulatory light chains of myosin are associated with a rare myopathy in human heart and skeletal muscle. *Nat Genet* 1996 May;13(1):63-9.

(212) Van Eyk JE, Powers F, Law W, Larue C, Hodges RS, Solaro RJ. Breakdown and release of myofilament proteins during ischemia and ischemia/reperfusion in rat hearts: identification of degradation products and effects on the pCa-force relation. *Circ Res* 1998 February 9;82(2):261-71.

(213) Casey TM, Arthur PG, Bogoyevitch MA. Proteomic analysis reveals different protein changes during endothelin-1- or leukemic inhibitory factor-induced hypertrophy of cardiomyocytes in vitro. *Mol Cell Proteomics* 2005 May;4(5):651-61.

(214) White MY, Cordwell SJ, McCarron HC, Tchen AS, Hambly BD, Jeremy RW. Modifications of myosin-regulatory light chain correlate with function of stunned myocardium. *J Mol Cell Cardiol* 2003 July;35(7):833-40.

(215) Bamburg JR, McGough A, Ono S. Putting a new twist on actin: ADF/cofilins modulate actin dynamics. *Trends Cell Biol* 1999 September;9(9):364-70.

(216) Arber S, Barbayannis FA, Hanser H et al. Regulation of actin dynamics through phosphorylation of cofilin by LIM-kinase. *Nature* 1998 June 25;393(6687):805-9.

(217) Huang YS, Wang SM, Hsu KL, Tseng YZ, Wu JC. Mechanism of oleic acid-induced myofibril disassembly in rat cardiomyocytes. *J Cell Biochem* 2007 October 15;102(3):638-49.

(218) Kim JS, Huang TY, Bokoch GM. Reactive Oxygen Species (ROS) Regulate a Slingshot-Cofilin Activation Pathway. *Mol Biol Cell* 2009 April 8.

(219) Flashman E, Redwood C, Moolman-Smook J, Watkins H. Cardiac myosin binding protein C: its role in physiology and disease. *Circ Res* 2004 May 28;94(10):1279-89.

(220) Stelzer JE, Patel JR, Moss RL. Protein kinase A-mediated acceleration of the stretch activation response in murine skinned myocardium is eliminated by ablation of cMyBP-C. *Circ Res* 2006 October 13;99(8):884-90.

(221) Palmer BM, McConnell BK, Li GH et al. Reduced cross-bridge dependent stiffness of skinned myocardium from mice lacking cardiac myosin binding protein-C. *Mol Cell Biochem* 2004 August;263(1-2):73-80.

(222) Yoshida M, Minamisawa S, Shimura M et al. Impaired Ca2+ store functions in skeletal and cardiac muscle cells from sarcalumenin-deficient mice. *J Biol Chem* 2005 February 4;280(5):3500-6.

(223) Muller-Brunotte R, Kahan T, Malmqvist K, Edner M. Blood pressure and left ventricular geometric pattern determine diastolic function in hypertensive myocardial hypertrophy. *J Hum Hypertens* 2003 December;17(12):841-9.

(224) Huang C, Zhou Q, Liang P et al. Characterization and in vivo functional analysis of splice variants of cypher. *J Biol Chem* 2003 February 28;278(9):7360-5.

(225) Arimura T, Hayashi T, Terada H et al. A Cypher/ZASP mutation associated with dilated cardiomyopathy alters the binding affinity to protein kinase C. *J Biol Chem* 2004 February 20;279(8):6746-52.

(226) Zheng M, Cheng H, Li X et al. Cardiac-specific ablation of Cypher leads to a severe form of dilated cardiomyopathy with premature death. *Hum Mol Genet* 2009 February 15;18(4):701-13.

(227) Alvarez BV, Johnson DE, Sowah D et al. Carbonic anhydrase inhibition prevents and reverts cardiomyocyte hypertrophy. *J Physiol* 2007 February 15;579(Pt 1):127-45.

(228) Stratmann B, Tschoepe D. Sweet heart - contributions of metabolism in the development of heart failure in diabetes mellitus. *Exp Clin Endocrinol Diabetes* 2008 September;116 Suppl 1:S40-S45.

(229) Nikolaidis LA, Mankad S, Sokos GG et al. Effects of glucagon-like peptide-1 in patients with acute myocardial infarction and left ventricular dysfunction after successful reperfusion. *Circulation* 2004 March 2;109(8):962-5.

(230) Vitale C, Wajngaten M, Sposato B et al. Trimetazidine improves left ventricular function and quality of life in elderly patients with coronary artery disease. *Eur Heart J* 2004 October;25(20):1814-21.

(231) Stanley WC, Chandler MP. Energy metabolism in the normal and failing heart: potential for therapeutic interventions. *Heart Fail Rev* 2002 April;7(2):115-30.

(232) Recchia FA. Role of nitric oxide in the regulation of substrate metabolism in heart failure. *Heart Fail Rev* 2002 April;7(2):141-8.

(233) Kurzelewski M, Duda M, Stanley WC, Boemke W, Beresewicz A. Nitric oxide synthase inhibition and elevated endothelin increase oxygen consumption but do not affect glucose and palmitate oxidation in the isolated rat heart. *J Physiol Pharmacol* 2004 March;55(1 Pt 1):27-38.

(234) Noguchi T, Chen Z, Bell SP, Nyland L, LeWinter MM. Endothelin receptor blockade has an oxygen-saving effect in Dahl salt-sensitive rats with heart failure. *Am J Physiol Heart Circ Physiol* 2003 October;285(4):H1428-H1434.

(235) Cwinn MA, Jones SP, Kennedy SW. Exposure to perfluorooctane sulfonate or fenofibrate causes PPAR-alpha dependent transcriptional responses in chicken embryo hepatocytes. *Comp Biochem Physiol C Toxicol Pharmacol* 2008 August;148(2):165-71.

(236) Yoon M. The role of PPARalpha in lipid metabolism and obesity: focusing on the effects of estrogen on PPARalpha actions. *Pharmacol Res* 2009 September;60(3):151-9.

(237) Bulhak AA, Sjoquist PO, Xu CB, Edvinsson L, Pernow J. Protection against myocardial ischaemia/reperfusion injury by PPAR-alpha activation is related to production of nitric oxide and endothelin-1. *Basic Res Cardiol* 2006 May;101(3):244-52.

(238) Irukayama-Tomobe Y, Miyauchi T, Sakai S et al. Endothelin-1-induced cardiac hypertrophy is inhibited by activation of peroxisome proliferator-activated receptor-alpha partly via blockade of c-Jun NH2-terminal kinase pathway. *Circulation* 2004 February 24;109(7):904-10.

(239) Yakubu MA, Nsaif RH, Oyekan AO. peroxisome proliferator-activated receptor alpha activation-mediated regulation of endothelin-1 production via nitric oxide and protein kinase C signaling pathways in piglet cerebral microvascular endothelial cell culture. *J Pharmacol Exp Ther* 2007 February;320(2):774-81.

(240) Vredendaal PJ, van dB, I, Stroobants AK, van der AD, Malingre HE, Berger R. Structural organization of the human short-chain L-3-hydroxyacyl-CoA dehydrogenase gene. *Mamm Genome* 1998 September;9(9):763-8.

(241) Janssen U, Stoffel W. Disruption of mitochondrial beta -oxidation of unsaturated fatty acids in the 3,2-trans-enoyl-CoA isomerase-deficient mouse. *J Biol Chem* 2002 May 31;277(22):19579-84.

(242) Sharma S, Sud N, Wiseman DA et al. Altered carnitine homeostasis is associated with decreased mitochondrial function and altered nitric oxide signaling in lambs with pulmonary hypertension. *Am J Physiol Lung Cell Mol Physiol* 2008 January;294(1):L46-L56.

(243) Sinatra ST. Metabolic cardiology: the missing link in cardiovascular disease. *Altern Ther Health Med* 2009 March;15(2):48-50.

(244) Calo LA, Pagnin E, Davis PA et al. Antioxidant effect of L-carnitine and its short chain esters: relevance for the protection from oxidative stress related cardiovascular damage. *Int J Cardiol* 2006 February 8;107(1):54-60.

(245) Schinetti ML, Rossini D, Greco R, Bertelli A. Protective action of acetylcarnitine on NADPH-induced lipid peroxidation of cardiac microsomes. *Drugs Exp Clin Res* 1987;13(8):509-15.

(246) McVeigh JJ, Lopaschuk GD. Dichloroacetate stimulation of glucose oxidation improves recovery of ischemic rat hearts. *Am J Physiol* 1990 October;259(4 Pt 2):H1079-H1085.

(247) Abe K, Hayashi N, Terada H. Effect of endogenous nitric oxide on energy metabolism of rat heart mitochondria during ischemia and reperfusion. *Free Radic Biol Med* 1999 February;26(3-4):379-87.

(248) Kakinuma Y, Miyauchi T, Suzuki T et al. Enhancement of glycolysis in cardiomyocytes elevates endothelin-1 expression through the transcriptional factor hypoxia-inducible factor-1 alpha. *Clin Sci (Lond)* 2002 August;103 Suppl 48:210S-4S.

(249) Tribulova N, Okruhlicova L, Bernatova I, Pechanova O. Chronic disturbances in NO production results in histochemical and subcellular alterations of the rat heart. *Physiol Res* 2000;49(1):77-88.

(250) Serradeil-Le GC, Jouneaux C, Sanchez-Bueno A et al. Endothelin action in rat liver. Receptors, free Ca2+ oscillations, and activation of glycogenolysis. *J Clin Invest* 1991 January;87(1):133-8.

(251) Kakinuma Y, Miyauchi T, Yuki K, Murakoshi N, Goto K, Yamaguchi I. Mitochondrial dysfunction of cardiomyocytes causing impairment of cellular energy metabolism induces apoptosis, and concomitant increase in cardiac endothelin-1 expression. *J Cardiovasc Pharmacol* 2000 November;36(5 Suppl 1):S201-S204.

(252) Piatti PM, Monti LD, Galli L et al. Relationship between endothelin-1 concentration and metabolic alterations typical of the insulin resistance syndrome. *Metabolism* 2000 June;49(6):748-52.

(253) Skalska A, Gasowski J, Grodzicki T. Antioxidants modify the relationship between endothelin-1 level and glucose metabolism-associated parameters. *Metabolism* 2009 September;58(9):1229-33.

(254) Fragasso G, Spoladore R, Cuko A, Palloshi A. Modulation of fatty acids oxidation in heart failure by selective pharmacological inhibition of 3-ketoacyl coenzyme-A thiolase. *Curr Clin Pharmacol* 2007 September;2(3):190-6.

(255) Ussher JR, Lopaschuk GD. Targeting malonyl CoA inhibition of mitochondrial fatty acid uptake as an approach to treat cardiac ischemia/reperfusion. *Basic Res Cardiol* 2009 March;104(2):203-10.

(256) Marin-Garcia J, Goldenthal MJ, Moe GW. Selective endothelin receptor blockade reverses mitochondrial dysfunction in canine heart failure. *J Card Fail* 2002 October;8(5):326-32.

(257) Yuki K, Suzuki T, Katoh S, Kakinuma Y, Miyauchi T, Mitsui Y. Endothelin-1 stimulates cardiomyocyte injury during mitochondrial dysfunction in culture. *Eur J Pharmacol* 2001 November 16;431(2):163-70.

(258) Iwai-Kanai E, Hasegawa K, Adachi S et al. Effects of endothelin-1 on mitochondrial function during the protection against myocardial cell apoptosis. *Biochem Biophys Res Commun* 2003 June 13;305(4):898-903.

(259) Brown GC, Cooper CE. Nanomolar concentrations of nitric oxide reversibly inhibit synaptosomal respiration by competing with oxygen at cytochrome oxidase. *FEBS Lett* 1994 December 19;356(2-3):295-8.

(260) Kojic ZZ, Flogel U, Schrader J, Decking UK. Endothelial NO formation does not control myocardial O2 consumption in mouse heart. *Am J Physiol Heart Circ Physiol* 2003 July;285(1):H392-H397.

(261) Loke KE, McConnell PI, Tuzman JM et al. Endogenous endothelial nitric oxide synthase-derived nitric oxide is a physiological regulator of myocardial oxygen consumption. *Circ Res* 1999 April 16;84(7):840-5.

(262) Visser G, Suormala T, Smit GP et al. 3-methylcrotonyl-CoA carboxylase deficiency in an infant with cardiomyopathy, in her brother with developmental delay and in their asymptomatic father. *Eur J Pediatr* 2000 December;159(12):901-4.

(263) Foker JE, Einzig S, Wang T. Adenosine metabolism and myocardial preservation. Consequences of adenosine catabolism on myocardial high-energy compounds and tissue blood flow. *J Thorac Cardiovasc Surg* 1980 October;80(4):506-16.

(264) Cronstein BN, Kramer SB, Rosenstein ED, Weissmann G, Hirschhorn R. Adenosine modulates the generation of superoxide anion by stimulated human neutrophils via interaction with a specific cell surface receptor. *Ann N Y Acad Sci* 1985;451:291-301.

(265) Tiranti V, Viscomi C, Hildebrandt T et al. Loss of ETHE1, a mitochondrial dioxygenase, causes fatal sulfide toxicity in ethylmalonic encephalopathy. *Nat Med* 2009 February;15(2):200-5.

(266) Parikh H, Nilsson E, Ling C et al. Molecular correlates for maximal oxygen uptake and type 1 fibers. *Am J Physiol Endocrinol Metab* 2008 June;294(6):E1152-E1159.

Publications

2009 N. Vignon-Zellweger, K. Relle, E. Kienlen, E. Dowuona-Hammond, J. Sharkovska, S. Heiden, P. Kalk, K. Schwab, B. Albrecht-Küpper, J-P. Stasch, F. Theuring, and B. Hocher. (Under review). Endothelin-1 overexpression restores cardiac function in eNOS knockout mice.

2009 N. Vignon-Zellweger, P. Seider, K. Relle, S. Heiden, B. Hocher, F. Theuring. (Manuscript in preparation). Sex dependent expression of cardiac fibrotic components in ET+/+eNOS-/- mice.

2008 S. Heiden, T. Pfab, K. Von Websky, N. Vignon-Zellweger, M. Godes, K. Relle, P. Kalk, F. Theuring, W. Zidek and B. Hocher. Tissue Specific Activation of the Endothelin System in Severe Acute Liver Failure. **Eur J Med Res 2008** 13: 327-329.

2007 T. Quaschning, F. Voss, K. Relle, P. Kalk, N. Vignon-Zellweger, T. Pfab, C. Bauer, F. Theilig, S. Bachmann, A. Kraemer-Guth, C. Wanner, F. Theuring, J. Galle and B. Hocher. Lack of eNOS Promotes Endothelin-Induced Hypertension: Lessons from Endothelin-1 transgenic/eNOS Knockout Mice. **J Am Soc Nephrol. 2007** Mar;18 (3):730-40**.**

Oral communications and posters

Sept. 9-12 2009 **ET-11, 11th international conference on endothelin, Montreal, Canada**
Oral Presentation: Endothelin-1 overexpression restores cardiac function in eNOS knockout mice but promotes cardiac fibrosis. N. Vignon-Zellweger, K. Relle, E. Kienlen, E. Dowuona-Hammond, J. Sharkovska, S. Heiden, P. Kalk, K. Schwab, B. Neuman, C. Scheler, B. Albrecht-Küpper, J-P. Stasch, F. Theuring, and B. Hocher.

Nov.8-12 2008 **Scientific Sessions of the American Heart Association, New Orleans, USA.**
Poster Presentation: Additional Lack Of eNOS Promotes Cardiac Fibrosis In ET-1 Transgenic Mice. N. Vignon-Zellweger, K. Relle, E. Kienlen, P. Seider, E. Dowuona-Hammond, J. Sharkovska, S. Heiden, F. Voss, P. Kalk, K. Schwab, B. Neuman, C. Scheler, B. Albrecht, S. Schäfer, F. Theuring, B. Hocher.

Sept 12-14 2008 **3rd International Congress of Gender Medicine, Stockholm, Sweden.**
Poster Presentation: Additional Lack Of eNOS Promotes Cardiac Fibrosis In ET-1 Transgenic Mice. N. Vignon-Zellweger, K. Relle, J. Rahnenführer, P. Seider, E. Dowuona-Hammond, J. Sharkovska, F. Voss, K. Schwab, P. Kalk, C. Scheler, F. Theuring, B. Hocher.

June 14-19 2008 **Hypertension 2008, 22nd Scientific Meeting International Society of Hypertension, Berlin, Germany**.
Oral Presentation: Additional Lack Of eNOS Promotes Cardiac Fibrosis in ET-1 Transgenic Mice. N. Vignon-Zellweger*, K. Relle, J. Rahnenführer, P. Seider, E. Dowuona-Hammond, J. Sharkovska, F. Voss, P. Kalk, C. Scheler, F. Theuring, B. Hocher.
**Nominated for the Austin Doyle Award of the International Society of Hypertension.*